Four Lectures on Turbulent Combustion

N. Peters

Institut für Technische Mechanik
RWTH Aachen

ERCOFTAC Summer School
September 15-19, 1997
Aachen, Germany

Contents

Lecture 1

Turbulent Combustion: Introduction and Overview

Technical processes in turbulent combustion are in general subdivided into two classes: premixed or non-premixed combustion. For example, combustion in homogeneous charge, spark-ignition engines occurs under premixed conditions. On the other hand, combustion in a Diesel engine or in furnaces essentially taakes place under non-premixed conditions.

In the spark-ignition engine fuel and oxidizer are being mixed by turbulence during a sufficiently long time down to the molecular level before combustion is initiated by a spark. The deposition of energy from the spark generates a flame kernel that grows at first by laminar, then by turbulent flame propagation. The turbulent burning velocity is therefore a very important quantity in premixed turbulent combustion.

In the Diesel engine a liquid fuel spray is injected into hot compressed air, the fuel evaporates and mixes partially with the air until auto-ignition occurs. The auto-ignition process is very rapid and the partially premixed gas is rapidly consumed. The final phase of burnout then occurs under non-premixed conditions.

Similarly, in furnaces jets of gaseous, liquid or solid fuels are injected into air which may be preheated or partially diluted by exhaust gases. Once the jet is ignited, the flame propagates towards the nozzle until it stabilizes at a distance, called the lift-off height downstream of the nozzle. Partial premixing then occurs within the region between the nozzle and the lift-off height, and determines the stabilization of the turbulent flame. Further downstream, combustion again occurs under non-premixed conditions.

It is clear, that in addition to premixed and non-premixed combustion, partially premixed combustion plays, at least locally, an important role in technical applications. An important example are modern gas turbine combustion chambers where fuel rich regions are used for flame stabilization but, in order to minimize NO_x formation, most of the combustion occurs under premixed fuel lean conditions. Similarly, combustion in direct injection or stratified charge spark-ignition

	premixed	partially and non-premixed
fast chemistry	spark-ignition engines	Diesel engines gas turbine engines combustion in furnaces
slow chemistry	NO_x formation in post-flame regions	low NO_x-burners

Table 1.1: Classification of combustion applications.

engines occurs under partially premixed conditions.

Another criterion to classify turbulent combustion is related to the ratio of turbulent to chemical time scales. If turbulence is very intense the turbulent time is likely to be short. Chemical time scales become short if the temperature is high and they become long with decreasing temperature. The case of short turbulent and long chemical time scales is simply called slow chemistry while the case of a comparatively long turbulent and short chemical time scale is called fast chemistry.

Slow chemistry is not very often of practical interest: there are a few situations like low NO_x burners which operate with strong exhaust gas recirculation and therefore lower temperature where the chemistry is slow compared to turbulent mixing. Also, in the post-flame region of a spark ignition engine NO_x production is slow while the temperature field is nearly homogeneous. On the other hand, reacting flows with fast chemistry occur in nearly all the applications mentioned above. The reason is simple: for combustion to be stable and efficient, the temperature must be high and therefore the chemical time scales are short. Therefore engines are designed such that only at limit conditions, i.e. at very high engine speeds, turbulent time scales may become comparable to chemical time scales.

Table 1.1 shows a diagram where combustion applications are classified with respect to both criteria mentioned above.

The four lectures on turbulent combustion are therefore organized as follows: In this lecture an overview of current modeling approaches for turbulent flows with combustion will be given. Regimes in premixed and non-premixed turbulent combustion will be defined in terms of velocity, length, time and mixing scales.

In the next lecture, treating premixed turbulent combustion, models based on the progress variable c and the distance function G will be presented. Damköhler's regimes of large scale and small scale turbulence will be associated with the corrugated flamelet regime and the thin reaction zones regime, respectively. Finally,

based on an equation for the total flame surface density, an expression for the burning velocity that is valid in both regimes, will be derived.

In the third lecture flamelet modeling for non-premixed combustion will be addressed. The unsteady flamelet equations will be derived and solutions will be presented. Coupling with solutions of the turbulent mixing field will be discussed. Finally, approximate solutions for the round turbulent jet and the influence of buoyancy on the flame length will be presented.

The last lecture is concerned with partially premixed combustion. The key element here is the triple flame, which will be discussed in detail. The distance function approach for premixed combustion and the flamelet approach for non-premixed combustion will be combined to obtain an expression for the turbulent burning velocity in partially premixed systems. This expression is used to calculate flame propagation in diffusion flames and to determine the lift-off height.

1.1 Moment Methods in Modeling Turbulence with Combustion

A classical way to describe turbulent flows is to split the three components of velocity and the scalar quantities like the temperature and mass fractions measured at a point $\mathbf{x}$ into a mean (denoted by an overbar) and a fluctuation, for example u

$$u(\mathbf{x},t) = \bar{u}(\mathbf{x},t) + u'(\mathbf{x},t), \quad \text{where} \quad \bar{u'}(\mathbf{x},t) = 0\ . \tag{1.1}$$

If the flow is stationary on the average, the mean is defined by the time average

$$\bar{u}(\mathbf{x}) = \lim_{\Delta t\to\infty}\left\{\frac{1}{\Delta t}\int_{t}^{t+\Delta t} u(\mathbf{x},t)dt\right\} \tag{1.2}$$

and the fluctuation is obtained by subtracting the mean from the instantaneous value. For instationary flows the time-dependent mean value may be obtained by low-pass filtering the signal. This requires that the mean velocity changes on a time scale that is significantly longer than the time scale of turbulent fluctuations. These two cases are shown in Fig. 1.1.

For flows with large density changes like in combustion it is often convenient to introduce a density weighted average $\tilde{u}$, called the Favre average, by splitting $u(\mathbf{x},t)$ into $\tilde{u}(\mathbf{x},t)$ and $u''(\mathbf{x},t)$ as

$$u(\mathbf{x},t) = \tilde{u}(\mathbf{x},t) + u''(\mathbf{x},t)\ . \tag{1.3}$$

This averaging procedure is defined by requiring that the average of the product of u'' with the density ρ (rather than $u''(\mathbf{x},t)$ itself) vanishes

$$\overline{\rho u''} = 0\ . \tag{1.4}$$

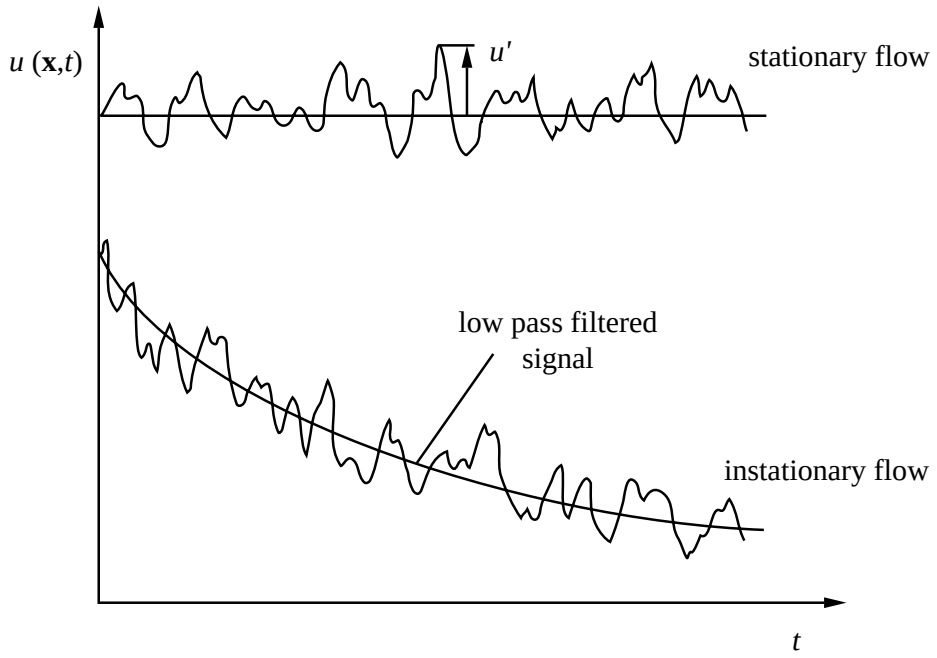

Figure 1.1: Mean and fluctuation of a velocity signal as a function of time for stationary and instationary flows.

The definition for $\tilde{u}$ may then be derived by multiplying (1.3) by the density ρ and averaging

$$\overline{\rho u} = \overline{\rho\tilde{u}} + \overline{\rho u''} = \bar{\rho}\tilde{u} \ . \tag{1.5}$$

Here the average of the product $\rho\tilde{u}$ is equal to the product of the averages $\bar{\rho}\tilde{u}$, since $\tilde{u}$ is already an average defined by

$$\tilde{u} = \overline{\rho u}/\bar{\rho} \ . \tag{1.6}$$

It can be calculated if simultaneous measurements of $\rho(\mathbf{x}, t)$ and $u(\mathbf{x}, t)$ are available by taking the average of the product $\rho(\mathbf{x}, t)u(\mathbf{x}, t)$ and dividing it by the average of $\rho(\mathbf{x}, t)$. While such measurements are often difficult to obtain, Favre averaging has considerable advantages for the mathematical development. In the balance equations of momentum, energy and chemical species, the convective terms are dominant in high Reynolds number flows. Since these contain the product of the dependent variable and the density, they are treated very simply by Favre averaging. For instance the average of the product of the density ρ with the velocity components v_α and v_β would lead with conventional averages to

$$\overline{\rho v_\alpha v_\beta} = \bar{\rho}\overline{v_\alpha}\ \overline{v_\beta} + \bar{\rho}\overline{v'_\alpha v'_\beta} + \overline{\rho' v'_\alpha}\overline{v_\beta} + \overline{\rho' v'_\beta}\overline{v_\alpha} + \overline{\rho' v'_\alpha v'_\beta} \ . \tag{1.7}$$

Using Favre averages one writes

$$\begin{aligned} \rho\widetilde{u_\alpha u_\beta} &= \rho(\tilde{u}_\alpha + \tilde{u}''_\alpha)(\tilde{u}_\beta + u''_\beta) \\ &= \rho\tilde{u}_\alpha\tilde{u}_\beta + \rho u''_\alpha\tilde{u}_\beta + \rho u''_\beta\tilde{u}_\alpha + \rho u''_\alpha u''_\beta \ . \end{aligned} \tag{1.8}$$

Here fluctuations of the density do not appear. Taking the average leads to

$$\overline{\rho u_\alpha u_\beta} = \bar{\rho}\tilde{u}_\alpha\tilde{u}_\beta + \bar{\rho}\widetilde{u''_\alpha u''_\beta} \tag{1.9}$$

where (1.4) and (1.6) have been applied. This expression is much simpler than (1.7) and has formally the same structure as the conventional average of $u_\alpha u_\beta$ for constant density flows

$$\overline{u_\alpha u_\beta} = \overline{u_\alpha}\ \overline{u_\beta} + \overline{u'_\alpha u'_\beta}\ . \tag{1.10}$$

Difficulties arising in the viscous and diffusive transport are of lower importance since these terms are usually neglected as compared to turbulent diffusion.

In Favre-averaged form the balance equations are written

Continuity

$$\frac{\partial\bar{\rho}}{\partial t} + \frac{\partial(\bar{\rho}\tilde{v}_\alpha)}{\partial x_\alpha} = 0 \tag{1.11}$$

Momentum

$$\bar{\rho}\frac{\partial\tilde{v}_\beta}{\partial t} + \bar{\rho}\tilde{v}_\alpha\frac{\partial\tilde{v}_\beta}{\partial x_\alpha} = -\frac{\partial\bar{p}}{\partial x_\beta} + \frac{\partial\bar{\tau}_{\alpha\beta}}{\partial x_\alpha} - \frac{\partial}{\partial x_\alpha}\left(\bar{\rho}\,\widetilde{v''_\alpha v''_\beta}\right) + \bar{\rho}g_\beta\ , \quad \beta = 1,2,3\ . \tag{1.12}$$

Here the l.h.s represents the local rate of change and convection, the first term on the r.h.s the pressure gradient, the second term molecular transport due to viscosity, the third term turbulent transport resulting from the decomposition in (1.9) and the last term forces due to buoyancy. Greek indices used twice indicate a summation over the three coordinate directions.

The mean viscous stress tensor $\bar{\tau}_{\alpha\beta}$ is often neglected compared to the Reynolds stress tensor $\bar{\rho}\,\widetilde{v''_\alpha v''_\beta}$. Balance equations for the components of the Reynolds stress tensor can be derived and closure assumptions have been proposed [1.1]. This is called second moment closure or Reynolds stress equation modeling. It leads to a number of additional terms that must be modelled, in particular the velocity-pressure gradient correlation and the dissipation tensor. Here we will introduce the eddy viscosity approach using a gradient transport hypothesis

$$\bar{\rho}\,\widetilde{v''_\alpha v''_\beta} = \begin{cases} -\bar{\rho}\tilde{\nu}_t\left[2\dfrac{\partial\tilde{v}_\alpha}{\partial x_\beta} - \dfrac{2}{3}\dfrac{\partial\tilde{v}_\gamma}{\partial x_\gamma}\right] + \dfrac{2}{3}\bar{\rho}\,\tilde{k}\,, & \alpha = \beta \\ -\bar{\rho}\tilde{\nu}_t\left[\dfrac{\partial\tilde{v}_\alpha}{\partial x_\beta} + \dfrac{\partial\tilde{v}_\beta}{\partial x_\alpha}\right], & \alpha \neq \beta\ . \end{cases} \tag{1.13}$$

The eddy viscosity $\tilde{\nu}_t$ is related to a Favre averaged turbulent kinetic energy $\tilde{k} = \widetilde{v''^2_\beta}/2$ and its dissipation $\tilde{\varepsilon}$ by

$$\tilde{\nu}_t = c_\mu\,\frac{\tilde{k}^2}{\tilde{\varepsilon}}\,, \qquad c_\mu = 0.09\ . \tag{1.14}$$

The $\tilde{k}$-$\tilde{\varepsilon}$-model leads to equations where the turbulent transport is diffusive and therefore is more easily handled by numerical methods than the modelled Reynolds stress equations. This is probably the most important reason for its wide use in many industrial codes. Equations for $\tilde{k}$ and $\tilde{\varepsilon}$ must be modelled using empirical information. These equations are

turbulent kinetic energy

$$\bar{\rho}\frac{\partial \tilde{k}}{\partial t} + \bar{\rho}\tilde{v}_\alpha \frac{\partial \tilde{k}}{\partial x_\alpha} = \frac{\partial}{\partial x_\alpha}\left(\bar{\rho}\tilde{\nu}_t \frac{\partial \tilde{k}}{\partial x_\alpha}\right) - \bar{\rho}\widetilde{v''_\alpha v''_\beta}\frac{\partial \tilde{u}_\alpha}{\partial x_\beta} - \bar{\rho}\tilde{\varepsilon} - \tilde{\nu}_t \frac{\partial \ln \bar{\rho}}{\partial x_\alpha}\frac{\partial \bar{p}}{\partial x_\alpha} , \quad (1.15)$$

Turbulent dissipation

$$\begin{aligned}\bar{\rho}\frac{\partial \tilde{\varepsilon}}{\partial t} + \bar{\rho}\tilde{v}_\alpha \frac{\partial \tilde{\varepsilon}}{\partial x_\alpha} = \frac{\partial}{\partial x_\alpha}\left(\bar{\rho}\frac{\nu_t}{\sigma_\varepsilon}\frac{\partial \tilde{\varepsilon}}{\partial x_\alpha}\right) &- c_{\varepsilon 1}\bar{\rho}\frac{\tilde{\varepsilon}}{\tilde{k}}\widetilde{v''_\alpha v''_\beta}\frac{\partial \tilde{u}_\alpha}{\partial x_\beta} - c_{\varepsilon 2}\bar{\rho}\frac{\tilde{\varepsilon}^2}{\tilde{k}} \\ &- c_{\varepsilon 3}\tilde{\nu}_t \frac{\tilde{\varepsilon}}{\tilde{k}}\frac{\partial \ln \bar{\rho}}{\partial x_\alpha}\frac{\partial \bar{p}}{\partial x_\alpha} .\end{aligned} \quad (1.16)$$

In these equations the two terms on the l.h.s represent the local rate of change and convection, respectively, the first term on the r.h.s represents the turbulent transport, the second one turbulent production and the third one turbulent dissipation. The last term accounts for the effect of pressure gradients which is absent in constant density flows [1.2]. As in the standard k-ε model, the constants $\sigma_\varepsilon = 1.3$, $c_{\varepsilon 1} = 1.44$, $c_{\varepsilon 2} = 1.92$ may be used. For $c_{\varepsilon 3}$ a value of $c_{\varepsilon 3} = 1.0$ has been proposed [1.1].

Favre averaged equations for the temperature and the mass fractions of the n chemical species are written as

Temperature

$$c_p\left(\bar{\rho}\frac{\partial \widetilde{T}}{\partial t} + \bar{\rho}\tilde{v}_\alpha \frac{\partial \widetilde{T}}{\partial x_\alpha}\right) = -\frac{\partial}{\partial x_\alpha}\overline{\mathrm{J}_{T,\alpha}} - c_p\frac{\partial}{\partial x_\alpha}(\bar{\rho}\widetilde{v''_\alpha T''}) + \frac{\partial \bar{p}}{\partial t} - \overline{\sum_{i=1}^{n} h_i \dot{m}_i} - \overline{q_R} , \quad (1.17)$$

Mass fraction

$$\bar{\rho}\frac{\partial \widetilde{Y}_i}{\partial t} + \bar{\rho}\tilde{v}_\alpha \frac{\partial \widetilde{Y}_i}{\partial x_\alpha} = -\frac{\partial}{\partial x_\alpha}\overline{\mathrm{J}_{i,\alpha}} - \frac{\partial}{\partial x_\alpha}(\bar{\rho}\widetilde{v''_\alpha Y''_i}) + \overline{\dot{m}_i} , \; i = 1, 2, \ldots, n . \quad (1.18)$$

In these equations the terms on the l.h.s represent the local rate of change and convection, the first terms on the r.h.s molecular transport and the second terms turbulent transport resulting from a decomposition of the convective terms similar to (1.9). In the equation for the temperature a constant heat capacity c_p has been assumed for simplicity. The molecular heat flux is denoted by $\mathrm{J}_{T,\alpha}$ and the diffusion flux by $\mathrm{J}_{i,\alpha}$. In addition, the small Mach number limit has been introduced such that spatial gradients of the pressure vanish in the temperature equations and only the unsteady change of pressure, which is important for reciprocating engines,

remains. The last two terms in the temperature equation represent the chemical heat release and the heat loss by radiation. The last term in the species equation is the chemical source term. The molecular transport terms in these equations can often be neglected compared to turbulent transport, which may be modelled using the gradient transport hypothesis as

$$-\bar{\rho}\widetilde{v_\alpha'' T''} = \bar{\rho}\frac{\tilde{\nu}_t}{\sigma_T}\frac{\partial \widetilde{T}}{\partial x_\alpha}\,, \tag{1.19}$$

$$-\bar{\rho}\widetilde{v_\alpha'' Y_i''} = \bar{\rho}\frac{\tilde{\nu}_t}{\sigma_i}\frac{\partial \widetilde{Y_i}}{\partial x_\alpha}\,. \tag{1.20}$$

Here σ_T and σ_i are the turbulent Prandtl and Schmidt numbers, respectively. This kind of modeling is based on the assumption that the instantaneous fields of temperature and species concentrations are smoothly varying which requires that chemistry is slow compared to turbulent mixing. This is hardly ever the case in practical applications.

In addition, the chemical source terms $\overline{\sum_{i=1}^{n} h_i \dot{m}_i}$ and $\overline{\dot{m}_i}$ appearing in (1.17) and (1.18) need to be modelled. Since these terms are highly non-linear and strongly dependent on temperature and species concentrations, a moment closure approach is inadequate. Therefore the modeling of the chemical source terms has often been considered as the main problem in turbulent combustion. An early attempt to solve this problem is due to Spalding [1.3] who realized that turbulent mixing may be viewed as a cascade process from large to small scales and that small scale mixing down to the molecular scales controls the chemical reactions. Then mixing rather than reaction is the rate determining process. This model was called the Eddy-Break-Up model (EBU). The turbulent mean reaction rate of products was expressed as

$$\overline{\dot{m}_{pr}} = \min\left\{\dot{m}_{pr}, c_{\mathrm{EBU}}\bar{\rho}\frac{\tilde{\varepsilon}}{\tilde{k}}\left(\widetilde{Y_{pr}''^{\,2}}\right)^{1/2}\right\} \tag{1.21}$$

where $\widetilde{Y_{pr}''^{\,2}}$ is the Favre variance of the product mass fraction and $c_{\mathrm{EBU}} = 0.35$ is the Eddy-Break-Up constant. The formulation in (1.21) takes into account that chemistry may be rate determining in cold regions of the flow or when chemical equilibrium in a homogeneous mixture has been reached.

The Eddy-Break-Up model marks an important step in the development of models for premixed turbulent combustion. For non-premixed combustion, however, it fails to recognize that the simultaneous mixing of fuel and air during the combustion poses an additional limitation. This limitation may be expressed as the probability of finding stoichiometric mixture at a position $\mathbf{x}$. For this case an expression for the mean turbulent reaction rate was derived in a rigorous way by Bilger [1.4] who showed that in the fast chemistry limit the mean consumption rate

of fuel may be expressed as

$$\overline{\dot{m}_F} = -\frac{1}{2}\bar{\rho}\frac{Y_{F,1}}{1-Z_{\rm st}}\widetilde{\chi}_{\rm st}\widetilde{P}(Z|Z=Z_{\rm st})\ . \tag{1.22}$$

Here $Y_{F,1}$ is the mass fraction of fuel in the fuel stream, $\widetilde{\chi}_{\rm st}$ is the scalar dissipation rate of the mixture fraction Z and $\widetilde{P}(Z|Z=Z_{\rm st})$ is the probability density function of Z, both conditioned at stoichiometric mixture fraction $Z=Z_{\rm st}$.

This expression introduces the probability density function (pdf) as an important concept in turbulent combustion.

1.2 Probability Methods

If the pdf of all reactive scalars was known, the turbulent mean reaction rate of species i could be expressed as

$$\overline{\dot{m}_i} \equiv \bar{\rho}\widetilde{S}_i = \bar{\rho}\int_T\int_{\underline{Y}} S_i(T,\underline{Y})\widetilde{P}(T,\underline{Y})\,dT\,d\underline{Y}\ . \tag{1.23}$$

Here S_i is defined as $S_i = \dot{m}_i/\rho$ and $\widetilde{P}(T,\underline{Y})$ is the multi-dimensional Favre pdf of the temperature T and the mass fractions Y_i of the reactive species. Since there are n reactive species, they are denoted by the set $\underline{Y} = (Y_i, Y_2, \ldots, Y_n)$. $\widetilde{P}(T,\underline{Y})$ is defined as the probability of finding at point $\mathbf{x}$ and time t the temperature T and the reactive scalars within a range of $T \pm dT$ and $Y_i \pm dY_i$. Therefore the pdf covers a space of $n+1$ dimensions. In the pdf formulation, the quantities T and $\underline{Y}$ are independent variables on which the pdf depends. They are considered as random variables since their balance equations cannot be solved exactly for high Reynolds number turbulent flows. In order to solve the problem of the turbulent reaction rate based on (1.23) transport equations for the joint pdf of temperature and the reactive scalars have been proposed (cf. [1.5]).

There are several ways proposed to derive this transport equation. We refer to a presentation in [1.1] and present the final result as

$$\begin{aligned}\bar{\rho}\frac{\partial\widetilde{P}}{\partial t} + \bar{\rho}\tilde{v}_\alpha\frac{\partial\widetilde{P}}{\partial x_\alpha} \quad &+ \quad \bar{\rho}\sum_{i=1}^{n}\frac{\partial}{\partial\psi_i}\left\{\dot{m}_i(\underline{\psi})\widetilde{P}\right\} \\ &= \quad -\frac{\partial}{\partial x_\alpha}\left\{\bar{\rho}\overline{u''_\alpha|\underline{\psi}}\widetilde{P}\right\} + \sum_{i=1}^{n}\frac{\partial}{\partial\psi_i}\left\{\overline{\frac{\partial \underline{\mathrm{J}_i}}{\partial x_\alpha}\Big|\underline{\psi}}\ \widetilde{P}\right\}\ .\end{aligned} \tag{1.24}$$

Here $\underline{\psi}$ is the set $\underline{Y}$ including the temperature as additional variable. Similarly the set $\underline{\mathrm{J}_i}$ includes all diffusive fluxes of species and the heat flux. The first two terms on the l.h.s of (1.24) are the local rate of change and convection in physical space. The third term is the chemical source term in $\underline{\psi}$ space. On the r.h.s the first term represents turbulent transport in physical space and the last term molecular

transport in $\underline{\psi}$ space. These two terms contain the velocity fluctuation u''_α and the gradient of molecular fluxes, respectively, both conditioned on the set $\underline{\psi}$ and therefore need to be modelled.

In spite of the high dimensionality (1.24) is often thought be superior to other formulations, because the chemical source term is exact. However, when chemistry is fast compared to turbulent mixing, chemistry takes place in thin layers where molecular transport and the chemical source term are the leading terms and balance each other. This will result in steep local gradients of the reacting scalars, which makes most closure assumptions applied to the molecular mixing term questionable. For the same reason the gradient transport approximation cannot be applied to the turbulent transport term in physical space.

In the case of fast chemistry, the pre-assumed pdf approach is widely used. It relies on the assumption that within the thin layers, but also in their vicinity, the profiles of temperature and the reactive species concentrations may be expressed as functions of the mixture fraction Z (for non-premixed combustion) the distance function G (for premixed combustion) or both (for partially premixed combustion). Then only the pdf of the independent variables Z and G must be known. Since these quantities are described by differential equations that do not contain chemical source terms, the main problem in turbulent combustion is circumvented. These equations and the modeling of the corresponding equations for calculating their mean and variance will be discussed in the lectures that follow. Once the Favre mean and variance are known at position $\mathbf{x}$ and time t, one may construct the entire pdf by assuming that it depends on two parameters only. Thereby the functional form of the pdf is "pre-assumed" and its local shape may be calculated by expressing the two parameters in terms of the known values of the mean and the variance.

For the distance function G, for instance, a Gaussian pdf has been shown to be appropriate. Then the Favre pdf of G is given by

$$\widetilde{P}(G,\mathbf{x},t) = \frac{1}{\sqrt{2\pi\,\widetilde{G''^2}}}\exp\left(-\frac{(G-\widetilde{G})^2}{2\,\widetilde{G''^2}}\right) \tag{1.25}$$

where the Favre mean $\widetilde{G}(\mathbf{x},t)$ and the variance $\widetilde{G''^2}(\mathbf{x},t)$ are presumed to be known.

For the mixture fraction Z, which varies between $Z=0$ and $Z=1$, the beta function pdf is widely used

$$\widetilde{P}(Z,\mathbf{x},t) = \frac{Z^{\alpha-1}(1-Z)^{\beta-1}}{\Gamma(\alpha+\beta)}\;\Gamma(\alpha)\Gamma(\beta)\;. \tag{1.26}$$

This function is shown in Fig. 1.2. Here Γ is the gamma function. The two parameters α and β are related to the Favre mean $\widetilde{Z}(\mathbf{x},t)$ and variance $\widetilde{Z''^2}(\mathbf{x},t)$ by

$$\begin{aligned} \gamma &= \frac{\widetilde{Z}(1-\widetilde{Z})}{\widetilde{Z''^2}} - 1 \geq 0\;, \\ \alpha &= \widetilde{Z}\gamma\;, \quad \beta = (1-\widetilde{Z})\gamma\;. \end{aligned} \tag{1.27}$$

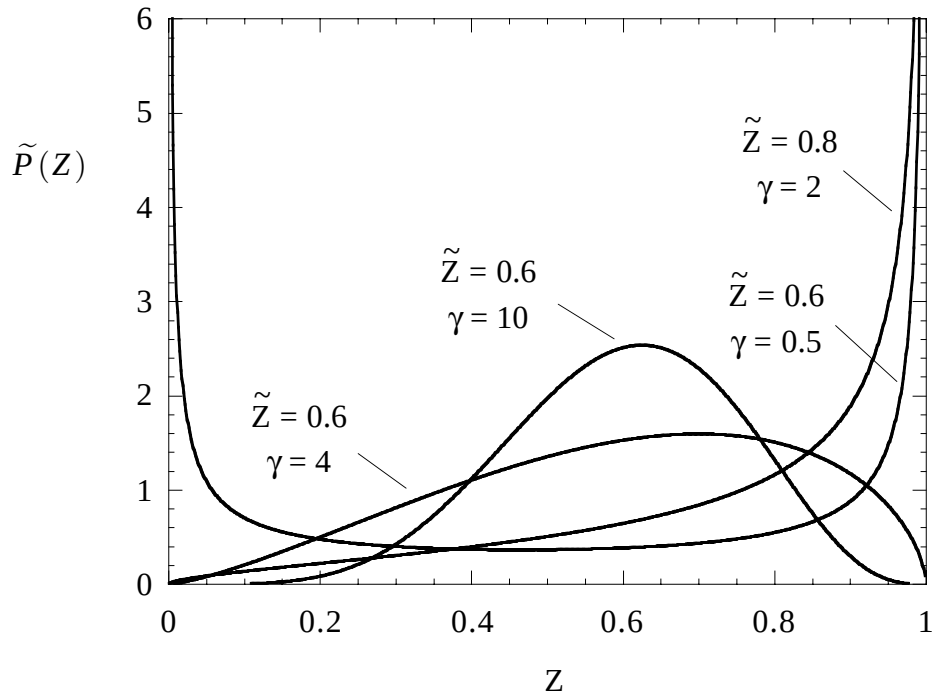

Figure 1.2: Shapes of the beta-function distribution.

When both, the profiles of the scalars and the pdf of the independent variables, are known, means and variances of any quantity depending on the reactive scalars may be calculated. In the case of non-premixed combustion, for instance, the mean temperature, its variance and the heat release rate may be obtained from

$$\widetilde{T}(\mathbf{x},t) = \int_0^1 T(Z)\widetilde{P}(Z,\mathbf{x},t)\,dZ\ , \tag{1.28}$$

$$\widetilde{T''^2} = \int_0^1 (T(Z)-\widetilde{T})^2\widetilde{P}(Z,\mathbf{x},t)\,dZ\ , \tag{1.29}$$

$$-\overline{\sum_{i=1}^{n} h_i\dot{m}_i} = \bar{\rho}\widetilde{S_T} = \bar{\rho}\int_0^1 S_T(Z)\widetilde{P}(Z,\mathbf{x},t)\,dZ\ . \tag{1.30}$$

where $S_T = -\sum_{i=1}^{n} h_i\dot{m}_i/\rho$.

A further quantity of interest is the mean density $\bar{\rho}$. Here, in using Favre averages, one must consider the Favre average of ρ^{-1}, which for non-premixed combustion would be

$$\widetilde{\rho^{-1}} = \frac{1}{\bar{\rho}} = \int_0^1 \frac{1}{\rho}\widetilde{P}(Z)\,dZ\ . \tag{1.31}$$

The profiles of the reactive scalars may not only be a function of the independent variable, but also of additional parameters. An example in non-premixed combustion is the dependence on the scalar dissipation rate χ (cf. lecture 3 below). If that

parameter is assumed to be a random variable and the joint pdf (of Z and χ in this example) is assumed to be known, then the means could be obtained by integrating over both variables. This approach, however, has turned out to be impracticable in many cases. Therefore the additional parameters are usually replaced by mean values.

1.3 Turbulent Length, Time and Velocity Scales

In order to be able to estimate whether chemistry is fast or slow compared to turbulent mixing, it is useful to define laminar and turbulent time, length and velocity scales.

A given turbulent flow field may locally be characterized by the root-mean-square velocity fluctuation v' and the turbulent macroscale ℓ, yielding a turbulent time scale $\tau = \ell/v'$. If the Favre averaged turbulent kinetic energy and its dissipation are used, one may relate v' and ℓ to $\tilde{k}$ and $\tilde{\varepsilon}$ by

$$v' = (2\tilde{k}/3)^{1/2}, \quad \ell = v'^3/\tilde{\varepsilon} \; . \tag{1.32}$$

The turbulent time is then

$$\tau = \frac{\tilde{k}}{\tilde{\varepsilon}} \; . \tag{1.33}$$

In terms of the kinematic viscosity ν and $\tilde{\varepsilon}$ the Kolmogorov length, time and velocity scales are

$$\eta = \left(\frac{\nu^3}{\tilde{\varepsilon}}\right)^{1/4}, \quad t_\eta = \left(\frac{\nu}{\tilde{\varepsilon}}\right)^{1/2}, \quad v_\eta = (\nu\tilde{\varepsilon})^{1/4} \; . \tag{1.34}$$

Furthermore, for non-premixed combustion, the non-homogeneous mixture field must be considered. Fluctuations of the mixture fraction are characterized by

$$Z' = \sqrt{\widetilde{Z''^2}} \; , \tag{1.35}$$

where $\widetilde{Z''^2}$ is the Favre averaged mixture fraction variance. The time scale of the flow may be expressed by the inverse of the scalar dissipation rate at stoichiometric mixture $\widetilde{\chi}_{\mathrm{st}}$ which was already used in (1.22).

The Taylor length scale λ as an intermediate scale between the integral and the Kolmogorov scale is defined by replacing the average gradient in the definition of the dissipation by u'/λ. This leads to the definition

$$\tilde{\varepsilon} = \nu \left(\frac{\partial \widetilde{u_\alpha}}{\partial x_\beta}\right)^2 = 15\nu \frac{v'^2}{\lambda^2} \; . \tag{1.36}$$

Here the factor 15 originates from considerations for isotropic homogeneous turbulence. Using (1.34) it is seen that λ is proportional to the product of the turnover velocity of the large eddies and the Kolmogorov time

$$\lambda = (15\nu\, v'^2/\tilde{\varepsilon})^{1/2} \sim v' t_\eta \,. \tag{1.37}$$

Therefore λ may be interpreted as the distance that a large eddy convects a Kolmogorov eddy during its turnover time t_η. As a somewhat artificially defined intermediate scale it has no direct physical significance in turbulent combustion.

According to Kolmogorov's 1941 theory on the universal range of turbulence, there is a transfer from the energy containing eddies of characteristic size of the integral length scale ℓ to smaller and smaller eddies. The energy transfer per unit turnover time of the large eddies is equal to the dissipation of energy at the dissipation scale η. Therefore

$$\tilde{\varepsilon} = \frac{v'^2}{\tau} = \frac{v'^3}{\ell} \,. \tag{1.38}$$

We may define a discrete sequence of eddies within the inertial range by defining

$$\ell_n = \frac{\ell}{2^n} \geq \eta, \quad n = 1, 2, \ldots \,. \tag{1.39}$$

Since the energy transfer $\tilde{\varepsilon}$ is constant within the inertial range, dimensional analysis relates the turnover time t_n and the velocity difference v_n across the eddy ℓ_n to $\tilde{\varepsilon}$ in that range as

$$\tilde{\varepsilon} = \frac{v_n^2}{t_n} = \frac{v_n^3}{\ell_n} = \frac{\ell_n^2}{t_n^3} \,. \tag{1.40}$$

This relation includes the integral scales and also holds for the dissipation scales

$$\tilde{\varepsilon} = \frac{v_\eta^2}{t_\eta} = \frac{v_\eta^3}{\eta} \,. \tag{1.41}$$

1.4 Regimes in Premixed Turbulent Combustion

For scaling purposes it is useful to assume a Schmidt number $\mathrm{Sc} = \nu/D$ of unity and to define the flame thickness ℓ_F as the ratio of the diffusivity D and the laminar burning velocity s_L

$$\ell_F = \frac{D}{s_L} \,. \tag{1.42}$$

Then, we may define the turbulent Reynolds number

$$\mathrm{Re} = v'\ell / s_L \ell_F \tag{1.43}$$

the turbulent Damköhler number

$$\mathrm{Da}_\ell = \tau / t_F = s_L \ell / v' \ell_F \tag{1.44}$$

and the turbulent Karlovitz number

$$\mathrm{Ka} = \mathrm{Da}_\eta^{-1} = t_F / t_\eta = \ell_F^2 / \eta^2 = v_\eta^2 / s_L^2. \tag{1.45}$$

The Karlovitz number is therefore equal to the inverse of a Damköhler number defined with the Kolmogorov time scale rather than with the integral time scale. Since the interaction between chemistry and turbulence occurs at the smallest scale only, the Damköhler number defined by (1.44) has no direct physical significance as far as the interaction between turbulence and chemistry is concerned. It will be shown, however, that the condition $\mathrm{Da}_\ell = 1$ corresponds to the largest value of a mixing length scale that will be introduced below. The definitions can be used to derive the following relations between the ratios v'/s_L and ℓ/ℓ_F in terms of the two non-dimensional numbers Re and Ka as

$$\begin{aligned} v'/s_L &= \mathrm{Re}(\ell/\ell_F)^{-1} \\ &= \mathrm{Ka}^{2/3}(\ell/\ell_F)^{1/3} \, . \end{aligned} \tag{1.46}$$

In the following we will discuss a regime diagram, Fig. 1.3, for premixed turbulent combustion where the logarithm of v'/s_L is plotted over the logarithm of ℓ/ℓ_F. In this diagram, the lines $\mathrm{Re} = 1$, $\mathrm{Ka} = 1$ and $\mathrm{Ka}_\delta = 1$ represent boundaries between the different regimes of premixed turbulent combustion. Another boundary of interest is the line $v'/s_L = 1$, which separates the wrinkled and corrugated flamelets and the line denoted by $\mathrm{Ka}_\delta = 1$, which separates thin reaction zones from broken reaction zones.

The line $\mathrm{Re} = 1$ separates all turbulent flame regimes characterized by $\mathrm{Re} > 1$ from the regime of laminar flames, which is situated in the lower-left corner of the diagram. Among the remaining four regimes, the wrinkled and corrugated flames belong to the flamelet regime, which is characterized by the inequalities $\mathrm{Re} > 1$ (turbulence) and $\mathrm{Ka} < 1$ (fast chemistry). The boundary to the thin reaction zones regime is given by $\mathrm{Ka} = 1$, which, according to (1.45), is equivalent to the condition that the flame thickness is equal to the Kolmogorov scale (the Klimov-Williams criterion). However, in addition, since viscosity as a molecular transport process relates Kolmogorov velocity, length, and time scales to each other in the same way as the velocity, length, and time scales are related in a laminar flame the flame time is equal to the Kolmogorov time and the burning velocity is equal to the Kolmogorov velocity. This is also apparent from (1.45).

The thin reaction zones regime is characterized by $\mathrm{Re} > 1$, $\mathrm{Ka}_\delta < 1$ and $\mathrm{Ka} > 1$, the last inequality indicating that the smallest eddies can enter into the flame structure since $\eta < \ell_F$. The smallest eddies of size η are still larger than the inner layer thickness

$$\ell_\delta = \delta \ell_F \tag{1.47}$$

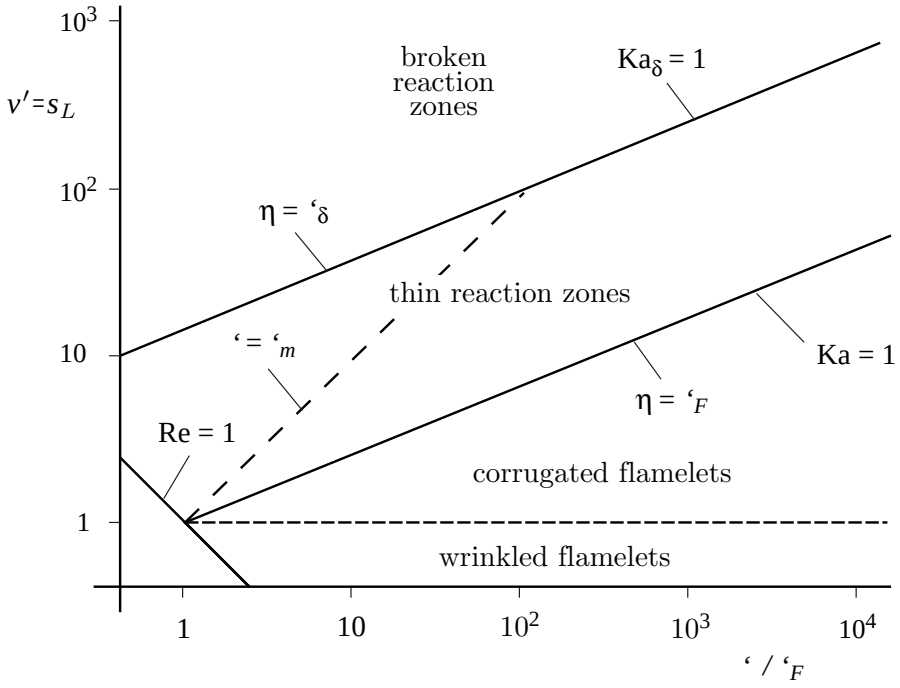

Figure 1.3: Regime diagram for premixed turbulent combustion.

and can therefore not penetrate into that layer. The non-dimensional thickness δ of the inner layer in a premixed flame is typically one tenth such that ℓ_δ is one tenth of the preheat zone thickness (cf. [1.6]), which is of the order of the flame thickness ℓ_F. We may therefore introduce a Karlovitz number based on the thickness of the inner layer

$$\mathrm{Ka}_\delta = \ell_\delta^2/\eta^2 = \delta^2 \mathrm{Ka} \; . \tag{1.48}$$

Therefore, if $\delta = 0.1$ the value $\mathrm{Ka}_\delta = 1$ corresponds to $\mathrm{Ka} = 100$.

We will now enter into a more detailed discussion of the various regimes. The flamelet regime is subdivided into the regimes of wrinkled and corrugated flamelets. In the wrinkled flamelet regime, where $v' < s_L$, v' may be interpreted as the turnover velocity of the large eddies. It follows that even those eddies cannot convolute the flame front enough to form multiple connected reaction sheets. Laminar flame propagation is dominating over turbulent flame propagation in this regime.

In the regime of corrugated flamelets there is an interaction between turbulent and laminar flame propagation. In view of (1.45), we have with $\mathrm{Ka} < 1$

$$v' \geq s_L \geq v_\eta \tag{1.49}$$

within this regime. Since the velocity of large eddies is larger than the burning velocity, these eddies will push the flame front around, causing a substantial corrugation. Conversely, the smallest eddies, having a turnover velocity less than the burning velocity, will not wrinkle the flame front.

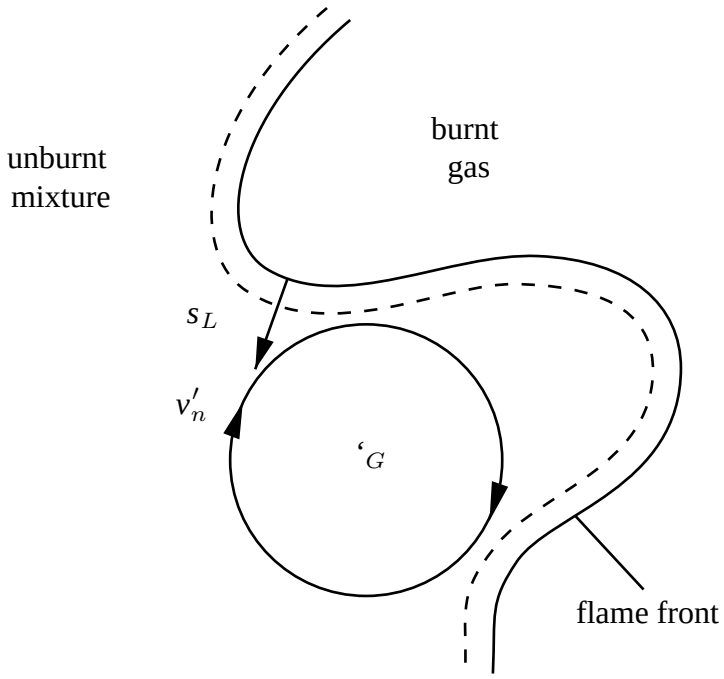

Figure 1.4: Kinematic interaction between a propagating flame front and an eddy of the size $\ell_n = \ell_G$. The dashed line marks the thickness of the preheat zone.

To determine the size of the eddy that interacts locally with the flame front, we set the turnover velocity v_n in (1.40) equal to the burning velocity s_L. This determines the Gibson scale [1.7]

$$\ell_G = s_L^3/\varepsilon \ . \tag{1.50}$$

The Gibson scale is the size of burnt pockets that move into the unburnt mixture with velocity s_L. These pockets try to grow there due to the advance of the flame front normal to itself, but are reduced in size again by newly arriving eddies of size ℓ_G with turnover velocity $v_n = s_L$. Therefore, there is kinematic equilibrium mechanism for the formation of burnt pockets, while unburnt pockets that penetrate into the burnt gas will be consumed by flame advancement. This is illustrated in Fig. 1.4. It is worth noting that ℓ_G increases with s_L if the turbulence properties are kept constant. Using $(1.32)_2$, one may also write (1.50) in the form

$$\ell_G/\ell = (s_L/v')^3 \ . \tag{1.51}$$

A graphical derivation of the Gibson scale ℓ_G within the inertial range is shown in Fig. 1.5. Here the logarithm of the velocity v_n is plotted over the logarithm of the length scale according to (1.40). We assume v' and ℓ and thereby ε, and also ν and thereby v_η and η to be fixed. If one enters on the vertical axis with the burning velocity s_L equal to v_n into the diagram, one obtains ℓ_G as the corresponding length

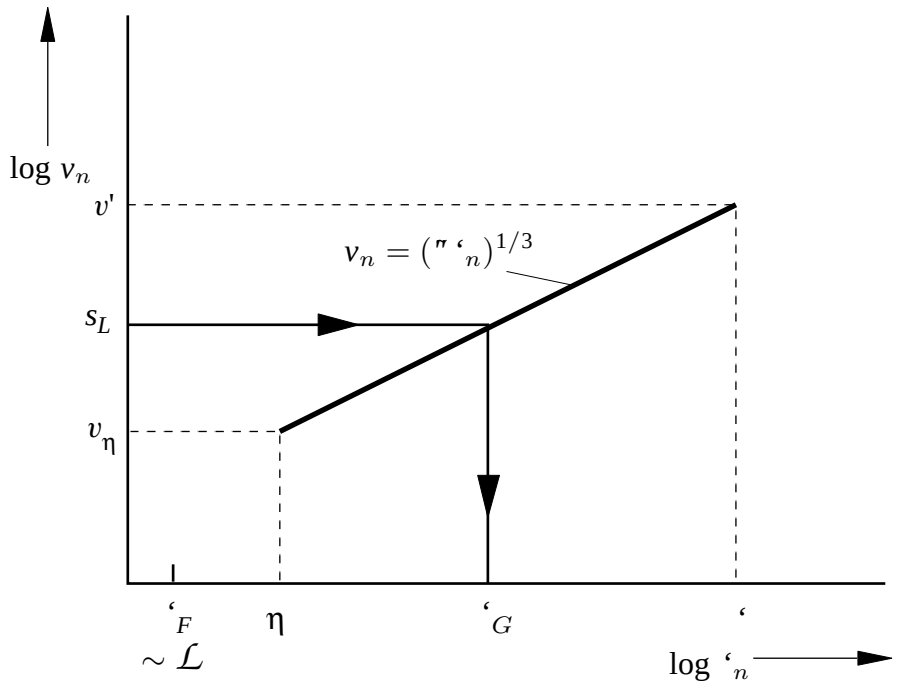

Figure 1.5: Graphical illustration of the Gibson scale ℓ_G within the inertial range.

scale on the horizontal axis. The laminar flame thickness ℓ_F, which is of the order of the Markstein length $\mathcal{L}$ (which will be defined in lecture 2) but is smaller than η in the corrugated flamelet regime is also shown. This diagram also illustrates the limiting values of ℓ_G: If the burning velocity is equal to v', ℓ_G is equal to the integral length scale ℓ. This case corresponds to the borderline between corrugated and wrinkled flamelets in Fig. 1.3. Conversely, if s_L is equal to the Kolmogorov velocity v_η, ℓ_G is equal to η. This corresponds to the line Ka $= 1$ in Fig. 1.3. Therefore, ℓ_G may vary between η and ℓ in the corrugated flamelet regime.

The next regime of interest in Fig. 1.3 is the regime of thin reaction zones. As noted earlier, since $\eta < \ell_F$, in this regime small eddies can enter into the preheat zone and increase the scalar mixing, but they cannot penetrate into the inner layer since $\eta > \ell_\delta$. The burning velocity cannot be defined as a property of the mixture anymore, but since the reaction zone also moves normal to itself due to reactive and normal diffusion, there is a displacement speed of the reaction zone which is of the same order of magnitude as the burning velocity s_L. The burning velocity is smaller than the Kolmogorov velocity in this regime which would lead to a Gibson scale that is smaller than η. Therefore the Gibson scale has no meaning in this regime. Another characteristic scale, however, can be defined since Ka > 1 and according to (1.45) the flame time is larger than the Kolmogorov time and therefore within the inertial range. For laminar flames the flame time may be defined as the

time that a flame needs to propagate across its own thickness

$$t_F = \frac{\ell_F}{s_L} \, . \tag{1.52}$$

If we use (1.42) it may also be related to the diffusivity indicating that it is the time needed for diffusion of heat or chemical species across the distance ℓ_F

$$t_F = \frac{\ell_F^2}{D} \, . \tag{1.53}$$

Then, by setting $t_F = t_n$ in (1.40), one obtains the length scale

$$\ell_m = (\tilde{\varepsilon} t_F^3)^{1/2} \, . \tag{1.54}$$

This scale may be interpreted as a mixing length scale. It is defined as the size of an eddy within the inertial range which has a turnover time equal to the time needed to diffuse heat over a distance equal to the thickness ℓ_F. During half its turnover time an eddy of size ℓ_m will interact with the advancing reaction front and will be able to transport preheated fluid from a region of thickness ℓ_F in front of the reaction zone over a distance corresponding to its own size. This is schematically shown in Fig. 1.6. Much smaller eddies will also do this but since their size is smaller, their action will be masked by eddies of size ℓ_m. Much larger eddies have a longer turn-over time and would therefore be able to transport thicker structures than those of thickness ℓ_F, namely of the thickness ℓ_m across their own width. They will therefore corrugate the broadened flame structure at scales larger than ℓ_m. The physical interpretation of ℓ_m is therefore that of the maximum distance that preheated fluid can be transported ahead of the flame.

Again, the derivation of ℓ_m is illustrated in a diagram in Fig. 1.7, showing (1.40) in a log-log plot of t_n over ℓ_n. If one enters the time axis at $t_F = t_n$, the scale ℓ_m on the length scale axis is obtained. It should be noted that all eddies having a size between η and ℓ_m have a shorter turnover time than ℓ_m and therefore are able to mix the scalar fields in front of the thin reaction zones more rapidly. If t_F is equal to the Kolmogorov time t_η, Fig. 1.7 shows that ℓ_m is equal to the Kolmogorov scale η. In this case, one obtains $\ell_m = \ell_F$ at the border between the thin reaction zones regime and the corrugated flamelet regime. Similarly, from Fig. 1.7, if the flame time t_F is equal to the integral time τ, ℓ_m is equal to the integral length scale. This corresponds to $\mathrm{Da}_\ell = 1$ which previously [1.7] was interpreted as the borderline between two regimes in turbulent combustion. Here, it turns out to merely set a limit for the mixing scale ℓ_m which cannot increase beyond the integral scale ℓ. The line $\ell_m = \ell$ is also shown in Fig. 1.3.

In Fig. 1.7 also the flame thickness ℓ_F and the Gibson scale ℓ_G are shown. The Gibson scale is smaller than the Kolmogorov scale and ℓ_F lies between η and ℓ_m. It may also be noted that, since we have assumed $\nu = D$, the Kolmogorov length is equal to the Obukhov-Corrsin scale

$$\ell_C = (D^3/\tilde{\varepsilon})^{1/4} \tag{1.55}$$

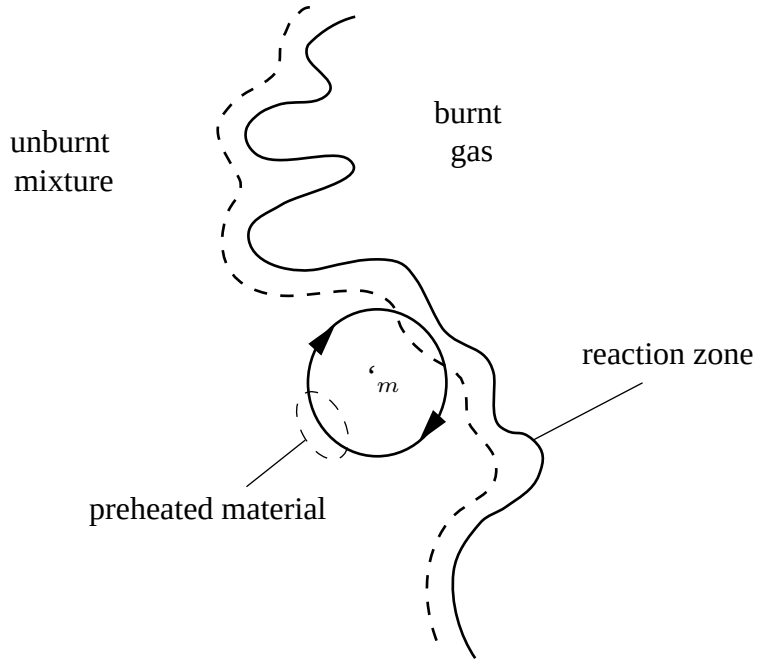

Figure 1.6: Transport of preheat gas from a region of thickness ℓ_F by an eddy of size $\ell_n = \ell_m$ during half a turnover time $t_n = t_F$.

which will be used in the next lecture.

As a final remark related to the thin reaction zones regime, it is important to realize that turbulence in real systems is not homogeneous and $\tilde{\varepsilon}$ is not a local constant but has a statistical distribution. This refinement of Kolmogorov's theory has led to the notion of intermittency, or "spottiness", of the activity of turbulence in a flow field. This may have important consequences on the physical appearance of turbulent flames at sufficiently large Reynolds numbers. One may expect that the flame front shows manifestations of strong local mixing by small eddies as well as of rather smooth regions where corrugated flamelets appear. The two regimes discussed above may well both be apparent in an experimentally observed turbulent flame.

Beyond the line $\mathrm{Ka}_\delta = 1$ there is a regime where Kolmogorov eddies are smaller than the reaction zone thickness ℓ_δ. They may therefore enter into these zones and perturb them until the reactions break down locally due to loss of radicals. This regime is called the broken reaction zones regime and corresponds to what has been called slow chemistry in the introduction.

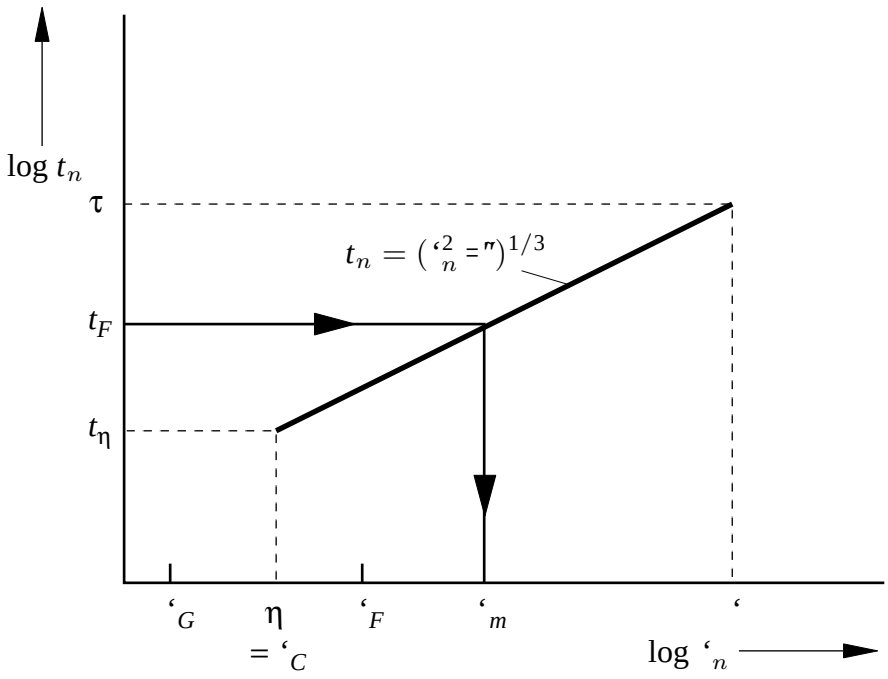

Figure 1.7: Graphical illustration of the mixing scale ℓ_m within the inertial range.

1.5 Regimes in Non-Premixed and Partially Premixed Turbulent Combustion

In order to analyze partially premixed and non-premixed turbulent combustion, it is necessary to identify the relevant quantities that influence the flame structure. In a non-homogeneous mixture field the reaction zone is attached to the high temperature region close to stoichiometric mixture and is advected and diffused with the mixture field. In contrast to premixed combustion, there is no burning velocity, which would move the combustion front relative to its previous position. There is a characteristic time scale, however, the chemical time which we relate to the inverse of the scalar dissipation rate χ_q. This value corresponds to the condition where heat loss by diffusion out of the reaction zone cannot be balanced by the heat release from the chemical reaction and therefore the flamelet is quenched. The scalar dissipation rate χ_q is an eigenvalue of the laminar diffusion flame problem similarly as s_L is an eigenvalue for the premixed laminar flame. Since it has the dimension of $\sec^{-1}$ it may be considered as the inverse of a characteristic chemical time. Since there is no physically meaningful velocity scale in diffusion flames no meaningful length scale can be defined. Because the mixture field fixes the flame position, mixture fraction space rather than physical space should be considered. Therefore one must define a flame thickness in mixture fraction space.

For a strained laminar diffusion flame, one may use the strain rate a and the

diffusion coefficient D to define a diffusion length scale

$$\ell_D = \sqrt{\frac{D}{a}} \; . \tag{1.56}$$

Here a corresponds to a velocity gradient and may be interpreted as the inverse of the characteristic flow time. The mixture fraction profile across the diffusion flame may be used to define the mixture fraction gradient normal to the reaction layer at stoichiometric mixture as $(dZ/dx_n)_{\rm st}$. Then the flame thickness in mixture fraction space may be defined as

$$(\Delta Z)_F = \left(\frac{dZ}{dx_n}\right)_{\rm st} \ell_D \; . \tag{1.57}$$

This thickness contains the diffusive layers surrounding the reaction zone and therefore corresponds to the preheat zone thickness of order $O(\ell_F)$ in premixed flames.

The instantaneous value of the scalar dissipation rate is defined as

$$\chi = 2D(\nabla Z)^2 \; . \tag{1.58}$$

Conditioning χ at $Z = Z_{\rm st}$ leads to

$$\chi_{\rm st} = 2D \left(\frac{dZ}{dx_n}\right)^2_{\rm st} \; , \tag{1.59}$$

since gradients in tangential direction on the isoline $Z = Z_{\rm st}$ are zero. Therefore one may combine (1.56), (1.57) and (1.59) to obtain

$$(\Delta Z)_F = \left(\frac{\chi_{\rm st}}{2a}\right)^{1/2} \; . \tag{1.60}$$

For strained laminar diffusion flames of hydrogen or hydrocarbon-air mixtures $Z_{\rm st}$ is small and (ΔZ_F) may be estimated as

$$(\Delta Z)_F \sim 2\, Z_{\rm st} \; . \tag{1.61}$$

In the regime diagram for partially premixed and non-premixed turbulent combustion shown in Fig. 1.8 the ratio $\widetilde{Z''^2}/(\Delta Z)_F^2$ is plotted over the time scale ratio $\chi_q/\widetilde{\chi}$. Let us consider mixture fraction fluctuations around stoichiometric mixture. For large mixture fraction variances $\widetilde{Z''^2} > (\Delta Z)_F^2$, mixture fraction fluctuations extend to sufficiently lean and rich mixtures such that the diffusion layers surrounding the reaction zones are separated. For small mixture fraction variances $\widetilde{Z''^2} < (\Delta Z)_F^2$, which may either be due to intense mixing or to partial premixing, a situation arises where diffusion layers surrounding the reaction zones are connected. Therefore the criterion $Z''^2/(\widetilde{\Delta Z})_F = 1$ distinguishes between two

regimes. If mixture fraction fluctuations are larger than $(\Delta Z)_F$ one has separated flamelets, otherwise connected flame zones.

However, when $\widetilde{\chi}_{\mathrm{st}} > \chi_q$ laminar flamelets can not exist in a diffusion flame. This corresponds to the regime denoted as flame extinction in Fig. 1.8.

Fig. 1.8 also shows schematically how local conditions on the centerline of a lifted jet diffusion flame would fit into these three regimes of non-premixed turbulent combustion. Since the flame is lifted, they would correspond to flame extinction close to the nozzle and enter into the flamelet regime at the lift-off height. Close to the flame tip where the variance has decayed to values of the order of $(\Delta Z)_F^2$ one enters into the connected flame zones regime. Since $\widetilde{Z''^2}$ decreases as x^{-2} and $\widetilde{\chi}$ as x^{-4} on the centerline in a jet flame, where x is the distance from the nozzle, local conditions follow a line with a slope $-1/2$ in the double-logarithmic plot in Fig. 1.8. When the fuel exiting from the nozzle is partially premixed the position of the centerline shown in Fig. 1.8 would shift to lower values of $\widetilde{Z''^2}/(\Delta Z)_F^2$ and therefore move more into the regime of connected flame zones.

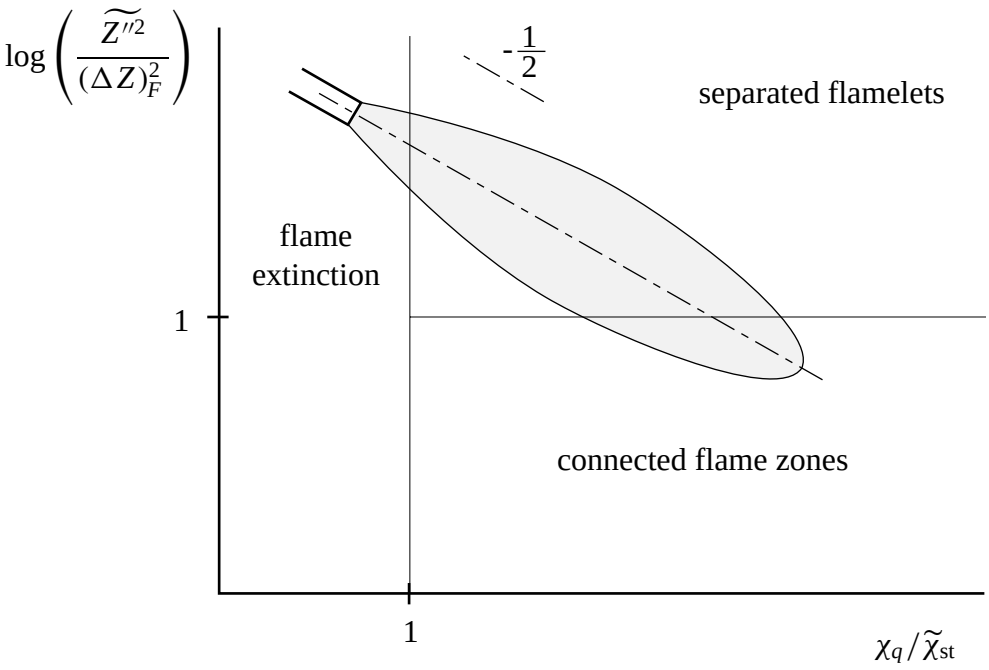

Figure 1.8: Regimes in non-premixed turbulent combustion.

Bibliography

[1.1] Jones, W. P., “Turbulence Modeling and Numerical Solution Methods for Variable Density and Combusting Flows”, in “Turbulent Reacting Flows” (P. A. Libby and F. A. Williams, Eds.) pp. 309–374, Academic Press, 1994.

[1.2] Jones, W. P., and Kakhi, M., “Mathematical Modeling of Turbulent Flames”, in “Unsteady Combustion” (F. Culick, M. V. Heitov and J. H. Whitelaw, Eds.) NATO ASI Series E, Vol 306, Kluwer Academic Publishers, 1996.

[1.3] Spalding, D. B., Thirteenth Symposium (International) on Combustion, The Combustion Institute, Pittsburgh, pp. 649–657, 1971.

[1.4] Bilger, R. W., Combust.Sci.Techn. **13**, 155–170 (1976).

[1.5] Pope, S. B., “Pdf Methods for Turbulent Reactive Flows”, Progress in Energy and Combustion Science, **11** (1985) 119–192.

[1.6] Peters, N., in “Numerical Approaches to Combustion Modeling”, (E.S. Oran, J.A. Boris, Eds.) Prog. Astronautics Aeronautics **135**, pp. 155–182, AIAA 1991.

[1.7] Peters, N., Twenty-First Symposium (International) on Combustion, pp. 1231–1256, The Combustion Institute, 1986.

Lecture 2

Premixed Turbulent Combustion

It was noted in lecture 1 that the most important application for premixed turbulent combustion are spark-ignition engines. In homogeneous charge spark-ignition engines fuel is injected into the intake manifold and mixes with the intake air. When this mixture enters into the cylinder it mixes further with the remaining burnt gas from the previous cycle during the subsequent compression. At approximately 40–20 degrees before top dead center (TDC) the mixture is nearly homogeneous. It is ignited by a spark forming at first a laminar flame kernel, which rapidly becomes turbulent. This kernel develops into a turbulent flame which grows spherically until it reaches the combustion chamber walls at the piston, the cylinder and the cylinder head. Fig. 2.1 shows Schlieren photographs of flame propagation in a dish shaped combustion chamber of a 1.6 liter transparent engine at 2000 rpm. The piston is equipped with a quartz window which allows to observe the combustion process. In this series of pictures, ignition occurred at approximately 40 degrees before TDC. At 22 degrees before TDC the flame kernel has grown to a few millimeters. It then develops further until at 14 degrees before TDC large turbulent structures become visible. The corrugated flame front is located within the bright regions where large density gradients occur. At 4 degrees before TDC there appears a dark region behind the front which corresponds to the burnt gas region. At TDC the flame has traveled across most of the visible part of the combustion chamber.

As the burnout of the charge must be completed within a crank angle range up to 40 degrees after TDC, it is clear that in spark ignition engines the turbulent burning velocity is a very important quantity that needs to be known. In this lecture we will focus on models for the turbulent burning velocity.

2.1 Experimental Devices

The most classical experiment to determine turbulent burning velocities uses the Bunsen burner. The only difference to the laminar Bunsen burner experiment is that the flow is turbulent rather than laminar. This may be achieved by running

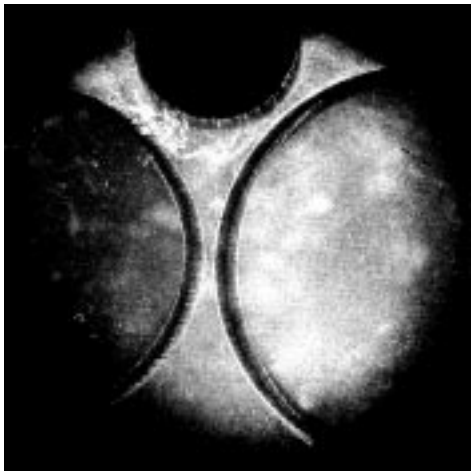

22 degrees BTDC

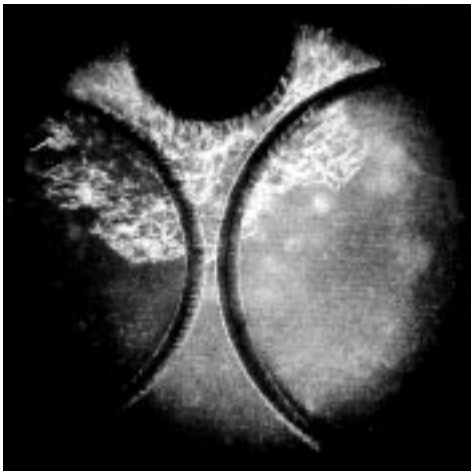

14 degrees BTDC

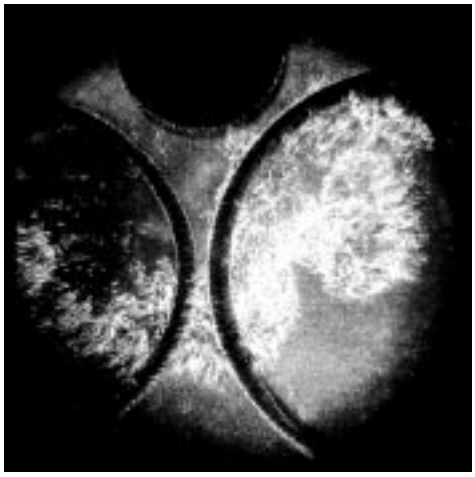

4 degrees BTDC

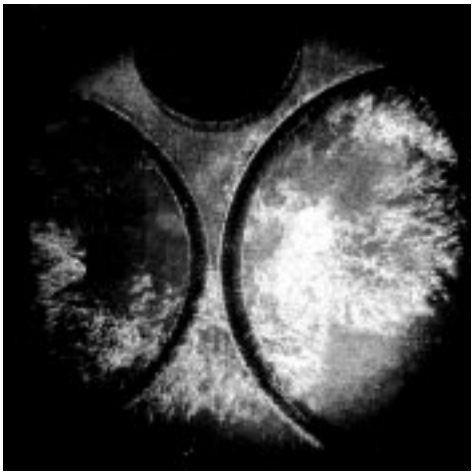

TDC

Figure 2.1: Schlieren photographs of flame propagation in a transparent engine.

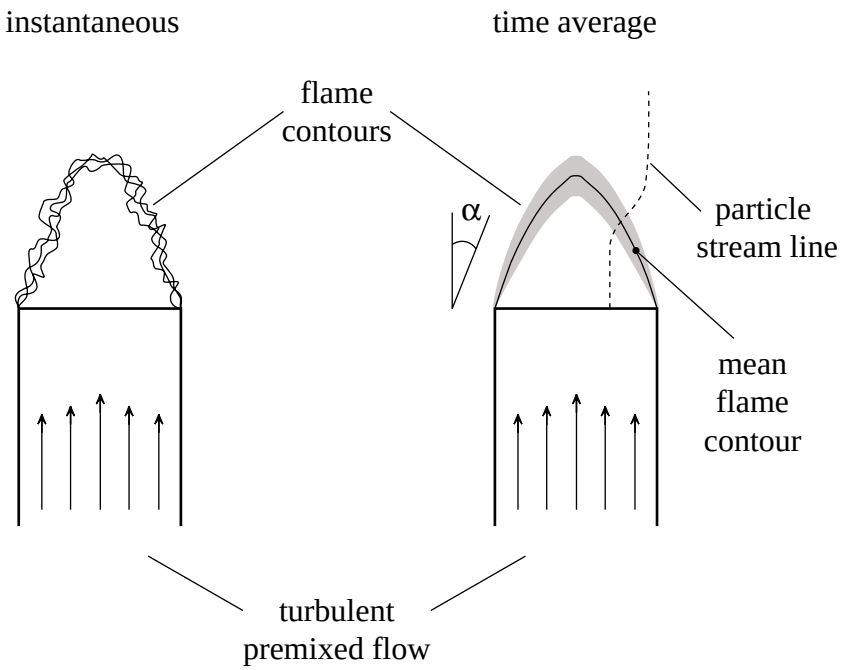

Figure 2.2: Instantaneous and time averaged Bunsen flames.

the experiment with a large enough diameter and velocity to exceed the critical Reynolds number in the pipe of the Bunsen burner or by adding a turbulence grid at the exit of the burner. The second arrangement has the advantage that the turbulence length and velocity scales may be controlled independently while in the case of a turbulent pipe flow they vary in radial direction and depend on whether the pipe flow is fully developed or not. In Fig. 2.2 the turbulent Bunsen cone is shown schematically as a collection of instantaneous flame contours and as a long-time exposure of the fluctuating flame front.

The second picture corresponds to a time-average description and shows the mean flame contour and the flame brush thickness which increases with downstream distances. Also, a mean stream line is shown. Due to thermal expansion in the flame the stream lines are deflected as in a laminar Bunsen flame. As in a laminar case the turbulent burning velocity may be determined by measuring the angle α of the mean flame contour with respect to the flow. Since this angle is not constant along the mean flame contour such a measurement provides only an estimate.

The **advantages** of the turbulent Bunsen flame experiment are the following:

- The mass flow rate through the Bunsen cone in known.
- There is an easy optical access to the flame.

The **disadvantages** are:

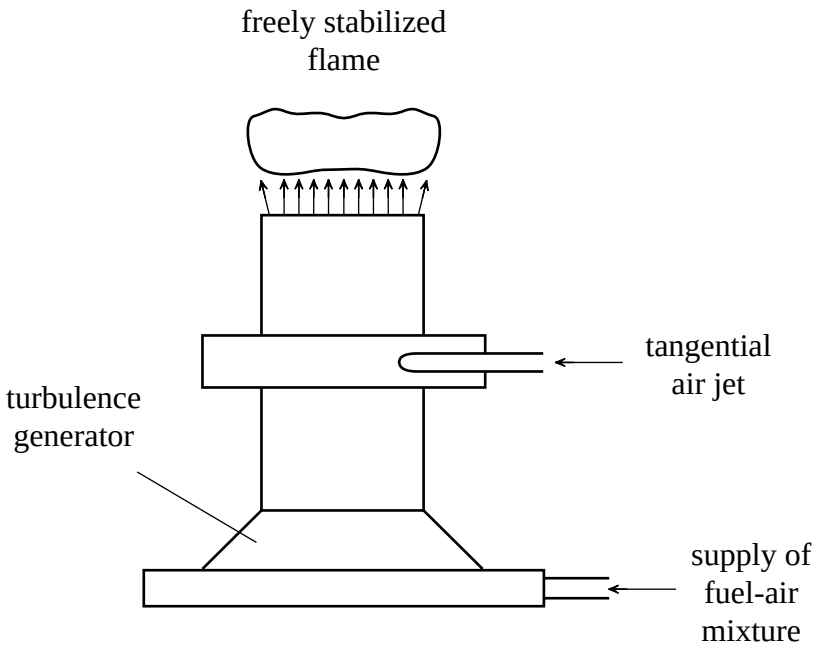

Figure 2.3: The weak swirl burner [2.1] with a freely stabilized premixed flame normal to the mean flow.

- The flow field is not uniform in the case of a fully developed pipe flow.
- Even if a turbulence grid is used within the pipe, shear layers develop outside of the tube and create non-uniformities of the flow.
- The mixing with the surrounding air will dilute the fuel-air mixture and generate mixture fraction non-uniformities.

In order to avoid the influence of non-homogeneities in studying turbulent burning velocities, it is useful to consider flames generated by a weak swirl burner [2.1]. Such a device is shown schematically in Fig. 2.3. It consists, as the Bunsen flame, of a flame tube which in addition to the main premixed flow has four tangential air inlets that generate a circumferential velocity component. This velocity component, however, is restricted only to a small portion of the outlet flow at the perimeter of the premixture close to the burner rim but leaves the center core flow undisturbed. The weak swirl generates a slightly diverging flow that stabilizes the premixed downward propagating flame at the vertical position where the mean flow velocity equals the turbulent burning velocity.

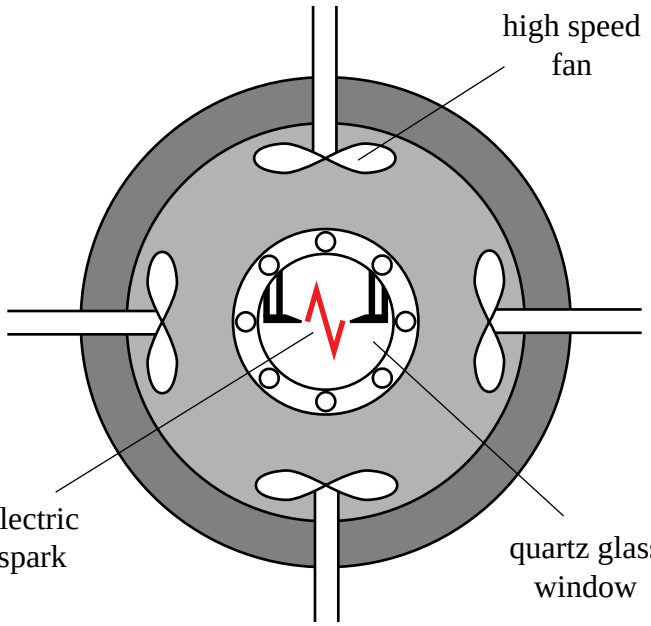

Figure 2.4: A fan-stirred combustion bomb for premixed turbulent combustion studies.

The **advantages** of the weak swirl flame experiment are:

- It is possible to generate a freely stabilized flame which has a one-dimensional steady structure in the mean.
- There is an easy optical access to the flame.

The **disadvantage** is:

- The mass flow rate through the flame is not known.

Since the main application of premixed turbulent combustion is in engines, it is important to study also unsteady flames. An isotropic turbulence field may, for instance, be established in a fan-stirred combustion bomb [2.21] shown in Fig. 2.4.

Such a device has been used extensively by D. Bradley and co-workers (cf. [2.3]). Four mutually opposed high speed fans create a nearly isotropic homogeneous turbulence field with a low mean velocity in the center region of the bomb. One or two flame kernels are initiated by electrical sparks and propagate either radially outwards or towards each other. They can be observed through quartz glass windows. Another device for measuring unsteady flame propagation is the single stroke compression machine with a square piston and a turbulence grid that is pulled through the combustion chamber before ignition. Such a configuration was used by Adomeit and co-workers [2.4].

During the flame kernel development the instantaneous flame front interacts with all sizes of turbulent eddies. Therefore, there is a time period during the early flame kernel development, where the interaction of the flame with the turbulent flow field is not fully established. An estimate of this time period will be given below.

The **advantage** of these configurations is the following:

- A nearly isotropic homogeneous turbulence field with high turbulence intensity is established.

The **disadvantages** are:

- The experiment is unsteady and the early flame development must be taken into account.
- The optical access through quartz glass windows is more difficult than in open flames.

2.2 Scaling Laws for the Turbulent Burning Velocity

Damköhler [2.5] was the first to present theoretical expressions for the turbulent burning velocity. He identified two different regimes which he called large scale and small scale turbulence, respectively. For large scale turbulence he assumed that the interaction between a wrinkled flame front and the turbulent flow field is purely kinematic and therefore independent of length scales. This corresponds to the corrugated flamelet regime that has been discussed in lecture 1. In the limit of a large ratio of the rms turbulent velocity v' to the laminar burning velocity s_L the turbulent burning velocity s_T is then proportional to v'

$$s_T \sim v' \quad \text{for} \quad v' >> s_L \ . \tag{2.1}$$

In order to derive this result consider a steady turbulent flow with constant mean velocity $\bar{v}$ and uniform turbulence properties characterized by the turbulent intensity v' and the integral length scale ℓ. Then a plane turbulent flame should propagate in opposite direction to the flow. A steady flame is obtained if the turbulent burning velocity s_T is equal to the turbulent mean flow velocity $\overline{v}$

$$s_T = \overline{v} \ . \tag{2.2}$$

This idealized one-dimensional steady flame as shown is very difficult to realize experimentally. If one reduces, for example, the flow velocity in a Bunsen flame the cone angle increases but the flame propagates into the tube rather than stabilizing at the exit of the burner when the mean velocity is equal to the burning velocity.

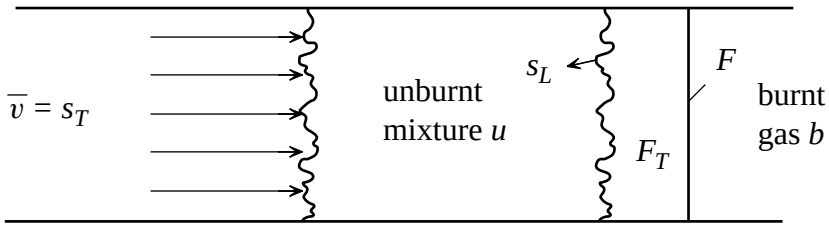

Figure 2.5: An idealized steady premixed flame in a duct with constant flow velocity.

This is due to inhomogeneities in the turbulent flow and the very dynamic response of the flame thereon. Therefore a plane turbulent flame can only be established if additional measures are taken to stabilize it. These will be discussed below, when flames in a divergent or swirling flow are discussed.

The definition of a turbulent burning velocity goes back to Damköhler who also introduced the concept of an instantaneous wrinkled turbulent flame surface, which for constant turbulence and combustion properties should have reached statistically a steady state. He equated the mass flux $\dot{m}$ of unburnt gas with the laminar burning velocity s_L through the turbulent flame surface area F_T to the mass flux through the cross sectional area F with the turbulent burning velocity s_T (cf. Fig. 2.5)

$$\dot{m} = \rho_u \, s_L \, F_T = \rho_u \, s_T \, F \; . \tag{2.3}$$

Here ρ_u is the density of the unburnt mixture. The burning velocities s_L and s_T are also defined with respect to the conditions in the unburnt mixture. This leads to

$$\frac{s_T}{s_L} = \frac{F_T}{F} \; . \tag{2.4}$$

Using the geometrical analogy with a Bunsen flame, Damköhler assumed that the area increase of the wrinkled flame surface area relative to the cross sectional area is proportional to the increase of flow velocity over the laminar burning velocity

$$\frac{F_T}{F} = \frac{s_L + v'}{s_L} \; . \tag{2.5}$$

Here v' is the velocity increase which finally is identified as the turbulence intensity v'. Combining (2.4) and (2.5) leads to

$$\frac{s_T}{s_L} = 1 + \frac{v'}{s_L} \tag{2.6}$$

or in the limit $v' \gg s_L$ to the law given by (2.1). It states that in the case of large scale turbulence the turbulent burning velocity should be independent of any laminar velocity, length and time scale of combustion. Therefore chemistry should not affect the process of turbulent flame propagation.

For small scale turbulence Damköhler argued that turbulence modifies the transport between the reaction zone and what he called the "preparation zone". He used the scaling relation for the laminar burning velocity

$$s_L \sim \sqrt{D/t_c} \tag{2.7}$$

where t_c is the chemical time scale and replaced the laminar diffusivity D by a turbulent diffusivity D_t to obtain

$$s_T \sim \sqrt{D_t/t_c} \tag{2.8}$$

and therefore the ratio

$$\frac{s_T}{s_L} = \sqrt{\frac{D_t}{D}} \tag{2.9}$$

where it is implicitly assumed that the chemical time scale is not affected by turbulence. Since the turbulent diffusivity is proportional to the product $v'\ell$ and the laminar diffusivity is proportional to the product of the laminar burning velocity s_L and the flame thickness ℓ_F (cf. (1.42)) one may write (2.9) as

$$\frac{s_T}{s_L} \sim \sqrt{\frac{v'}{s_L}\frac{\ell}{\ell_F}} \tag{2.10}$$

showing that in the small scale turbulence regime the ratio of the turbulent to the laminar burning velocity not only depends on the velocity ratio v'/s_L but also on the length scale ratio ℓ/ℓ_F.

There were many attempts to modify Damköhler's analysis and to derive expressions that would reproduce the large amount of experiment data on turbulent burning velocities. Expressions of the form

$$\frac{s_T}{s_L} = 1 + C\left(\frac{v'}{s_L}\right)^n \tag{2.11}$$

have been proposed that contain (2.1) and (2.10) as limiting cases. When the ratio s_T/s_L is plotted as a function of v'/s_L which is called the turbulent velocity diagram, the exponent is found to be in the vicinity of 0.7 or 0.75 [2.6]. Attempts to justify a single exponent on the basis of dimensional analysis, however, fall short even of Damköhler's pioneering work who had recognized the existence of two different regimes in premixed turbulent combustion.

The deviation from the straight line of the large scale turbulence limit is called the bending of the turbulent burning velocity. In Fig. 2.6 two empirical approximations are plotted in the turbulent velocity diagram for a length scale ratio of $\ell/\ell_F = 50$ showing the bending effect. The reason for this bending is not fully understood. This is often considered to be the most important unresolved problem in premixed turbulent combustion. We will discuss this question in the context of combustion regimes that were presented in Fig. 1.3. It will be shown below that Damköhler's case of large scale turbulence falls into the corrugated flamelet regime while his small scale turbulence case falls into the thin reaction zones regime.

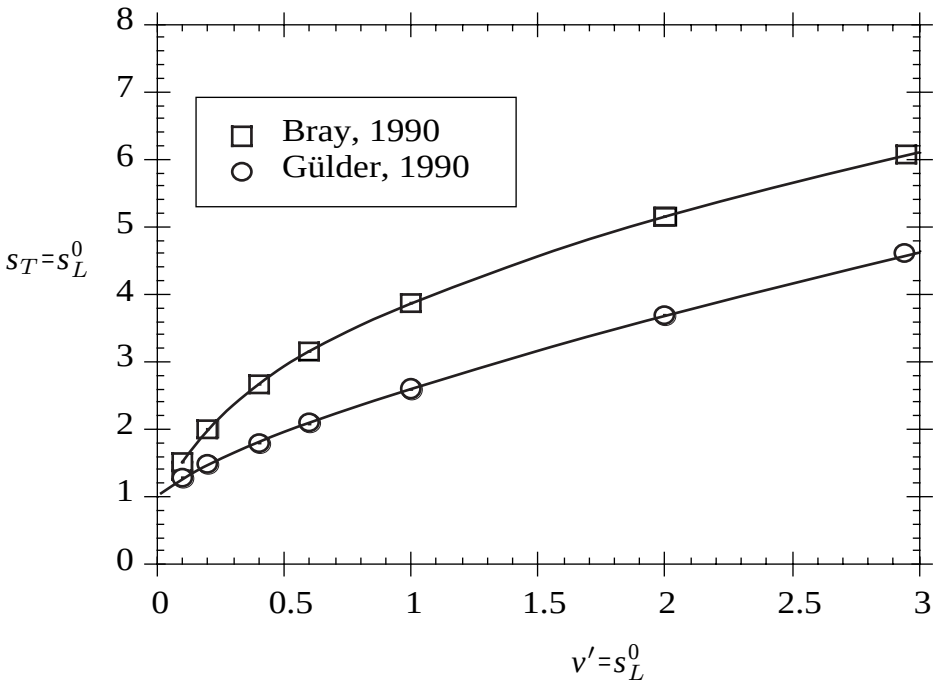

Figure 2.6: Comparison of different correlations for the ratio of the turbulent and the laminar burning velocity as a function of v'/s_L^0 for $\ell/\ell_F = 50$.

2.3 The Bray-Moss-Libby Model

This widely used concept in premixed turbulent combustion (cf. [2.7], [2.8]) assumes that chemical reactions are localized in a thin surface which may be represented as a sheet separating unburnt mixture from burnt gas. This approximation clearly places the BML model within the flamelet regime in Fig. 1.3. The formulation is based on introducing a progress variable which, by definition is $c = 0$ in the unburnt mixture and $c = 1$ in the burnt gas. The progress variable can be interpreted in the context of a one-step reaction either as a non-dimensional temperature

$$c = \frac{T - T_u}{T_b - T_u} \tag{2.12}$$

or as a non-dimensional product mass fraction. This interpretation is somewhat misleading, since the basic assumption of the model states that reaction is infinitely thin and no intermediate values of temperature between T_u and T_b can be resolved. The progress variable is better interpreted as a step function that separates unburnt mixture and burnt gas in a given flow field. It is therefore related to the spatial structure of the flame front and its statistics rather than to a reacting scalar such as the temperature or the reactants and products. This property of c becomes more

evident when the pdf of c at a given location $\mathbf{x}$ is considered. It is introduced as

$$P(c,\mathbf{x}) = \alpha(\mathbf{x})\delta(c) + \beta(\mathbf{x})\delta(1-c) + \gamma(\mathbf{x})\, f(c,\mathbf{x}) \tag{2.13}$$

where α, β and γ are the probabilities of finding unburnt, fully burnt and burning mixture, respectively, at location $\mathbf{x}$, δ is the Dirac function and $f(c,\mathbf{x})$ is the pdf of finding values between $c = 0$ and $c = 1$. Due to the basic assumption of an infinitely thin sheet the limit $\gamma = 0$ is taken which leads to a two-delta function description of the pdf with

$$\alpha(\mathbf{x}) + \beta(\mathbf{x}) = 1\ . \tag{2.14}$$

Here $\alpha(\mathbf{x})$ corresponds to the probability of finding unburnt mixture, $\beta(\mathbf{x})$ to that of finding burnt gas at the location $\mathbf{x}$. Then the mean progress variable is calculated as

$$\overline{c} = \int_0^1 c\, P(c,\mathbf{x}) dc = \beta(\mathbf{x}) \tag{2.15}$$

indicating $\overline{c}(\mathbf{x})$ is nothing else than the probability of finding burnt gas at location $\mathbf{x}$.

Assuming constant pressure and a constant mean molecular weight the density ratio is inversely proportional to the temperature ratio. Then, using (2.12) one may also express the density as a function of the progress variable

$$\frac{\rho}{\rho_u} = \frac{T_u}{T} = \frac{1}{1+\tau c} \tag{2.16}$$

where $\tau = (T_b - T_u)/T_u$. Then the ratio of the mean density to ρ_u can be calculated from the pdf by taking only the entries at $c = 0$ and $c = 1$ into account

$$\frac{\overline{\rho}(\mathbf{x})}{\rho_u} = \int_0^1 \rho\, P(c) dc = \alpha(\mathbf{x}) + \frac{\beta(\mathbf{x})}{1+\tau} = 1 - \beta(\mathbf{x}) + \frac{\beta(\mathbf{x})}{1+\tau} \tag{2.17}$$

where (2.14) has been used. The Favre averaged progress variable $\tilde{c}$ may be obtained by using its definition as

$$\tilde{c}(\mathbf{x}) \equiv \frac{\overline{\rho c}}{\bar{\rho}} = \frac{\rho_u}{\bar{\rho}} \int_0^1 \frac{c}{1+\tau c}\, P(c) dc = \frac{\rho_u}{\bar{\rho}}\, \frac{\beta(\mathbf{x})}{1+\tau}\ . \tag{2.18}$$

Combining (2.17) and (2.18) one may express $\beta(\mathbf{x})$ and therefore $\overline{c}(\mathbf{x})$ as a function of $\tilde{c}(\mathbf{x})$

$$\overline{c}(\mathbf{x}) = \beta(\mathbf{x}) = \frac{(1+\tau)\tilde{c}(\mathbf{x})}{1+\tau\tilde{c}(\mathbf{x})}\ . \tag{2.19}$$

This also yields a simple expression for the density ratio in terms of $\tilde{c}$

$$\frac{\bar{\rho}(\mathbf{x})}{\rho_u} = \frac{1}{1+\tau\tilde{c}(\mathbf{x})} \tag{2.20}$$

which shows an interesting analogy to (2.16).

The BML model has been extended to express higher moments of the progress variable and also correlations between the velocity and the progress variable in terms of mean quantities. These results illustrate the consequences of the bi-modal form of the pdf in (2.13) but they unfortunately do not lead to a closure of the unknown terms in the balance equations.

2.4 The Level-Set Approach for the Kinematic G-Equation

If chemistry is sufficiently fast it occurs in layers that are thin compared to the length scales of the flow. All the chemistry is then confined to these thin layers and the chemical source term in the equations for the reacting scalars could be represented by a delta function rather than a continuous smooth function in physical space. In order to circumvent the difficulty of modelling series of delta functions, it is useful to formulate the problem of premixed turbulent combustion in terms of a field equation that does not explicitly contain a chemical source term. Such an equation may be derived from a kinematic balance between the flow velocity $\mathbf{v}$, the burning velocity normal to the front $s_L\mathbf{n}$ and the resulting propagation velocity $d\mathbf{x}/dt$ of the front

$$\frac{d\mathbf{x}}{dt} = \mathbf{v} + \mathbf{n}\, s_L \tag{2.21}$$

Bby defining the normal vector as

$$\mathbf{n} = -\frac{\nabla G}{|\nabla G|} \tag{2.22}$$

and considering an arbitrary iso-scalar surface

$$G(\mathbf{x}, t) = G_0\ . \tag{2.23}$$

This surface divides the flow field into two regions where $G > G_0$ is the region of burnt gas and $G < G_0$ that of the unburnt mixture (Fig. 2.7). This is called the level-set approach. If one differentiates (2.23) with respect to t

$$\frac{dG}{dt} + \nabla G \cdot \frac{d\mathbf{x}}{dt}\Big|_{G=G_0} = 0 \tag{2.24}$$

and introduces (2.21) one obtains

$$\frac{dG}{dt} + \mathbf{v} \cdot \nabla G = s_L |\nabla G| \tag{2.25}$$

which will be called kinematic G-equation in the following. It contains a local and a convective term on the l.h.s, the Eikonal term with the burning velocity s_L on the

r.h.s but no diffusion term. It is valid in the corrugated flamelet regime where the flame thickness is smaller than the Kolmogorov scale. Although G represents an arbitrary scalar, it is convenient to interpret it as the distance from the flame front by imposing the condition $|\nabla G| = 1$ for $G \neq G_0$ numerically. This numerical procedure is called re-initialization [2.9]. Then G has the dimension of a length. It will be called the distance function in the following. This use of the level-set approach is by no means compulsory. In fact (2.25) also satisfies any variable that is a unique function of G. This is immediately evident for a linear function $\hat{G} = aG + b$, but also, for example, for the progress variable $c(G)$. If we define

$$c = H(G - G_0) = \begin{cases} 0, & \text{for } G < G_0 \\ 1, & \text{for } G > G_0 \end{cases} \tag{2.26}$$

where H is the Heaviside function, the derivative of c is

$$dc = \delta(G - G_0)\, dG \tag{2.27}$$

and therefore the normal vector is also

$$\mathbf{n} = -\frac{\nabla c}{|\nabla c|} \,. \tag{2.28}$$

Introducing (2.27) into (2.25) leads to

$$\frac{dc}{dt} + \mathbf{v} \cdot \nabla c = s_L |\nabla c| \tag{2.29}$$

since the delta function cancels.

The burning velocity s_L appearing in (2.25) is defined with respect to the unburnt mixture. It may be modified to account for the effect of flame curvature and flame strain. In asymptotic analyses employing the limit of a large ratio of the fluid dynamic length scale to the flame thickness resulting in a quasi-steady structure of the preheat zone, first order corrections to the burning velocity due to curvature κ and straining of the flame may be derived [2.10]–[2.12] yielding

$$s_L = s_L^0 - s_L^0 \mathcal{L} \kappa + \mathcal{L} \mathbf{n} \cdot \nabla \mathbf{v} \cdot \mathbf{n} \,. \tag{2.30}$$

Here s_L^0 is the burning velocity of the unstretched flame and $\mathcal{L}$ is the Markstein length. The ratio of the Markstein length to the flame thickness is called the Markstein number and depends on the density ratio between the burnt and the unburnt gas, the Lewis number and the Zeldovich number. For the case of a one-step large activation energy reaction and a constant thermal conductivity, dynamic viscosity and heat capacity c_p, the ratio of $\mathcal{L}$ to the flame thickness ℓ_F is

$$\frac{\mathcal{L}}{\ell_F} = \frac{1}{\gamma} \ln \frac{1}{1-\gamma} + \frac{\mathrm{Ze}(\mathrm{Le} - 1)}{2} \frac{(1-\gamma)}{\gamma} \int_0^{\gamma/(1-\gamma)} \frac{\ln(1+x)}{x}\, dx \,. \tag{2.31}$$

This expression was first derived by Clavin and Williams [2.13]. Here $\gamma = (T_b - T_u)/T_b$ where T_b and T_u are the temperatures in the burnt and the unburnt gas, respectively, $\mathrm{Ze} = E(T_b - T_u)/\mathrm{R}T_b^2$ is the Zeldovich number, where E is the activation energy and R the universal gas constant, and $\mathrm{Le} = \lambda/\rho\, c_p\, D$ is the Lewis number of the reactant.

The flame curvature κ in (2.30) is defined as

$$\kappa = \nabla \cdot \mathbf{n} = \nabla \cdot \left(-\frac{\nabla G}{|\nabla G|} \right) = -\frac{\nabla^2 G - \mathbf{n} \cdot \nabla(\mathbf{n} \cdot \nabla G)}{|\nabla G|} \; . \tag{2.32}$$

If (2.30) is introduced into (2.25) the kinematic G-equation may be written as

$$\frac{\partial G}{\partial t} + \mathbf{v} \cdot \nabla G = s_L^0 \sigma - D_{\mathcal{L}}\, \kappa \sigma + \mathcal{L}\, \mathbf{n} \cdot \nabla \mathbf{v} \cdot \mathbf{n} \sigma \; , \tag{2.33}$$

where $D_{\mathcal{L}} = s_L^0 \mathcal{L}$ is the Markstein diffusivity and

$$\sigma = |\nabla G| \tag{2.34}$$

is the absolute value of the gradient of the distance function G.

The curvature term adds a second order derivative to the kinematic G-equation. This avoids the formation of cusps and non-unique solutions that would result from (2.25) with a constant value of s_L. The mathematical nature of (2.33) is that of a Hamilton-Jacobi equation with a parabolic second order differential operator coming from the curvature term. It is easily shown that the progress variable also satisfies (2.33).

The properties of the G-equation for turbulent flow fields have been investigated in a number of papers. In particular, Kerstein et al. [2.14] have performed direct numerical simulations for the constant density (passive) G-equation in a cubic box and have shown that for larger times the mean absolute gradient of G may be interpreted as the total flame surface density of the front equal to the ratio of the turbulent to the laminar burning velocity

$$\bar{\sigma} = \overline{|\nabla G|} = \frac{s_T}{s_L} \; . \tag{2.35}$$

In view of (2.4) this may also be interpreted as the ratio of the turbulent flame surface area F_t to the cross sectional area F.

In [2.15] Reynolds-averaged equations for the mean $\overline{G}$ and the variance $\overline{G'^2}$ have been derived. A constant density was assumed and G, σ and the velocity component v_α were split into a mean and a fluctuation

$$G = \overline{G} + G' \; , \quad \sigma = \bar{\sigma} + \sigma' \; , \quad v_\alpha = \overline{v_\alpha} + v'_\alpha \; . \tag{2.36}$$

The equation for the mean $\overline{G}$ is simply

$$\frac{\partial \overline{G}}{\partial t} + \overline{\mathbf{v}} \cdot \nabla \overline{G} + \nabla \cdot \overline{\mathbf{v}' G'} = s_L^0 \bar{\sigma} - D_{\mathcal{L}}\, \overline{\kappa \sigma} + \mathcal{L}\, \overline{\mathbf{n} \cdot \nabla \mathbf{v} \cdot \mathbf{n}\, \sigma} \; . \tag{2.37}$$

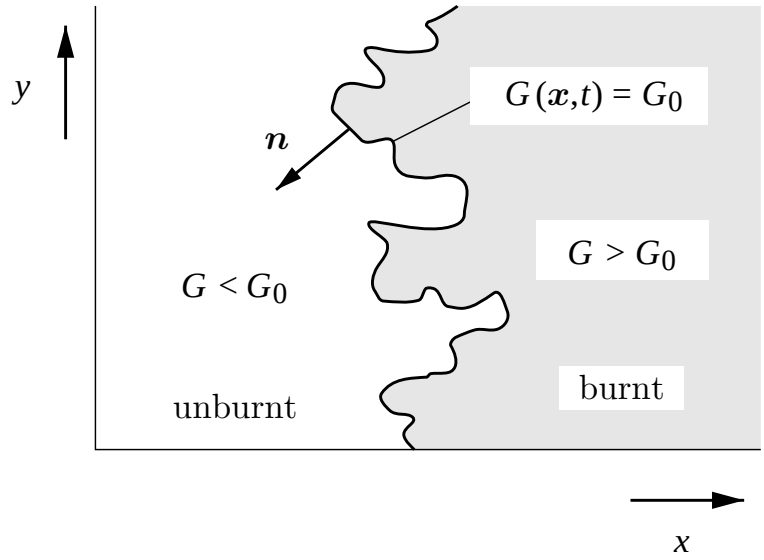

Figure 2.7: A schematic representation of the flame front as an iso-scalar surface of $G(\mathbf{x}, t)$.

The condition $\overline{G} = G_0$ now defines the location of the mean flame front, while the variance $\overline{G'^2}$ accounts for flame front fluctuations and thereby is a measure of the flame brush thickness. An equation for $\overline{G'^2}$ may be derived by subtracting (2.37) from (2.33) to obtain an equation for G'. After multiplying this by $2G'$ and averaging one obtains the equation

$$\frac{\partial \overline{G'^2}}{\partial t} + \mathbf{v} \cdot \nabla \overline{G'^2} + \nabla \cdot (\overline{\mathbf{v}' G'^2}) = -2\overline{\mathbf{v}' G'} \cdot \nabla \overline{G} - \overline{\omega} - \overline{\chi}_{\mathcal{L}} - \overline{\Sigma}_{\mathcal{L}} \,. \tag{2.38}$$

Here, the local and convection term and the turbulent transport term on the l.h.s as well as the production term $2\,\overline{\mathbf{v}' G'} \cdot \nabla \overline{G}$ on the r.h.s result from local and convective terms in (2.33). The second term on the r.h.s of (2.38) results from the Eikonal term $s_L^0 \sigma$ in (2.33) and is defined as

$$\overline{\omega} = -2\, s_L^0 \overline{\sigma' G'} \,. \tag{2.39}$$

This term was called kinematic restoration in order to emphasize the kinematic effect of local laminar flame propagation. It accounts for the smoothing effect of the G-field and thereby the flame surface by flame advancement with the laminar burning velocity. Flame front corrugations produced by turbulence are restored by this kinematic effect. The third term on the r.h.s of (2.38) results from the second term on the r.h.s in (2.33) and is defined as

$$\overline{\chi}_{\mathcal{L}} = 2\, D_{\mathcal{L}} \overline{G' \kappa \sigma} \,. \tag{2.40}$$

Since it contains the Markstein diffusivity it is called the Markstein dissipation. The last term in (2.38) results from the last term in (2.33) and is called the scalar-strain

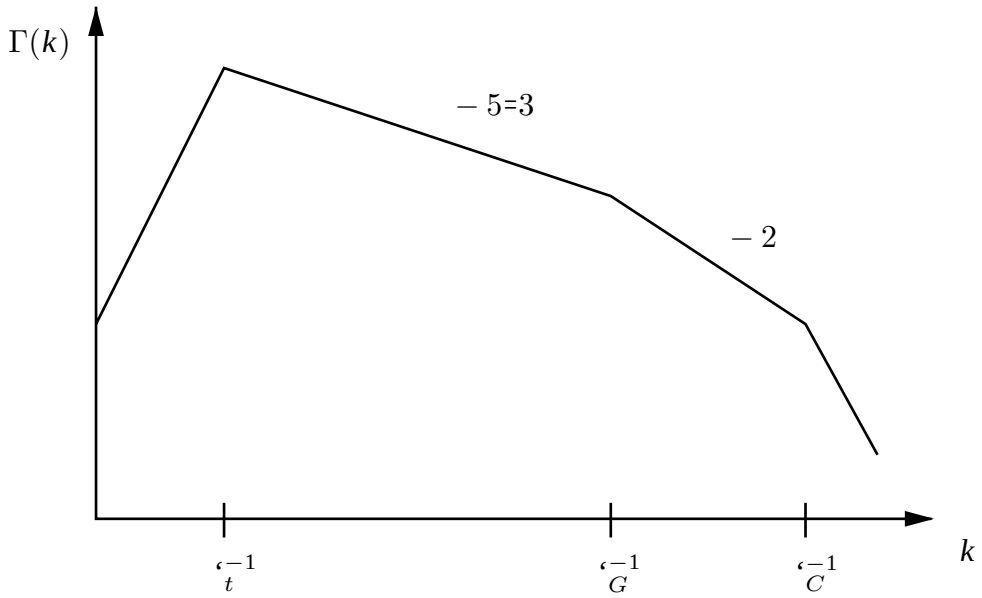

Figure 2.8: Double logarithmic plot of the scalar spectrum Γ as a function of the wave number k.

co-variance

$$\overline{\Sigma}_{\mathcal{L}} = -2\mathcal{L}\overline{G'\mathbf{n}\cdot\nabla\mathbf{v}\cdot\mathbf{n}\sigma} \ . \tag{2.41}$$

2.5 Closure of the Kinematic G-Equation

The kinematic restoration $\overline{\omega}$ is the most important destruction term in (2.38). It counterbalances the production term and thereby limits the variance and therefore flame front fluctuations in the corrugated flamelet regime. In [2.15] a closure of this term was achieved by deriving a scalar spectrum function for two-point correlations of G.

The scalar spectrum function is schematically shown in Fig. 2.8. It contains an inertial range with slope -5/3 between the integral length scale and the Gibson scale ℓ_G and a range with slope -2 between the Gibson scale and the Obukhov-Corrsin scale ℓ_C.

In [2.15] it was shown that kinematic restoration is active at the Gibson scale

$$\ell_G = \frac{s_L^0}{\tilde{\varepsilon}} \tag{2.42}$$

since ℓ_G represents the first cut-off from the inertial range in the scalar spectrum function and therefore is responsible for removing scalar fluctuations. It was already shown in Fig. 1.5 that in the corrugated flamelet regime the Gibson scale is larger than the Obukhov-Corrsin scale ℓ_C and the Markstein length $\mathcal{L}$. From the

analysis in [2.15] results an expression which relates $\overline{\omega}$ to the variance $\overline{G'^2}$ and the turbulent time $\tau = \bar{k}/\bar{\varepsilon}$

$$\overline{\omega} = c_\omega \frac{\bar{\varepsilon}}{\bar{k}} \overline{G'^2} \tag{2.43}$$

with $c_\omega = 1.62$. This expression shows that the kinematic restoration plays a similar role for fluctuations of the flame front as the scalar dissipation plays for concentration fluctuations of diffusive scalars.

The scalar dissipation is active at the Obukhov-Corrsin scale and the scalar-strain co-variance is active at the Markstein length which is of the order of the flame thickness. Therefore both are smaller than the kinematic restoration in the corrugated flamelet regime. While $\overline{\Sigma}_\mathcal{L}$ can probably be neglected in all practical applications, $\overline{\chi}_\mathcal{L}$ should be included for cases close to the Klimov-Williams line Ka $= 1$ in Fig. 1.4 where ℓ_G approaches η.

In order to derive a more consistent closure formulation we may split the product $G'\kappa\sigma$ that appears in (2.40) into two terms

$$2\,G'\kappa\sigma = -\nabla\cdot\left(2\frac{G'\nabla G}{|\nabla G|}\right) + 2\nabla G'\nabla G\ . \tag{2.44}$$

After averaging one may replace products like $\overline{G\,G'}$ and $\overline{\nabla G'\nabla G}$ by $\overline{G'^2}$ and $\overline{\nabla G'\nabla G'}$, respectively, such that

$$-\overline{2G'\kappa\sigma} = -\overline{\kappa''} - 2\overline{\nabla G'\nabla G'} \tag{2.45}$$

where κ'' is a curvature-like term defined by

$$\kappa'' = \nabla\cdot\left(-\frac{\nabla G'^2}{|\nabla G|}\right)\ . \tag{2.46}$$

The last term in (2.45) contains the product of scalar gradients. If G was a diffusive scalar, the product $2\,D\overline{\sigma'^2}$ would be modelled in a similar way as $\overline{\omega}$ in (2.43). This will be shown for the thin reaction zones regime where this term will be the most important destruction term that limits reaction zone fluctuations. In [2.16] an approximation for the sum of both destruction terms is derived which is valid in both the corrugated flamelet regime and the thin reaction zones regime

$$\overline{\omega} + \overline{\chi}_\mathcal{L} = c_s\frac{\bar{\varepsilon}}{\bar{k}}\overline{G'^2} \tag{2.47}$$

where $c_s = 2.0$.

The last terms on the l.h.s of (2.37) and (2.38) are turbulent transport terms that also need to be modelled. A classical gradient transport approximation cannot be used for these terms, because this would lead to elliptic equations for $\overline{G}$ and $\overline{G'^2}$. If one wants to obtain an equation for $\overline{G}$ that is consistent with the parabolic form of the equation for G the term $\nabla\cdot\overline{\mathbf{v}'G''^2}$ in (2.38) should be modelled as a

curvature term. In fact, a transformation similar to (2.32) shows that the second order elliptic operator, that would result from a gradient flux approximation, can be split into a second order normal derivative and a curvature term

$$\nabla(D_t \nabla \overline{G}) = \mathbf{n} \cdot \nabla(D_t \mathbf{n} \cdot \nabla \overline{G}) - D_t \bar{\kappa}(\overline{G}) |\nabla \overline{G}| \ . \tag{2.48}$$

Here D_t is the turbulent diffusivity and $\bar{\kappa}(\overline{G})$ is defined as in (2.32) but with $\overline{G}$ instead of G. Since diffusion normal to the G-isoline is not present in the instantaneous G-equation, it cannot appear in the equation for $\overline{G}$. In a model for high intensity turbulence, the curvature term in (2.37) may therefore be combined with the turbulent transport term as

$$-\mathcal{D}_{\mathcal{L}} \overline{\kappa \sigma} - \nabla \cdot \overline{\mathbf{v}' G'} = -(D_{\mathcal{L}} + D_t) \bar{\kappa}(\overline{G}) |\nabla \overline{G}| \ . \tag{2.49}$$

The inclusion of this term in the equation for $\overline{G}$ avoids the formation of cusps of the mean flame front.

The turbulent transport term in the variance equation must also be modelled as a curvature term. Equation (2.45) suggests that there is also a contribution proportional to $\mathcal{D}_{\mathcal{L}}$. Therefore, combining these two curvature terms in a similar way as in (2.49) one obtains

$$-\mathcal{D}_{\mathcal{L}} \overline{\kappa'' |\nabla G|} - \nabla \cdot (\overline{\mathbf{v}' G'^2}) = -(\mathcal{D}_{\mathcal{L}} + D_t) \bar{\kappa}(\overline{G'^2}) |\nabla \overline{G'^2}| \tag{2.50}$$

where $\bar{\kappa}(\overline{G'^2})$ is defined as in (2.32) but with the variance $\overline{G'^2}$ instead of G. For the turbulent production term classical gradient transport modelling is appropriate since second order derivatives are not involved

$$-\overline{\mathbf{v}' G'} \cdot \nabla \overline{G} = D_t \, (\nabla \overline{G})^2 \ . \tag{2.51}$$

Finally, the last term in (2.37), presenting the effect of local strain on the flame surface may be interpreted as a stretch term. Numerical simulations by Ashurst [2.17] show that the strain is statistically independent of σ and that the mean strain $\overline{\mathbf{n} \cdot \nabla \mathbf{v} \cdot \mathbf{n}}$ on the flame surface is always negative. When this term, divided by $s_L^0 \bar{\sigma}$ is plotted over v'/s_L^0 it is seen to be linear and independent of $\mathcal{L}$ (cf. Fig. 2.9). This leads to the closure model

$$-\mathcal{L} \overline{\mathbf{n} \cdot \nabla \mathbf{v} \cdot \mathbf{n} \sigma} = b_3 \frac{\mathcal{L}}{\ell} v' \bar{\sigma} \tag{2.52}$$

where $b_3 = 1.3$ with the integral length scale defined as

$$\ell = 0.37 v'^3 / \bar{\varepsilon} \tag{2.53}$$

and the r.m.s velocity fluctuations as

$$v' = \sqrt{2/3 \, \bar{k}} \ . \tag{2.54}$$

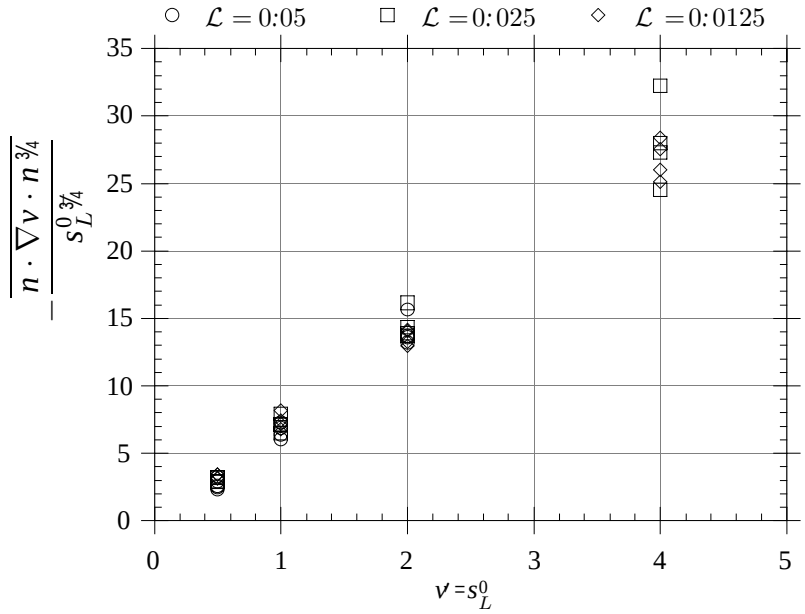

Figure 2.9: Results of numerical simulation of the strain rate term.

We will combine the first and the last term on the l.h.s of (2.37) as

$$s_L^0 \bar{\sigma} + \mathcal{L}\,\overline{\mathbf{n} \cdot \nabla \mathbf{v} \cdot \mathbf{n} \sigma} = s_T |\nabla \overline{G}| \tag{2.55}$$

where

$$s_T = s_L^0 \bar{\sigma} \left(1 - b_3 \frac{\mathcal{L}}{\ell} \frac{v'}{s_L^0} \right) \tag{2.56}$$

is the turbulent burning velocity. For $\mathcal{L}/\ell \to 0$ this is equal to (2.35). With all these closure assumptions we may write the equations for $\overline{G}$ and $\overline{G'^2}$ as

$$\frac{\partial \overline{G}}{\partial t} + \overline{\mathbf{v}} \cdot \nabla \overline{G} = -(\mathcal{D}_{\mathcal{L}} + D_t) \bar{\kappa}(\overline{G}) |\nabla \overline{G}| + s_T |\nabla \overline{G}| \,, \tag{2.57}$$

$$\frac{\partial \overline{G'^2}}{\partial t} + \overline{\mathbf{v}} \cdot \nabla \overline{G'^2} = -(\mathcal{D}_{\mathcal{L}} + D_t) \bar{\kappa}(\overline{G'^2}) |\nabla \overline{G'^2}| + 2 D_t (\nabla \overline{G})^2 - c_s \frac{\bar{\varepsilon}}{\bar{k}} \overline{G'^2} \,. \tag{2.58}$$

The only quantity that still needs to be determined is the flame surface area ratio $\bar{\sigma}$. The scaling relation (2.43) together with the definition (2.39) for the kinematic restoration shows that for large turbulent Reynolds numbers the laminar burning velocity s_L^0 plays a similar role in the kinematic restoration $\overline{\omega}$ as the viscosity ν plays in the dissipation $\bar{\varepsilon}$. In this limit both, $\overline{\omega}$ and $\bar{\varepsilon}$, are to be modelled in terms of quantities defined at the integral scales. Therefore the variance equation becomes independent of s_L^0 as the turbulent kinetic energy equation becomes independent of ν. This also indicates that the term $s_L^0 \bar{\sigma}$ in (2.57) should be independent of s_L^0 in the large Reynolds number limit. Introducing an artificial dimension for G, say

g, one finds that $\overline{\omega}$ has the dimension g^2/s and $\bar{\sigma}$ the dimension g/m. Dimensional analysis then suggests that

$$s_L^0 \bar{\sigma} \sim \left(\frac{\bar{\varepsilon}}{\bar{k}} \overline{\omega} \right)^{1/2} \sim \frac{\bar{\varepsilon}}{\bar{k}} (\overline{G'^2})^{1/2} \sim \frac{v'}{\ell} (\overline{G'^2})^{1/2} \; . \tag{2.59}$$

With these closure assumptions one may readily calculate the turbulent burning velocity of a one-dimensional unsteady planar flame. Since the variance $\overline{G'^2}$ is a property of the entire turbulent flame and does not vary across the flame brush, it is appropriate to assign zero gradient boundary conditions on both sides of the flame brush. Then the gradient $\overline{\nabla G'^2}$ normal to the flame vanishes. If the turbulence quantities D_t, $\bar{k}$ and $\bar{\varepsilon}$ are constant, the gradient $\nabla \overline{G'^2}$ in the convective term also does not change in tangential direction and therefore disappears entirely. Furthermore, in interpreting $\overline{G}$ as a distance function for the turbulent flame, $|\nabla \overline{G}|$ is equal to unity in the production term and since the flame is planar the curvature term vanishes in (2.56). Using (1.14), (2.53) and (2.54) and a turbulent Schmidt number Sc $= \nu_t / D_t = 0.7$ one obtains for the turbulent diffusivity

$$D_t = 0.78 \, v' \ell \; . \tag{2.60}$$

Likewise we may replace $\bar{\varepsilon}/\bar{k}$ in (2.58) by

$$\frac{\bar{\varepsilon}}{\bar{k}} = 0.247 \, \frac{v'}{\ell} \tag{2.61}$$

where $\bar{k}/\bar{\varepsilon} = \tau$ which is the integral time scale. The variance equation is then written in terms of the non-dimensional time t/τ with $c_s = 2$ as

$$\frac{\partial \overline{G'^2}}{\partial (t/\tau)} = 6.32 \, \ell^2 - 2 G'^2 \; . \tag{2.62}$$

This has the solution

$$\overline{G'^2} = b_2^2 \, \ell^2 \left[1 - \exp(-2t/\tau) \right] + \overline{G_0'^2} \exp(-2t/\tau) \tag{2.63}$$

where $b_2 = \sqrt{3.16} = 1.78$. Here $\overline{G'^2} = \overline{G_0'^2}$ is the initial value at $t = 0$. This may be set equal to ℓ_F^2, if one assumes the flame to start as a plane laminar flame.

The quantity $(\overline{G'^2})^{1/2}/|\nabla \overline{G}|$ may be interpreted as the turbulent flame brush thickness $\ell_{F,t}$. In the limit $\overline{G_0'^2}/\ell^2 \to 0$ this quantity would evolve as

$$\ell_{F,t} = \frac{(\overline{G'^2})^{1/2}}{|\nabla \overline{G}|} = b_2 \, \ell [1 - \exp(-2t/\tau)]^{1/2} \tag{2.64}$$

This shows that for large times the turbulent flame brush thickness is proportional to the integral length scale. Equation (2.63) may be inserted into (2.59) to write

$$s_L^0 \bar{\sigma} = b_1 v' \left[1 - \exp(-2t/\tau) + \frac{\overline{G_0'^2}}{3.16 \, \ell^2} \exp(-2t/\tau) \right]^{1/2} \; . \tag{2.65}$$

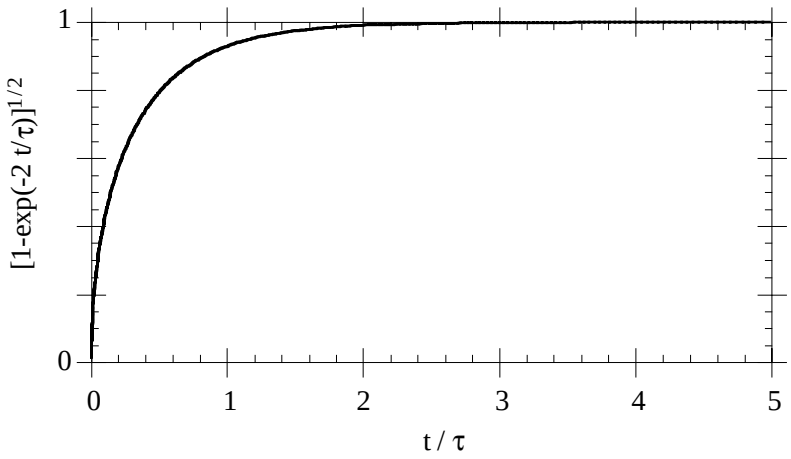

Figure 2.10: Time evolution of the turbulent flame brush thickness and the turbulent burning velocity.

This may be introduced into the expression (2.56) for the turbulent burning velocity s_T. One obtains in the limit $\overline{G_0'^2}/\ell^2 \to 0$

$$s_T = b_1\, v'[1-\exp(-2t/\tau)]^{1/2}\left(1 - b_3\frac{\mathcal{L}}{\ell}\frac{v'}{s_L^0}\right)\ . \tag{2.66}$$

This reaches for large times $t/\tau \to \infty$ and for $\mathcal{L}/\ell \to 0$ the steady state limit

$$s_T = b_1\, v' \tag{2.67}$$

which is equivalent to Damköhler's expression (2.1) for large scale turbulence. The modelling constant b_1 may be determined by the slope in the burning velocity diagram and lies between 1.0 and 2.0. The term in square brackets in (2.64) and (2.66) is plotted in Fig. 2.10 showing that the steady state condition is approached rather rapidly.

We may conclude that, apart from unsteady effects, modelling of the kinematic G-equation for high Reynolds number turbulence leads to well-known results, namely that the flame brush thickness is proportional to the integral length scale and that the turbulent burning velocity is proportional to the turbulent intensity. These findings are reassuring but they do not explain the "bending" of the turbulent burning velocity when the ratio s_T/s_L is plotted as a function of v'/s_L as shown in Fig. 2.6. As discussed in the beginning of this lecture this bending was found in many experimental situations. In order to understand the bending effect we will extend the level set approach to the thin reaction zones regime.

2.6 The Level-Set-Approach for the Diffusive G-Equation

We will consider a flame which contains a single reaction zone–which may contain several reaction layers–that separates the preheat zone from the post-flame equilibrium layers. The most upstream of these reaction layers adjacent to the preheat zone will be called the inner layer. We will furthermore assume that the binary diffusion approximation is valid and that the diffusivities of fuel, oxidizer and temperature differ only by a small amount. We want to derive an equation for the propagation velocity $d\mathbf{x}/dt$ of the thin reaction zone similar to (2.21). For that purpose we must define the location of the inner layer by specifying either concentrations or reaction rates in that zone. Since we do not intend to resolve the thin reaction zone we do not need to specify the chemistry. Asymptotic analyses [2.18] show that for lean, stoichiometric and slightly rich flames the fuel is the deficient species which disappears completely in the inner layer. Although the asymptotic analysis for very rich flames with realistic chemistry has not yet been performed, one may expect that in that case oxygen is the deficient species and disappears in the inner layer. We define the location of the reaction zone by the iso-scalar surface of either the fuel mass fraction Y_F or the oxygen mass fraction Y_{O_2} in the limit $Y_F \to 0$ or $Y_{O_2} \to 0$, respectively. We denote the mass fraction of the deficient species by Y and consider its balance equation

$$\rho\left(\frac{\partial Y}{\partial t} + \mathbf{v}\cdot\nabla Y\right) = \nabla\cdot(\rho D\nabla Y) + \dot{m} \tag{2.68}$$

where D is its diffusion coefficient and $\dot{m}$ its chemical source term. Similar to (2.23) the iso-scalar surface $Y(\mathbf{x}, t) = Y_0$ must satisfy the condition

$$\frac{\partial Y}{\partial t} + \nabla Y \cdot \frac{d\mathbf{x}}{dt}\Big|_{Y=Y_0} = 0\ . \tag{2.69}$$

Replacing $\partial Y/\partial t$ from (2.68) this leads to

$$\frac{d\mathbf{x}}{dt}\Big|_{Y=Y_0} = \mathbf{v} - \left[\frac{\nabla\cdot(\rho D\nabla Y) + \dot{m}}{\rho|\nabla Y|}\right]_0 \mathbf{n}\ . \tag{2.70}$$

Here the term in square brackets is the displacement speed of the thin reaction zone. For diffusive scalars (2.70) was first derived in [2.19]. The normal vector on the iso-concentration surface is defined as

$$\mathbf{n} = \frac{\nabla Y}{|\nabla Y|}\ . \tag{2.71}$$

We want to derive a G-equation that describes the location of the thin reaction zones such that the iso-surface $Y(\mathbf{x}, t) = Y_0$ coincides with the iso-surface defined

by $G(\mathbf{x}, t) = G_0$. Then the normal vector defined by (2.71) is equal to that defined by (2.22) and also points towards the unburnt mixture. Using (2.22) and (2.24) together with (2.70) leads to

$$\frac{\partial G}{\partial t} + \mathbf{v} \cdot \nabla G = - \left[\frac{\nabla \cdot (\rho D \nabla Y) + \dot{m}}{\rho |\nabla Y|} \right]_0 |\nabla G| \; . \tag{2.72}$$

The diffusive term appearing on the r.h.s of (2.72) may be split in a similar way as in (2.32) into one term accounting curvature and another for diffusion normal to the iso-surface

$$\nabla \cdot (\rho D \nabla Y) = \rho D |\nabla Y| \nabla \cdot \mathbf{n} + \mathbf{n} \cdot \nabla (\rho D \mathbf{n} \cdot \nabla Y) \tag{2.73}$$

where the definition (2.71) has been used. When (2.73) is introduced into (2.72) it can be written as

$$\frac{\partial G}{\partial t} + \mathbf{v} \cdot \nabla G = - D \, \kappa |\nabla G| + (V_n + V_r) |\nabla G| \; . \tag{2.74}$$

Here κ may be expressed by (2.32) in terms of the G-field. The quantities V_n and V_r are contributions due to normal diffusion and reaction to the displacement speed of the thin reaction zone and are defined as

$$V_n = - \frac{\mathbf{n} \cdot \nabla (\rho D \mathbf{n} \cdot \nabla Y)}{\rho |\nabla Y|} \; , \tag{2.75}$$

$$V_r = - \frac{\dot{m}}{\rho |\nabla Y|} \; . \tag{2.76}$$

In a steady, unstretched planar laminar flame the sum of V_n and V_r would be equal to the laminar burning velocity s_L^0. Here, however, the unsteady mixing and diffusion of all chemical species and the temperature in the regions ahead of the thin reaction zone will influence the local displacement speed. Therefore the sum of V_n and V_r cannot be prescribed, but is a fluctuating quantity, that couples the G-equation to the solution of the balance equations of the reactive scalars. There is reason to expect, however, that the sum of V_n and V_r is of the same order of magnitude as the laminar burning velocity s_L^0.

Furthermore, in the thin reaction zones regime the last term in (2.74) is small compared to the other terms. This can be shown by normalizing the independent quantities and the curvature in this equation with respect to Kolmogorov length and time scales

$$\begin{aligned} \hat{t} &= t / t_\eta \; , \quad \hat{x}_\alpha = x_\alpha / \eta \; , \quad \alpha = 1, 2, 3 \\ \hat{\kappa} &= \eta \kappa \; , \quad \hat{\nabla} = \eta \nabla \; . \end{aligned} \tag{2.77}$$

Using $\eta^2 / t_\eta = \nu$ one obtains

$$\frac{\partial G}{\partial \hat{t}} + \frac{\mathbf{v} \cdot \hat{\nabla} G}{v_\eta} = - \frac{D}{\nu} \hat{\kappa} |\hat{\nabla} G| + \frac{V_n + V_r}{v_\eta} |\hat{\nabla} G| \; . \tag{2.78}$$

Since Kolmogorov eddies can perturb the flow field that acts on the G-field, all derivatives, the curvature and the velocity ratio $\mathbf{v}_0/v_\eta$ are typically of order unity. It was assumed that D/ν is also of order unity. However, in the thin reaction zones regime the Karlovitz number is larger than unity and thereby, due to (1.45)

$$v_\eta > s_L^0 \sim V_n + V_r \tag{2.79}$$

indicating that the last term in (2.78) will be small.

In order to be able to analyze the properties of (2.74), we replace the sum of V_n and V_r by their statistical mean value, which we denote by s_L^* and consider in the following as a model equation for the thin reaction zone regime

$$\frac{\partial G}{\partial t} + \mathbf{v} \cdot \nabla G = -D\kappa|\nabla G| + s_L^*|\nabla G| \tag{2.80}$$

which will be called the diffusive G-equation. This equation is very similar to (2.33), which was derived for the corrugated flamelet regime. An important difference, apart from the difference between s_L and s_L^*, is the difference between $D_{\mathcal{L}}$ and D and the disappearance of the strain term in (2.80) as compared to (2.33). The Markstein diffusivity $D_{\mathcal{L}}$, although of the same order of magnitude as D, may even be negative if the Lewis number is sufficiently smaller than unity as can be seen from (2.31). In an analytical study of the response of one-dimensional constant density flames to time-dependent stretch and curvature, Joulin [2.20] has shown that for high frequency perturbations the effect of strain disappears entirely and Lewis-number effects on the Markstein length also disappear such that $D_{\mathcal{L}}$ approaches D. This analysis was based on one-step large activation energy asymptotics with the assumption of a single thin reaction zone. It suggests that (2.80) could also have been derived from (2.33) for the limit of high frequency perturbations of the chemically inert structure surrounding the thin reaction zone. This strongly supports the physical picture derived for the thin reaction zones regime.

Based on (2.80) equations for the mean $\overline{G}$ and the variance $\overline{G'^2}$ are readily derived. Modelling of these equations is very similar to that performed for the kinematic G-equation and (2.57) and (2.58) remain unchanged. The only fundamental difference concerns the scalar dissipation which now is based on D rather than $D_{\mathcal{L}}$. The scalar dissipation is then the dominating destruction term in the variance equation, while the kinematic restoration based on s_L^* is small. This is shown rigorously in [2.16]. The derivation is again based on the scalar spectrum function for two-point correlations of G. But as it is shown in Fig. 1.7, the Gibson scale is smaller than the Obukhov-Corrsin scale

$$\ell_C = \left(\frac{D^3}{\bar{\varepsilon}}\right)^{1/4} . \tag{2.81}$$

Therefore the range with slope -2 in Fig. 2.8 disappears and ℓ_C is the relevant cut-off scale. The closure relation for the scalar dissipation is similar to that in

(2.43) for the kinematic restoration

$$\chi = 2D\overline{\sigma'^2} = c_\chi \frac{\bar{\varepsilon}}{\bar{k}} \overline{G'^2} \tag{2.82}$$

with $c_\chi = 1.62$. Now the kinematic restoration is small, but the sum of both destruction terms may also be approximated by (2.47).

An important consequence of (2.82) is, however, that the scaling of $\bar{\sigma}$, that is presented by (2.59) for the corrugated flamelets regime is different for the distributed reaction zones regime. Dimensional analysis now leads to

$$\bar{\sigma}^2 \sim \frac{\bar{\varepsilon}}{\bar{k}} \frac{\overline{G'^2}}{D} \; . \tag{2.83}$$

This also has important consequences for the scaling of the turbulent burning velocity. The result for the variance given by (2.63) remains unchanged since the modelled variance equation is the same for both regimes. However, when (2.63) is introduced into (2.83) and (2.60) and (2.61) are combined to express $\bar{\varepsilon}/\bar{k}$ in terms of D_t/ℓ^2 one obtains

$$\bar{\sigma} = b_4 (D_t/D)^{1/2} \left[1 - \exp(-2t/\tau) + \frac{\overline{G_0'^2}}{3.16\,\ell^2} \exp(-2t/\tau) \right]^{1/4} \; . \tag{2.84}$$

Using (2.35) this reduces for large times to the steady state limit

$$\frac{s_T}{s_L^0} = b_4 \sqrt{\frac{D_t}{D}} \tag{2.85}$$

which, with $b_4 = 1$, is equal to Damköhler's expression (2.9) for small scale turbulence.

This surprising result which is based on simple scaling arguments needs a further physical explication. As noted below (2.9), Damköhler had implicitly assumed that the chemical time scale is not affected by turbulence in the small scale turbulence limit. This assumption was difficult to accept if one follows the arguments on the modelling difficulties of the turbulent mean reaction rate in lecture 1. However, the physical picture in the thin reaction zones regime is based on turbulent eddies that enter into the chemically inert preheat zone, not into the reaction zone. Therefore they affect the chemical reaction only indirectly by controlling the diffusion processes into that zone. Damköhler's assumption therefore defines the upper limit for the thin reaction zone regime which was given by $\eta = \ell_\delta$ in the combustion diagram in Fig. 1.3.

2.7 A Model Equation for the Flame Surface Area Ratio for Both Regimes

In this paragraph we want to derive a model equation for the quantity $\bar{\sigma} = \overline{|\nabla G|}$ which, according to (2.35) may be interpreted as the flame surface ratio. By applying the ∇-operator to both sides of (2.80) and multiplying it with $-\mathbf{n} = \nabla G/|\nabla G|$ one obtains an equation for σ

$$\frac{\partial \sigma}{\partial t} + \mathbf{v} \cdot \nabla \sigma = -\mathbf{n} \cdot \nabla \mathbf{v} \cdot \mathbf{n} \sigma + s_L^0 (\kappa \sigma + \nabla^2 G) - D[\nabla \cdot (\kappa \nabla G) + \kappa^2 \sigma] \; . \quad (2.86)$$

Here the terms proportional to D are a result of the transformation

$$\mathbf{n} \cdot \nabla(\kappa\sigma) = -\nabla G \cdot \nabla \kappa - \kappa \nabla^2 G - \kappa^2 \sigma = -\nabla \cdot (\kappa \nabla G) - \kappa^2 \sigma \; . \quad (2.87)$$

As in the variance equation the term containing the laminar burning velocity is important in the corrugated flamelet regime only. Therefore we have replaced s_L^* by s_L^0. The first term on the r.h.s of (2.86) accounts for straining by the flow field. It will lead to a production of flame surface ratio. The second term is proportional to s_L^0 and will have the same effect as the kinematic restoration has on the variance $\overline{G'^2}$. The last term is proportional to D and its effect will be similar to that of scalar dissipation on $\overline{G'^2}$. Since closure relations for these terms cannot be derived in a systematic way as for those in the variance equation we place ourselves in the context of two-equation modelling based on the constant density analogue to equations (1.15) and (1.16) for the turbulent kinetic energy $\tilde{k}$ and the dissipation $\tilde{\varepsilon}$.

With the scaling relations between $\bar{\sigma}$ and $\tilde{\varepsilon}/\tilde{k}$ obtained in both regimes, namely (2.59) and (2.83), we are now able to derive model equations for $\bar{\sigma}$ in the two regimes. We will start with the corrugated flamelet regime and will use (2.59) to derive a differential relation between $\bar{\sigma}$ and $\tilde{\varepsilon}$, $\tilde{k}$ and $\overline{G'^2}$ as

$$\frac{d\bar{\sigma}}{\bar{\sigma}} = \frac{d\tilde{\varepsilon}}{\tilde{\varepsilon}} - \frac{d\tilde{k}}{\tilde{k}} + \frac{1}{2}\frac{d\overline{G'^2}}{\overline{G'^2}} \; . \quad (2.88)$$

Combining the constant density analogues of (1.15) and (1.16) with (2.58) one obtains an equation for $\bar{\sigma}$ of the form

$$\begin{aligned} \frac{\partial \bar{\sigma}}{\partial t} + \overline{\mathbf{v}} \cdot \nabla \bar{\sigma} \;\; &= \;\; -D_t \tilde{k}(\bar{\sigma}) |\nabla \bar{\sigma}| + (c_{\varepsilon 1} - 1) \frac{(-\overline{v'_\alpha v'_\beta})}{\tilde{k}} \frac{\partial \overline{v_\alpha}}{\partial x_\beta} \bar{\sigma} \\ &+ \;\; \frac{-\overline{\mathbf{v}' G'} \cdot \nabla \overline{G}}{\overline{G'^2}} - (c_{\varepsilon 2} - 1 + \frac{c_s}{2}) \frac{\tilde{\varepsilon}}{\tilde{k}} \bar{\sigma} + (\text{additional terms}) \; . \end{aligned} \quad (2.89)$$

In this equation the terms on the l.h.s. represent the unsteady change and convection of $\bar{\sigma}$ by the mean velocity field. The first term on the r.h.s. describes the turbulent transport of $\bar{\sigma}$, which in the spirit of (2.48) and the discussion thereafter was

modelled as a curvature term. Here, $\bar{k}(\bar{\sigma})$ is defined as in (2.32) but with $\bar{\sigma}$ instead of G. The second term represents the production of the flame surface area ratio by mean velocity gradients and the third term by local turbulent fluctuations. The last term accounts for the destruction of the flame surface ratio by kinematic restoration. The additional terms originate from the curvature term in (2.58) and the turbulent transport terms in (1.15) and (1.16) and contain the squares of derivatives of $\bar{\varepsilon}$, $\bar{k}$ and $\overline{G'^2}$. It is common practice in turbulence modelling to interpret the squares of derivatives of mean quantities as dissipation terms and to subsume them within the last term in (2.89). This term may be cast into a form proportional to s_L^0 by replacing $\bar{\varepsilon}/\bar{k}$ using (2.59) as

$$\frac{\bar{\varepsilon}}{\bar{k}} \sim s_L^0 \frac{\bar{\sigma}}{(\overline{G'^2})^{1/2}} \; . \tag{2.90}$$

In the corrugated flamelet regime the model equation for the total flame surface density then reads

$$\begin{aligned} \frac{\partial \bar{\sigma}}{\partial t} + \overline{\mathbf{v}} \cdot \nabla \bar{\sigma} &= -D_t \bar{k}(\bar{\sigma}) |\nabla \bar{\sigma}| + c_0 \frac{(\overline{-v'_\alpha v'_\beta})}{\bar{k}} \frac{\partial \overline{v_\alpha}}{\partial x_\beta} \bar{\sigma} \\ &+ c_1 \frac{D_t (\nabla \overline{G})^2}{\overline{G'^2}} \bar{\sigma} - c_2 \frac{s_L^0 \bar{\sigma}^2}{(\overline{G'^2})^{1/2}} \end{aligned} \tag{2.91}$$

where $c_0 = c_{\varepsilon 1} - 1 = 0.44$. In the turbulent production term we have used (2.51).

A similar approach can be taken in the thin reaction zones regime where now the scalar dissipation $\overline{\chi}$ is the main term responsible for reducing fluctuations of the reaction zone. Using (2.83) this leads to the differential form

$$2\frac{d\bar{\sigma}}{\bar{\sigma}} = \frac{d\bar{\varepsilon}}{\bar{\varepsilon}} - \frac{d\bar{k}}{\bar{k}} + \frac{d\overline{G'^2}}{\overline{G'^2}} \tag{2.92}$$

rather than (2.88). We then obtain a similar equation as (2.89), except with a factor 2 in front of the turbulent production term and c_s replacing $c_s/2$ in the last term. In the last term, however, we now use (2.83) to replace $\bar{\varepsilon}/\bar{k}$ as

$$\frac{\bar{\varepsilon}}{\bar{k}} \sim \frac{D\bar{\sigma}^2}{\overline{G'^2}} \; . \tag{2.93}$$

Therefore, in the thin reaction zones regime an equation similar to (2.91) can be derived, namely

$$\begin{aligned} \frac{\partial \bar{\sigma}}{\partial t} + \overline{\mathbf{v}} \cdot \nabla \bar{\sigma} &= -D_t \bar{k}(\bar{\sigma}) |\nabla \bar{\sigma}| + c_0 \frac{(\overline{-v'_\alpha v'_\beta})}{\bar{k}} \frac{\partial \overline{v}_\alpha}{\partial x_\beta} \bar{\sigma} \\ &+ 2\frac{D_t (\nabla \overline{G})^2}{\overline{G'^2}} \bar{\sigma} - c_3 \frac{D\bar{\sigma}^3}{\overline{G'^2}} \; . \end{aligned} \tag{2.94}$$

The last term in (2.94) being proportional to $\bar{\sigma}^3$ differs from (2.91) where the last term was proportional to $\bar{\sigma}^2$. This shows a fundamental difference between the two regimes.

At this point we may take guidance from (2.86) which, after averaging, contains source terms proportional to s_L^0 and to D. Therefore the last terms in (2.91) and (2.94) are assumed to be additive, the former accounting for flame surface area ratio destruction in the corrugated flamelet regime and the latter in the thin reaction zones regime. A model equation for $\bar{\sigma}$ that covers both regimes would therefore read

$$\begin{aligned}\frac{\partial\bar{\sigma}}{\partial t}+\overline{\mathbf{v}}\cdot\nabla\bar{\sigma} = -D_t\bar{k}(\bar{\sigma})|\nabla\bar{\sigma}| \quad &+ \quad c_0\frac{(-\overline{v'_\alpha v'_\beta})}{\bar{k}}\frac{\partial\overline{u_\alpha}}{\partial x_\beta}\bar{\sigma}+c_1\frac{D_t(\nabla\overline{G})^2}{\overline{G'^2}}\bar{\sigma}\\ &- \quad c_2\frac{s_L^0\bar{\sigma}^2}{(\overline{G'^2})^{1/2}}-c_3\frac{D\bar{\sigma}^3}{\overline{G'^2}}\ .\end{aligned} \tag{2.95}$$

The last three terms in this equation represent the turbulent production, the kinematic restoration and the scalar dissipation of the flame surface area ratio, respectively, and correspond to the three terms on the r.h.s of (2.86). A constant c_1 has been introduced for a model of the production term that would be valid in both regimes.

We now want to fix the constants c_1, c_2 and c_3 in Eq. 2.95 at least tentatively. Existing collections and burning velocity data [2.21], [2.3] provide some guidance, but it must be recognized that in many experiments quantitative information about length scales is missing. Also, in interpreting many experimental data the burning velocity was assumed to have reached its steady state while it was still developing. The effect of mean velocity gradients on the development of the total flame surface density has hardly ever been taken into account.

For simplicity we will consider the case of isotropic fully developed turbulence and a fully developed turbulent flame in the limit of large times t/τ. This corresponds to the limit of turbulent production of flame surface area ratio equals kinematic restoration and scalar dissipation in (2.95) as

$$c_1\frac{D_t}{\ell_{F,t}^2}\bar{\sigma}-c_2\frac{s_L^0}{\ell_{F,t}}\bar{\sigma}^2-c_3\frac{D}{\ell_{F,t}^2}\bar{\sigma}^3=0\ . \tag{2.96}$$

Here the variance has been replaced by the turbulent flame brush thickness using (2.63) and $|\nabla\overline{G}|$ has been set equal to unity as before. In the corrugated flamelet regime the last term in (2.96) may be neglected. The turbulent diffusivity is expressed by (2.60) as a function of v' and ℓ. Then it follows from (2.64) for $t/\tau\to\infty$ that $\ell_{F,t}=b_2\ell$ and therefore

$$c_2\,b_2\,s_L^0\bar{\sigma}=0.78\,c_1v'\ . \tag{2.97}$$

Experimental data for fully developed flames suggest that the turbulent burning velocity is approximately $s_T=2.0v'$ in the large scale turbulence limit [2.21]. It

follows that $\bar{\sigma} = 2.0 v'/s_L^0$ and therefore

$$c_2\, b_2 = 0.39\, c_1 \ . \tag{2.98}$$

Similarly, for the thin reaction zones regime the second term in (2.96) may be neglected. We use (2.9) which Damköhler believed to be exact to obtain

$$c_3 = c_1 \ . \tag{2.99}$$

In order to define the laminar flame thickness unambiguously in the present context we set

$$D = s_L^0 \ell_F \ . \tag{2.100}$$

Then the limit where production equals kinematic restoration and scalar dissipation leads to a quadratic equation

$$\bar{\sigma}^2 + 0.39 \frac{\ell}{\ell_F} \bar{\sigma} - 0.78 \frac{v' \ell}{s_L^0 \ell_F} = 0 \tag{2.101}$$

with the solution

$$\bar{\sigma} = -\frac{0.39}{2} \frac{\ell}{\ell_F} + \sqrt{\left(\frac{0.39}{2} \frac{\ell}{\ell_F} \right)^2 + 0.78 \frac{v' \ell}{s_L^0 \ell_F}} \ . \tag{2.102}$$

This equation satisfies the limits $\ell/\ell_F \to \infty$ corresponding to $\bar{\sigma} = 1.5\, v'/s_L^0$ for the corrugated flamelet regime and $\ell/\ell_F \to 0$ corresponding to $\sigma = (D_t/D)^{1/2}$ for the thin reaction zones regime. Since the equation for the flame surface area ratio was derived for the limit of large turbulent Reynolds numbers (2.102) does not cover the laminar limit $\bar{\sigma} = 1$ for $v' \to 0$, $\ell \to 0$. In order to obtain an expression similar to (2.11), it is proposed to replace (2.56) by

$$s_T = s_L^0 + \bar{\sigma} \left(1 - b_3 \frac{\mathcal{L}}{\ell} \frac{v'}{s_L^0} \right) \ . \tag{2.103}$$

In Fig. 2.11 the ratio of the turbulent to the laminar burning velocity has been plotted using (2.103) for $\mathcal{L} = 0$ and for constant length scale ratios ranging from 1 to 100. A constant length scale ratio is typical for experiments at constant pressure with a fixed geometry. Fig. 2.11 then shows the "bending" behaviour of the turbulent burning velocity as v'/s_L^0 increases. It corresponds to the deviation from the straight line $s_T = s_L^0 + 2.0\, v'$ and leads to smaller values of s_T/s_L^0 for small length scale ratios.

There remains the problem of assigning a value to the constant c_1. Since after averaging the mean strain term in (2.86) is identical to that in (2.37) one may use the closure (2.52) derived by direct numerical simulations. This leads with (2.60) to

$$c_1 = 1.3\, b_2^2/0.547 = 5.261 \ . \tag{2.104}$$

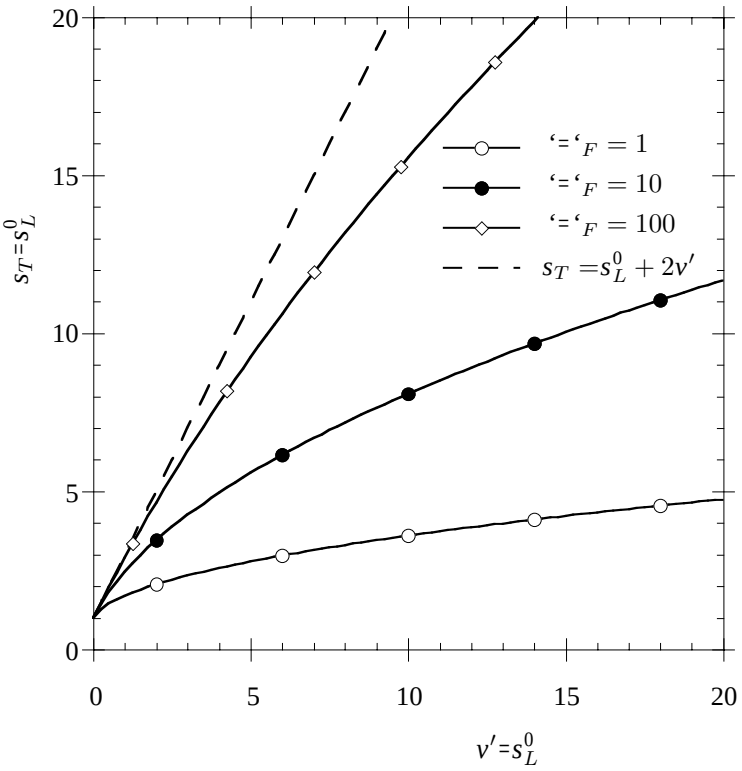

Figure 2.11: Ratio of the turbulent to the laminar burning velocity as a function of v'/s_L^0 for different length scale ratios.

For strong shear flows one may now also assume production equals dissipation in the turbulent kinetic energy equation (1.15). Using (2.61) the production term due to velocity gradients may then be expressed as

$$c_0 \frac{\bar{\varepsilon}}{\bar{k}} \bar{\sigma} = 0.109 \frac{v'}{\ell} \bar{\sigma} \psi \tag{2.105}$$

showing that production by mean gradients is of minor importance compared to production by strain.

2.8 Derivation of an Equation for the Mean Progress Variable

Numerical solutions of the $\overline{G}$-equation present certain difficulties. The location defined by $\overline{G}(\mathbf{x}, t) = G_0$ is the location of the mean flame front. Since $\overline{G}$ is interpreted as a distance function, initial conditions should satisfy the equation

$$|\nabla \overline{G}| = 1 \tag{2.106}$$

for $\overline{G} \neq G_0$. For instance, if flame propagation starting from a spherical spark of radius R_0 is to be calculated, initial $\overline{G}$ iso-lines would correspond to spherical shells around the spark with $\overline{G} - G_0 = R_0 - r$ where r is the radial distance from the center of the spark. As the calculation proceeds, it may be necessary to re-initialize the $\overline{G}$-field outside $\overline{G} = G_0$ such that it satisfies (2.106). A numerical procedure for doing this is given in [2.9] where it is proposed to solve the time-dependent equation for re-initialization

$$\frac{\partial g}{\partial t} = \text{sign}(\overline{G}(\mathbf{x}, t) - G_0)(1 - |\nabla g|) \tag{2.107}$$

starting from $g(\mathbf{x}, t = t_0) = \overline{G}(\mathbf{x}, t)$ until the stationary final solution $g_\infty(\mathbf{x})$ is reached. Then the solution $\overline{G}(\mathbf{x}, t)$ is set equal to $g_\infty(\mathbf{x})$ for $\overline{G} \neq G_0$ such that it satisfies (2.106) while it remains unchanged at $\overline{G} = G_0$. This numerical process is time-consuming. Therefore it would be useful to find an alternative to determine the location of the mean flame front.

Classical models of premixed turbulent combustion are based on the mean progress variable $\bar{c}$ rather than the mean distance function $\overline{G}$. Starting from (2.29) an equation for the mean progress variable can be derived using the same closure assumption that led to (2.57)

$$\frac{\partial \bar{c}}{\partial t} + \mathbf{v} \cdot \nabla \bar{c} = -(D_{\mathcal{L}} + D_t)\bar{k}(\bar{c})|\nabla \bar{c}| + s_T|\nabla \bar{c}| \ . \tag{2.108}$$

An iso-surface of, say, $\bar{c}(\mathbf{x}, t) = 0.5$ then would represent the location of the mean flame front $\mathbf{x} = \mathbf{x}_F$. This equation, however, bears no advantage over (2.57). In fact, numerical diffusion will decrease the gradient $|\nabla \bar{c}|$ in the last term of (2.108) which in turn will decrease the convective term. This will quickly lead to a spreading of the region where $\bar{c}$ is between 0 and 1 which is inconsistent with the physical interpretation of $\bar{c}(\mathbf{x})$ as the probability of finding burnt gas at the location $\mathbf{x}$. Therefore, if an equation for $\bar{c}$ is preferred for numerical calculations, the particular character of the Eikonal term in (2.108) must be examined. A more fundamental derivation of the equation for the progress variable starts from the transport equation for the pdf $P(G, \mathbf{x})$ [2.22]. Following [2.22] one may derive from (2.33) an equation similar to (1.24) by interpreting the eikonal term $s_L^0\sigma$ and the strain term as source terms and the curvature term as a transport term. The resulting pdf transport equation will then read

$$\begin{aligned} \frac{\partial P}{\partial t} + \overline{\mathbf{v}} \cdot \nabla P \quad &+ \quad s_L^0 \frac{\partial}{\partial G}\{< |\nabla G| >_G P\} + \mathcal{L}\frac{\partial}{\partial G}\{< \mathbf{n} \cdot \nabla \mathbf{v} \cdot \mathbf{n}\sigma >_G P\} \\ &+ \quad (D_{\mathcal{L}} + D_t)\bar{k}(P)|\nabla P| = 0 \ . \end{aligned} \tag{2.109}$$

Here, in the spirit of (2.48) and (2.49) we have combined the turbulent transport term and the curvature term into a mean curvature term. The quantities $< |\nabla G| >_G$ and $< \mathbf{n} \cdot \nabla \mathbf{v} \cdot \mathbf{n}\sigma >_G$ are conditional ensemble averages. An equation for $\bar{c}$ may

now be derived by multiplying (2.109) by c and integrating from $G = -\infty$ to $G = \infty$. Here it should be taken into account that c is a random variable that does not depend on t and $\mathbf{x}$ in (2.109). Then, since

$$\bar{c}(\mathbf{x}) = \int_{-\infty}^{+\infty} c(G) P(G, \mathbf{x}) dG \tag{2.110}$$

one obtains

$$\begin{aligned} \frac{\partial \bar{c}}{\partial t} + \overline{\mathbf{v}} \cdot \nabla \bar{c} = & - (D_{\mathcal{L}} + D_t) \bar{k}(\bar{c}) |\nabla \bar{c}| \\ & + s_L^0 \int_{-\infty}^{+\infty} \delta(G - G_0) < |\nabla G| >_G P dG \\ & + \mathcal{L} \int_{-\infty}^{+\infty} \delta(G - G_0) < \mathbf{n} \cdot \nabla \mathbf{v} \cdot \mathbf{n} \sigma >_G P dG \; . \end{aligned} \tag{2.111}$$

Here, (2.27) has been taken into account and partial integration was performed in order to obtain the last two terms on the r.h.s of (2.111). The delta function in these integrals makes them equal to the values of the integrand at $G = G_0$. Therefore, we obtain the following equation for the mean progress variable

$$\frac{\partial \bar{c}}{\partial t} + \overline{\mathbf{v}} \cdot \nabla \bar{c} = -(D_{\mathcal{L}} + D_t) \bar{k}(\bar{c}) |\nabla \bar{c}| + s_T P(G = G_0, \mathbf{x}) \; . \tag{2.112}$$

Here the turbulent burning velocity was identified in agreement with (2.56) as

$$s_T = s_L^0 < |\nabla G| >_{G=G_0} + \mathcal{L} < \mathbf{n} \cdot \nabla \mathbf{v} \cdot \mathbf{n} \sigma >_{G=G_0} = s_L^0 \bar{\sigma} \left(1 - b_3 \frac{\mathcal{L}}{\ell} \frac{v'}{s_L^0} \right) \; . \tag{2.113}$$

Equation (2.112) is very similar to (2.108) except for the last term which now contains the conditional pdf at $G = G_0$. The pdf $P(G = G_0, \mathbf{x})$ is a function of $\mathbf{x}$ only. This may be shown if one assumes, for instance, a Gaussian function for the pdf of G

$$P(G, \mathbf{x}) = \frac{1}{\sqrt{2\pi \overline{G'^2}}} \exp \left(- \frac{(G - \overline{G})^2}{2 \overline{G'^2}} \right) \tag{2.114}$$

where $\overline{G}$ and $\overline{G'^2}$ are functions of $\mathbf{x}$. Then, if G is interpreted as a distance function, it may be expressed as

$$G(\mathbf{x}, t) - G_0 = x + F(y, z, t) \tag{2.115}$$

where x measures the distance normal to the mean flame position at $x = 0$ and y and z are coordinates in tangential direction. Therefore $F(y, z, t)$ describes the fluctuation around the mean flame position. Taking the mean of (2.115) leads to

$$\overline{G} - G_0 = x \tag{2.116}$$

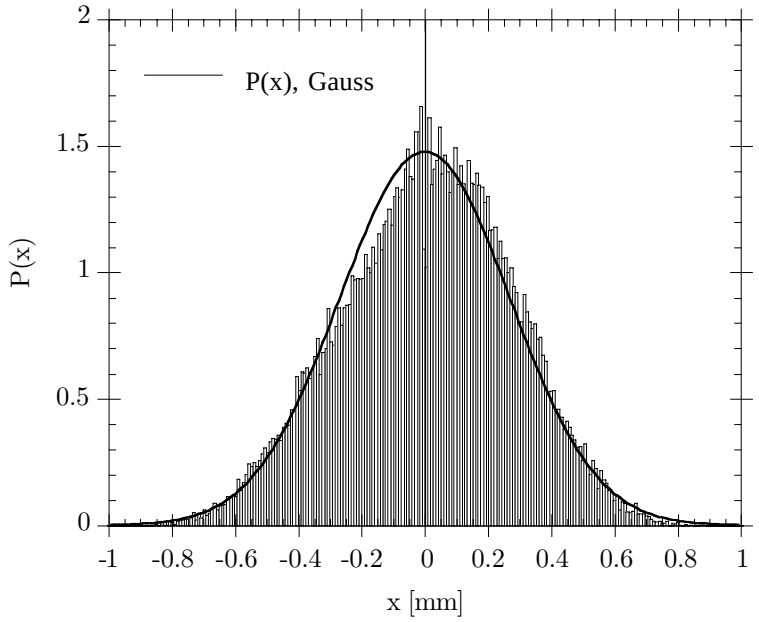

Figure 2.12: Probability density function of normal flame front fluctuations.

since $\overline{F} = 0$. Then for $G = G_0$

$$G - \overline{G} = F = -x \ . \tag{2.117}$$

Inserting this into (2.114) leads to

$$P(G = G_0, \mathbf{x}) = P(\mathbf{x}) = \frac{1}{\sqrt{2\pi\overline{G'^2}}} \exp\left(-\frac{x^2}{2\overline{G'^2}}\right) \ . \tag{2.118}$$

The variance $\overline{G'^2}$ does not vary in normal direction $x = \mathbf{n} \cdot (\mathbf{x} - \mathbf{x}_F)$ within the flame brush but it may vary in tangential direction.

Closure of (2.112) therefore uses the preassumed pdf $P(x)$ which then is a function of the coordinate normal to the flame brush x and the variance $\overline{G'^2}$.

In Fig. 2.12 the Gaussian pdf is compared with experimental data from flame front fluctuations obtained by Mie-scattering in a transparent spark ignition engine. Details may be found in [2.23] and [2.24]. It is seen that the Gaussian pdf fits the data quite well.

It should be noted that (2.112) has a non-local character since the variance must be evaluated at the location of the mean flame front $\mathbf{x} = \mathbf{x}_F$. Therefore, expansion effects that would modify the flow field ahead and behind the flame front will have no influence on the flame propagation mechanism.

Bibliography

[2.1] Bédat, B. and Cheng, R. K., Comb.Flame **100**, pp. 485–494 (1995).

[2.2] Abdel-Gayed, R. G:, Al-Kishali, K. J. and Bradley, D., Proc.R.Soc.Lond. A391, 393–419 (1984).

[2.3] Bradley, D., Twenty-Fourth Symposium (International) on Combustion, The Combustion Institute, Pittsburgh, pp. 247–262, 1992.

[2.4] Trautwein, S. E., Grudno, A., Adomeit, G., Twenty-Third Symposium (Int.) on Combustion, pp.723–728, (1990).

[2.5] Damköhler, G., Z. Eletrochem. **46**: 601–652 (1940), English translation NACA Techn. Memo. No.1112 (1947).

[2.6] Williams, F. A., *Combustion Theory* (2nd Edition), Addison -Wesley, 1985, p. 429ff.

[2.7] Bray, K. N. C, Twenty-Sixth Symposium (International) on Combustion, The Combustion Institute, Pittsburgh, pp. 1–26, 1996.

[2.8] Bray, K. N. C, and Libby, P. A., In "Turbulent Reacting Flows" (P. A. Libby and F. A. Williams, Eds.) Academic Press, 1994, pp. 115–151.

[2.9] Sussman, M, Fatemi, E., and Osher, S., J.Comp.Phys. **114**:146–159 (1994).

[2.10] Pelce, P., and Clavin, P., J.Fluid Mech. **124**:219–237 (1982).

[2.11] Matalon, M., and Matkowsky, B. J., J.Fluid Mech. **124**:239–259 (1982).

[2.12] Keller, D., and Peters, N., Theoret.Comput.Fluid Dynamics **6**:141–149 (1994).

[2.13] Clavin, P., Williams, F.A., J. Fluid Mech. **116**:251–282 (1982).

[2.14] Kerstein, A. R., Ashurst, Wm. T., and Williams, F. A., Phys.Rev. **A37**:2728–2731 (1988).

[2.15] Peters, N., J.Fluid Mech. **242**:611–629, 1992.

[2.16] Peters, N., *Propagating Thin Reaction Zones in Premixed Turbulent Combustion*, unpublished manuscript, 1997.

[2.17] Ashurst, Wm. T., private communication.

[2.18] Seshadri, K., Twenty-Sixth Symposium (International) on Combustion, The Combustion Institute, Pittsburgh, 1996, pp. 831–846.

[2.19] Gibson, C. H., Phys.Fluids **11**:2316–2327 (1968).

[2.20] Joulin, G., Combust. Sci. and Tech. **97**:219–229 (1994).

[2.21] Abdel-Gayed, R. G., Bradley, D., Phil.Trans.R.Soc.Lond. **A301**:1–25 (1981).

[2.22] Bray, K. N. C. and Peters, N., In "Turbulent Reacting Flows" (P. A. Libby and F. A. Williams Eds.) Academic Press, 1994, pp. 63–113.

[2.23] Wirth, M., Peters, N., Twenty-Fourth Symposium (International) on Combustion, The Combustion Institute, Pittsburgh, 1992, pp. 493–501.

[2.24] Wirth, M., Keller, P. and Peters, N., SAE-paper 932646 (1993).

Lecture 3

Non-Premixed Turbulent Combustion

A process where the mixing of fuel and oxidizer occurs simultaneously with combustion is called non-premixed combustion. Typical examples are fires and combustion in furnaces and in Diesel engines. As it was noted in lecture 1, combustion is nearly always fast compared to molecular mixing and therefore takes place in layers that are much thinner than the typical scales of turbulence. Under these conditions the flamelet concept for non-premixed combustion is applicable. This concept has been presented in previous reviews [3.1], [3.2]. For the case of a one-step reaction it may be viewed as a non-equilibrium derivation from the classical Burke-Schumann limit. However, the concept is much more general and may be used with detailed chemistry and for cases far from equilibrium. We will base this lecture essentially on the flamelet approach.

A very important quantity for the theory of non-premixed combustion is the mixture fraction Z which plays a similar role as the distance function G does in premixed combustion. Therefore, before going into the description of current modelling approaches we will present the mixture fraction as an independent coordinate of the Burke-Schumann solution.

3.1 The Mixture Fraction Coordinate and the Burke-Schumann Solution

The definition of the mixture fraction is best derived for a homogeneous system in the absence of diffusion. Then, by writing the global reaction equation for complete combustion of a hydrocarbon fuel, for instance, as

$$\nu'_{\mathrm{F}}\,\mathrm{F} + \nu'_{\mathrm{O_2}}\mathrm{O_2} \rightarrow \nu''_{\mathrm{CO_2}}\,\mathrm{CO_2} + \nu''_{\mathrm{H_2O}}\,\mathrm{H_2O}$$

one defines the stoichiometric coefficients ν'_{F} and $\nu'_{\mathrm{O_2}}$. The reaction equation relates to each other the changes of mass fraction of oxygen $dY_{\mathrm{O_2}}$ and fuel dY_{F} by

$$\frac{dY_{\mathrm{O_2}}}{\nu'_{\mathrm{O_2}} W_{\mathrm{O_2}}} = \frac{dY_{\mathrm{F}}}{\nu'_{\mathrm{F}} W_{\mathrm{F}}} \tag{3.1}$$

where W_i is the molecular weight. For a homogeneous system this equation may be integrated to

$$\nu Y_{\mathrm{F}} - Y_{\mathrm{O_2}} \;=\; \nu Y_{\mathrm{F},u} - Y_{\mathrm{O_2},u} \;, \tag{3.2}$$

where $\nu = \nu'_{\mathrm{O_2}} W_{\mathrm{O_2}} / \nu'_{\mathrm{F}} W_{\mathrm{F}}$ is the stoichiometric oxidizer-to-fuel mass ratio and the subscript u denotes the initial conditions in the unburnt mixture. The mass fractions Y_{F} and $Y_{\mathrm{O_2}}$ correspond to any state of combustion between the unburnt and the burnt state. If the diffusivities of fuel and oxidizer are equal, (3.2) can also be used for spatially non-homogeneous systems such as diffusion flames.

In a two-feed system, subscript 1 denotes the fuel stream with mass flux $\dot{m}_1$ and subscript 2 denotes the oxidizer stream with mass flux $\dot{m}_2$ into the system. Then the mixture fraction is defined as the local mass fraction of all elements within the mixture originating from the fuel feed

$$Z = \frac{\dot{m}_1}{\dot{m}_1 + \dot{m}_2} \;. \tag{3.3}$$

Both fuel and oxidizer streams may contain inerts such as nitrogen. The local mass fraction $Y_{\mathrm{F},u}$ of the fuel is the same fraction as in the original fuel stream, so

$$Y_{\mathrm{F},u} = Y_{\mathrm{F},1} Z \;, \tag{3.4}$$

where $Y_{\mathrm{F},1}$ denotes the mass fraction of fuel in the fuel stream. Similarly, since $1 - Z$ represents the mass fraction of the oxidizer stream locally in the unburnt mixture, one obtains for the local mass fraction of oxygen

$$Y_{\mathrm{O_2},u} \;=\; Y_{\mathrm{O_2},2}(1 - Z) \;, \tag{3.5}$$

where $Y_{\mathrm{O_2},2}$ represents the mass fraction of oxygen in the oxidizer stream ($Y_{\mathrm{O_2},2} = 0.232$ for air). Introducing (3.4) and (3.5) into (3.2) one obtains for the mixture fraction at any state of combustion

$$Z \;=\; \frac{\nu Y_{\mathrm{F}} - Y_{\mathrm{O_2}} + Y_{\mathrm{O_2},2}}{\nu Y_{\mathrm{F},1} + Y_{\mathrm{O_2},2}} \;. \tag{3.6}$$

Since a stoichiometric mixture is defined by $\nu Y_{\mathrm{F}} = Y_{\mathrm{O_2}}$ the stoichiometric mixture fraction is

$$Z_{\mathrm{st}} \;=\; \left[1 + \frac{\nu Y_{\mathrm{F},\,1}}{Y_{\mathrm{O_2},2}}\right]^{-1} \;. \tag{3.7}$$

For pure fuels ($Y_{\mathrm{F},1} = 1$) mixed with air the stoichiometric mixture fraction is, for instance 0.0284 for H_2, 0.055 for CH_4, 0.0635 for C_2H_4, 0.0601 for C_3H_8 and

0.072 for C_2H_2. This indicates that typically 20 times the mass of air, compared to the fuel, is needed to obtain a stoichiometric mixture.

The mixture fraction is a quantity that is conserved during combustion. It can be related to the fuel-air equivalence ratio which is defined as the fuel-to-air ratio in the unburnt mixture normalized by that of a stoichiometric mixture

$$\phi = \frac{Y_{\mathrm{F},u}/Y_{\mathrm{O}_2,u}}{(Y_{\mathrm{F},u}/Y_{\mathrm{O}_2,u})_{\mathrm{st}}} = \frac{\nu\, Y_{\mathrm{F},u}}{Y_{\mathrm{O}_2,u}} \,. \tag{3.8}$$

Introducing (3.4) and (3.5) into (3.8) leads to

$$\phi = \frac{Z}{1-Z}\frac{(1-Z_{\mathrm{st}})}{Z_{\mathrm{st}}} \,. \tag{3.9}$$

In the limit of infinitely fast chemistry the reaction zone is an infinitely thin layer at $Z = Z_{\mathrm{st}}$. Outside of this layer the temperature is a piecewise linear function of Z. When the profiles of temperature and mass fractions are plotted as a function of mixture fraction, one obtains the Burke-Schumann solution.

$$\begin{aligned} T(Z) &= T_u(Z) + \frac{(-\Delta H)Y_{\mathrm{F},1}}{c_p \nu'_{\mathrm{F}} W_{\mathrm{F}}}\, Z \,, \quad Z \le Z_{\mathrm{st}} \\ T(Z) &= T_u(Z) + \frac{(-\Delta H)Y_{\mathrm{O},2}}{c_p \nu'_{\mathrm{O}_2} W_{\mathrm{O}_2}}(1-Z) \,, \quad Z \ge Z_{\mathrm{st}} \\ T_u(Z) &= T_2 + Z(T_1 - T_2) \,. \end{aligned} \tag{3.10}$$

The quantity $(-\Delta H)$ may be identified as the heat of reaction, since the reaction enthalpy ΔH is negative for exothermic reactions. Both, $(-\Delta H)$ and the specific heat c_p have been assumed to be constant. The maximum temperature at $Z = Z_{\mathrm{st}}$ is obtained from (3.10) as

$$\begin{aligned} T_{\mathrm{st}} &= T_u(Z_{\mathrm{st}}) + \frac{(-\Delta H)Y_{\mathrm{F},1}}{c_p \nu'_{\mathrm{F}} W_{\mathrm{F}}} Z_{\mathrm{st}} \\ &= T_u(Z_{\mathrm{st}}) + \frac{(-\Delta H)Y_{\mathrm{O},2}}{c_p \nu'_{\mathrm{O}_2} W_{\mathrm{O}_2}}(1-Z_{\mathrm{st}}) \end{aligned} \tag{3.11}$$

The mass fractions of the reactants are also piecewise linear functions of Z

$$\begin{aligned} Y_{\mathrm{O}_2} &= Y_{\mathrm{O}_2,2}\left(1 - \frac{Z}{Z_{\mathrm{st}}}\right) \,, \quad Z \le Z_{\mathrm{st}} \\ Y_{\mathrm{F}} &= Y_{\mathrm{F},1}\frac{Z - Z_{\mathrm{st}}}{1 - Z_{\mathrm{st}}} \,, \quad Z \ge Z_{\mathrm{st}} \,. \end{aligned} \tag{3.12}$$

The mass fractions of product species may be written similarly. The Burke-Schumann solution is shown in Fig. 3.1.

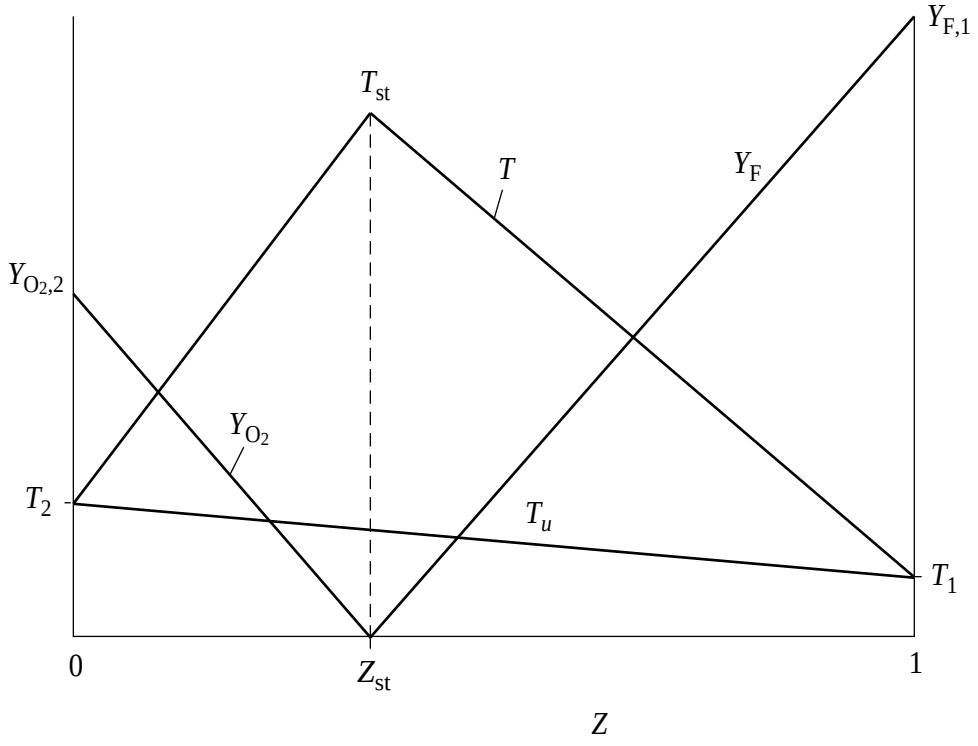

Figure 3.1: The Burke-Schumann solution as a function of mixture fraction.

3.2 Flamelet Structure of a Diffusion Flame

Different from previous formulations we will interpret Z similar to G as a variable that fixes the location of the thin reaction zone, namely at

$$Z(\mathbf{x}, t) = Z_{\text{st}} \ . \tag{3.13}$$

We do not explicitly relate Z to any combinations of mass fractions, but define it as the solution of a convective diffusive equation

$$\rho \frac{\partial Z}{\partial t} + \rho \mathbf{v} \cdot \nabla Z = \nabla \cdot (\rho D \nabla Z) \tag{3.14}$$

which has no chemical source term. The diffusion coefficient D in this equation is in principle arbitrary, but it is convenient to set it equal to the thermal diffusivity

$$D = \frac{\lambda}{\rho c_p} = D_T \ . \tag{3.15}$$

Here λ is the thermal conductivity. Independent of (3.14) the reactive-diffusive structure of the flamelet is determined by the equations for the
mass fractions Y_i

$$\rho \frac{\partial Y_i}{\partial t} + \rho \mathbf{v} \cdot \nabla Y_i = \frac{1}{\text{Le}_i} \nabla \cdot (\rho D_T \nabla Y_i) + \dot{m}_i \quad (i = 1, 2, \ldots, n) \tag{3.16}$$

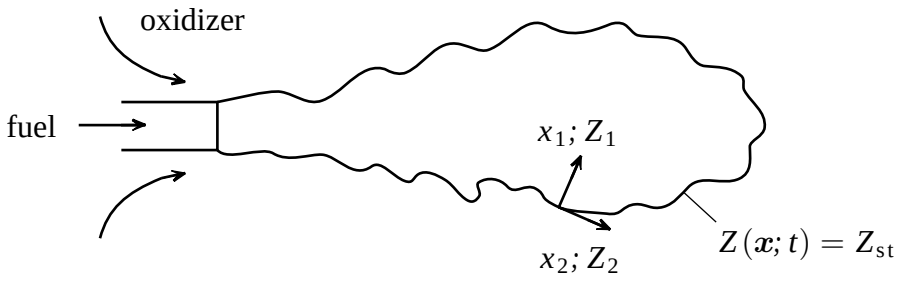

Figure 3.2: Surface of stoichiometric mixture in a turbulent jet.

and the temperature

$$\rho c_p \frac{\partial T}{\partial t} + \rho c_p \mathbf{v} \cdot \nabla T = \nabla \cdot (\rho c_p D_T \nabla T) - \sum_{i=1}^{n} h_i \dot{m}_i + q_R + \frac{\partial p}{\partial t} \; . \qquad (3.17)$$

In these equations $\dot{m}_i$ denotes the chemical source term of species i and $\sum_{i=1}^{n} h_i \dot{m}_i$ the heat release rate. We have assumed the Lewis numbers for all species

$$\mathrm{Le}_i = \frac{\lambda}{\rho c_p D_i} = \frac{D_T}{D_i} \quad (i = 1, 2, \ldots, n) \qquad (3.18)$$

to be constant. In the temperature equation the low Mach number limit leading to zero spatial pressure gradients has been employed, but the temporal pressure change $\partial p/\partial t$ has been retained. The heat capacity c_p is assumed to be constant for simplicity. Finally, q_R denotes the heat loss due to radiation which in many cases can be calculated by using the thin gas approximation.

We assume the mixture fraction Z to be given in the flow field as a function of space and time by solution of (3.14). Then the surface of the stoichiometric mixture can be determined from (3.13). This is shown schematically in Fig. 3.2 for a turbulent jet flame. Fuel and oxidizer interdiffuse at the lip of the nozzle. The surface of stoichiometric mixture starts there and is highly convoluted by the turbulent flow.

In turbulent combustion we are not so much interested in the instantaneous flame location, but in mean quantities. Modelling of (3.14) in a similar way as in (1.17) and (1.18) leads to the equation for the Favre mean mixture fraction

$$\bar{\rho} \frac{\partial \widetilde{Z}}{\partial t} + \bar{\rho} \overline{\mathbf{v}} \cdot \nabla \widetilde{Z} = \nabla \cdot (\bar{\rho} D_t \nabla \widetilde{Z}) \; . \qquad (3.19)$$

Since the molecular diffusivity D in (3.14) is typically much smaller than the turbulent diffusivity D_t, it has been neglected in (3.19). Therefore the arbitrariness of the choice of D has no influence on the mean mixture fraction and the mean flame contour given by $\widetilde{Z}(\mathbf{x}, t) = Z_{\mathrm{st}}$.

In addition to the mean mixture fraction we need an equation for the Favre variance $\widetilde{Z''^2}$ which is modelled by standard procedures as

$$\bar{\rho}\frac{\partial \widetilde{Z''^2}}{\partial t} + \bar{\rho}\overline{\mathbf{v}} \cdot \nabla \widetilde{Z''^2} = \nabla \cdot \left(\bar{\rho} D_t \nabla \widetilde{Z''^2}\right) + 2\bar{\rho} D_t (\nabla \widetilde{Z})^2 - \bar{\rho}\widetilde{\chi} \ . \tag{3.20}$$

Here $\widetilde{\chi}$ is the mean scalar dissipation rate, which is defined as

$$\widetilde{\chi} = 2\, D(\nabla \widetilde{Z''})^2 \tag{3.21}$$

and will be modelled similar to (2.83) as

$$\widetilde{\chi} = c_\chi \frac{\tilde{\varepsilon}}{\tilde{k}} \widetilde{Z''^2} \tag{3.22}$$

where $c_\chi = 2.0$.

Let us locally introduce an orthogonal coordinate system x_1, x_2, x_3, t attached to the surface of stoichiometric mixture as shown in Fig. 3.2, where x_1 points normal to the surface $Z(x_\alpha, t) = Z_{\text{st}}$ and x_2 and x_3 lie within the surface. We replace the coordinate x_1 by the mixture fraction Z and x_2, x_3 and t by $Z_2 = x_2$, $Z_3 = x_3$ and $\tau = t$. By definition the new coordinate Z is locally normal to the surface of stoichiometric mixture. With the transformation rules

$$\begin{aligned}
\frac{\partial}{\partial t} &= \frac{\partial}{\partial \tau} + \frac{\partial Z}{\partial t}\frac{\partial}{\partial Z}\,, \\
\frac{\partial}{\partial x_k} &= \frac{\partial}{\partial Z_k} + \frac{\partial Z}{\partial x_k}\frac{\partial}{\partial Z}\ , \quad (k = 2, 3) \\
\frac{\partial}{\partial x_1} &= \frac{\partial Z}{\partial x_1}\frac{\partial}{\partial Z}
\end{aligned} \tag{3.23}$$

we obtain the temperature equation in the form

$$\begin{aligned}
&\rho c_p \left(\frac{\partial T}{\partial \tau} + v_2 \frac{\partial T}{\partial Z_2} + v_3 \frac{\partial T}{\partial Z_3}\right) - \sum_{k=2}^{3} \frac{\partial(\rho c_p D_T)}{\partial x_k}\frac{\partial T}{\partial Z_k} \\
&-\rho c_p D_T \left[(\nabla Z)^2 \frac{\partial^2 T}{\partial Z^2} + 2\sum_{k=2}^{3}\frac{\partial Z}{\partial x_k}\frac{\partial^2 T}{\partial Z \partial Z_k} + \sum_{k=2}^{3}\frac{\partial^2 T}{\partial Z_k^2}\right] \\
&+ \left\{\rho\frac{\partial Z}{\partial t} + \rho \mathbf{v}\cdot\nabla Z - \nabla\cdot(\rho D_T \nabla Z)\right\} c_p \frac{\partial T}{\partial Z} = -\sum_{i=1}^{n} h_i \dot{m}_i + q_R + \frac{\partial p}{\partial t}\,.
\end{aligned} \tag{3.24}$$

A similar form can be derived for the species equations. In the species equations, however, D_i appears instead of D_T. It is immediately seen that due to (3.14) the term in braces on the l.h.s drops out in the temperature equation if one assumes $D = D_T$, but the corresponding term cannot be neglected in the species equations.

If the flamelet is thin in the Z direction, an order-of-magnitude analysis shows that the second derivative with respect to Z is the dominating term on the left-hand side of (3.24). This term must balance the terms on the right-hand side. All other terms containing spatial derivatives in Z_2 and Z_3 directions can be neglected to leading order. This is equivalent to the assumption that the temperature derivatives normal to the flame surface are much larger than those in tangential direction. The term containing the time derivative is important if the flamelet undergoes rapid changes, such as ignition or extinction events. It is also necessary to satisfy initial conditions if those are not equal to the steady state solution. This will be discussed below.

Neglecting the terms containing derivatives in Z_2 and Z_3 direction, one obtains the one-dimensional time-dependent temperature equation

$$\rho c_p \frac{\partial T}{\partial t} - \rho c_p \frac{\chi_{\mathrm{st}}}{2} \frac{\partial^2 T}{\partial Z^2} = -\sum_{i=1}^{n} h_i \dot{m}_i + q_R + \frac{\partial p}{\partial t} \,. \tag{3.25}$$

This equation is valid in the vicinity of stoichiometric mixture. We have introduced the quantity

$$\chi_{\mathrm{st}} = 2 D_T \left(\frac{\partial Z}{\partial x_\alpha} \right)^2_{\mathrm{st}} \tag{3.26}$$

as the instantaneous scalar dissipation rate at stoichiometric conditions. For turbulent non-premixed combustion it must be replaced by a conditional average value $\widetilde{\chi}_{\mathrm{st}}$. It has the dimension 1/s and may be interpreted as the inverse of a characteristic diffusion time. It may depend on t and Z and acts as a prescribed parameter in (3.25), representing the flow and the mixture field. As a result of the transformation, it implicitly incorporates the influence of convection and diffusion normal to the surface of stoichiometric mixture. In the limit $\chi \to 0$, the temperature equation for the homogeneous reactor is obtained.

The corresponding equations for the species are similarly

$$\rho \frac{\partial Y_i}{\partial t} - \frac{\rho}{\mathrm{Le}_i} \frac{\chi_{\mathrm{st}}}{2} \frac{\partial^2 Y_i}{\partial Z^2} + \left\{ \rho \frac{\partial Z}{\partial t} + \rho \mathbf{v} \cdot \nabla Z - \nabla \cdot (\rho D_i \nabla Z) \right\} \frac{\partial Y_i}{\partial Z} = \dot{m}_i \,. \tag{3.27}$$

The term in braces may be expressed in a more convenient form. Since, by exchanging the dependent variables, a second derivative d^2y/dx^2 may be transformed to $(dz^2/dy)/2$ with $z = dy/dx$, we obtain with (3.14) for that term

$$\begin{aligned} \left\{ \left(1 - \frac{1}{\mathrm{Le}_i} \right) \nabla (\rho D_T \nabla Z) \right\} &= \left(1 - \frac{1}{\mathrm{Le}_i} \right) \left\{ \nabla Z \cdot \frac{\partial}{\partial Z} (\rho D_T \nabla Z) \right\} \\ &= \frac{1}{4} \left(1 - \frac{1}{\mathrm{Le}_i} \right) \frac{\partial \rho \chi_{\mathrm{st}}}{\partial Z} \end{aligned} \tag{3.28}$$

where ρD_T has been assumed to be constant for simplicity. For the case of non-unity Lewis numbers the flamelet equations for the chemical species can therefore be written

$$\rho\frac{\partial Y_i}{\partial t}-\frac{\rho}{\mathrm{Le}_i}\frac{\chi_{\mathrm{st}}}{2}\frac{\partial^2 Y_i}{\partial Z^2}+\frac{1}{4}\left(1-\frac{1}{\mathrm{Le}_i}\right)\frac{\partial\rho\chi_{\mathrm{st}}}{\partial Z}\frac{\partial Y_i}{\partial Z}=\dot{m}_i\ . \tag{3.29}$$

The last term in this expression accounts for differential diffusion effects. Here the gradient of the scalar dissipation rate acts as a velocity in mixture fraction space. However, it should be noted that the assumption of constant Lewis numbers different from unity conflicts with the requirement that the sum of the diffusion fluxes should be zero. Therefore, if the binary diffusion approximation is used, correction terms must be considered that lead to much more complicated expressions than (3.29). Species equations containing those expressions are derived in [3.3]. These equations should be used to correctly account for differential diffusion effects when flamelet profiles are calculated with the mixture fraction as independent variable. A procedure to avoid this difficulty is to calculate species and temperature profiles in physical space, for a counterflow flame for example, and solve (3.14) simultaneously [3.4]. Then the scalar profiles may be plotted as a function of Z.

In [3.5] the counterflow diffusion flame in the stagnation region of a porous cylinder has been calculated using the four-step reduced mechanism

$$\begin{aligned}\mathrm{CH_4+2H+H_2O} &= \mathrm{CO+4H_2}\\ \mathrm{CO+H_2O} &= \mathrm{CO_2+H_2}\\ \mathrm{H+H+M} &= \mathrm{H_2+M}\\ \mathrm{O_2+3H_2} &= \mathrm{2H+2H_2O}\ .\end{aligned}$$

This flow configuration, used by Tsuji and Yamaoka [3.6] has the advantage that a similarity transformation can be formulated in order to derive a system of one-dimensional equations.

Temperature and fuel and oxygen mass fractions profiles from numerical simulation are plotted in Figs. 3.3 and 3.4 as a function of mixture fraction for the strain rates of $a = 100$/s and $a = 400$/s where a is the velocity gradient. Here the mixture fraction was calculated from the chemical species using the definition [3.7]

$$Z=\frac{2\,Z_{\mathrm{C}}/M_{\mathrm{C}}+\frac{1}{2}Z_{\mathrm{H}}/M_{\mathrm{H}}+(Z_{\mathrm{O,O}}-Z_{\mathrm{O}})/M_{\mathrm{O}}}{2\,Z_{\mathrm{C,F}}/M_{\mathrm{C}}+\frac{1}{2}Z_{\mathrm{H,F}}/M_{\mathrm{H}}+Z_{\mathrm{O,O}}/M_{\mathrm{O}}} \tag{3.30}$$

where Z_m is the mass fraction of the element m, $Z_{m,\mathrm{F}}$ is the mass fraction of the element m in the fuel stream, and $Z_{m,\mathrm{O}}$ is the mass fraction of the element m in the oxidant stream. The higher value of the strain rate in Figs. 3.3 and 3.4 corresponds to a condition close to extinction. It is seen that the temperature in the reaction zone decreases and the oxygen leakage through the reaction zone increases as extinction is approached.

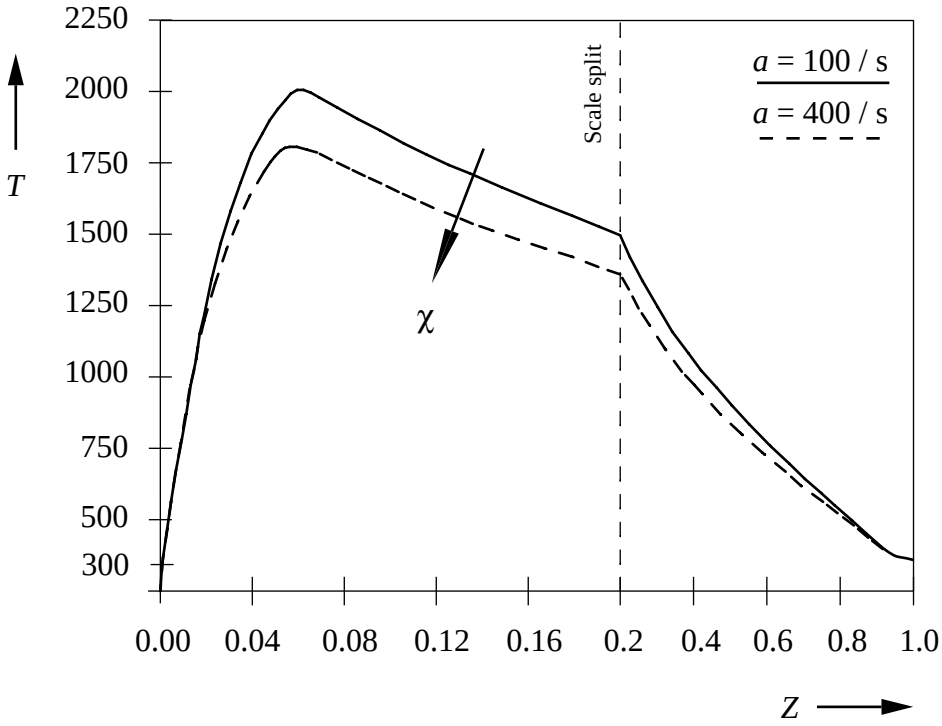

Figure 3.3: Temperature profiles of methane-air diffusion flames for strain rates of $a = 100$/s and $a = 400$/s as a function of mixture fraction.

For the counter-flow geometry, the scalar dissipation rate may be approximated as a function of mixture fraction diffusivity, assuming constant density and diffusivity, by

$$\chi = \frac{a}{\pi} \exp\{-2[\mathrm{erfc}^{-1}(2Z)]^2\} \approx 4aZ^2[\mathrm{erfc}^{-1}(2Z)]^2 \qquad (3.31)$$

where erfc^{-1} is the inverse of the complementary error function. For example, $(\mathrm{erfc}^{-1}(2Z))$ is 1.13 for methane-air flames at $Z = 0.055$. The second expression in (3.31) is derived using an approximation of the error function for small values of Z. It shows that χ is proportional to Z^2 for small Z but it becomes inaccurate even at Z as small as 0.05. For a non-constant density profile, which is typical for diffusion flames, (3.31) was improved to [3.8]

$$\chi(Z) = \frac{a_\infty}{4\pi} \frac{3\left(\sqrt{\rho_\infty/\rho}+1\right)^2}{2\sqrt{\rho_\infty/\rho}+1} \exp\left\{-2\left[\mathrm{erfc}^{-1}(2Z)\right]^2\right\} . \qquad (3.32)$$

Extinction of a CH_4-air counter-flow flame occurs approximately at a strain rate of $a = 550$/s. With (3.31) this corresponds to a scalar dissipation rate at quenching conditions of $\chi_q = 13.6$/s. At these values heat release by chemistry just balances heat loss by diffusion imposed by the flow. This corresponds to the situation in

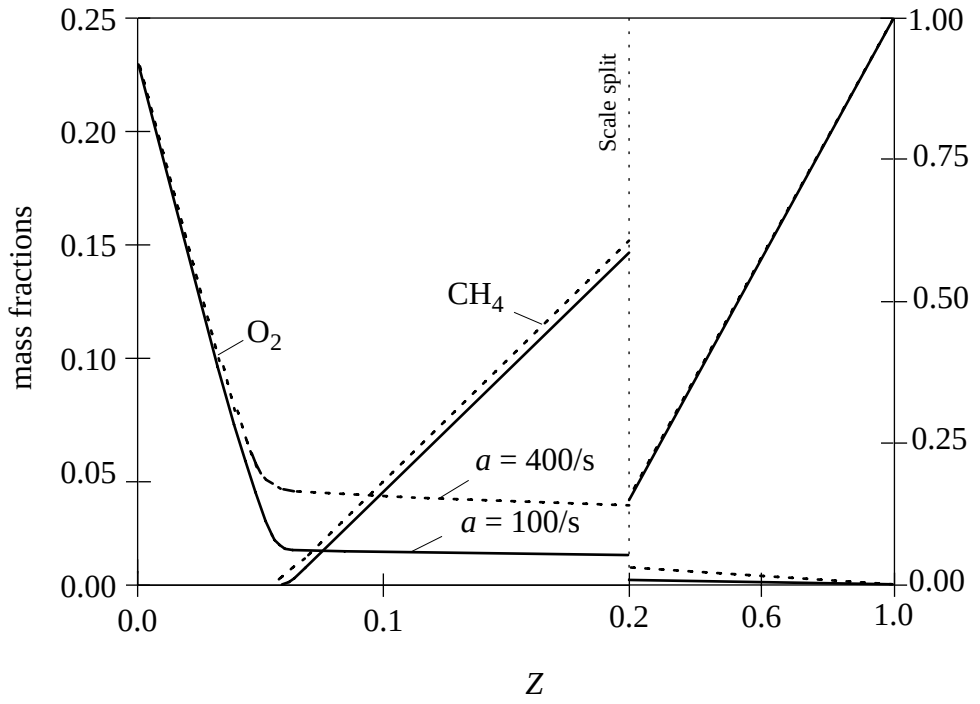

Figure 3.4: Fuel and oxygen mass fractions for strain rates of $a = 100$/s and $a = 400$/s as a function of mixture fraction.

premixed flames, where the burning velocity is such that heat release in the reaction zone just balances heat loss by diffusion towards the unburnt mixture.

The flamelet equations may also be used to describe ignition in a non-premixed system. If fuel and oxidizer are initially at the unburnt temperature $T_u(Z)$, as shown in Fig. 3.1, but sufficiently close to the ignition temperature, heat release by chemical reactions will lead to a thermal runaway. This auto-ignition process occurs in Diesel engines, where the air is heated by compression to temperatures of about 800K. During mixing the scalar dissipation rate decreases until it reaches the ignition value χ_i. For values larger than χ_i, heat loss out of the reaction zone is larger than the heat release by chemical reactions, thereby restricting the temperature rise and preventing a thermal runaway. This corresponds to a steady state condition.

The solution of the steadystate flamelet equations is shown schematically in Fig. 3.5. Here the maximum temperature is plotted as a function of the inverse of the scalar dissipation rate. The lower branch corresponds to the non-reacting flamelet prior to ignition. As the scalar dissipation rate is decreased the ignition point I is reached. For values smaller than χ_i a rapid unsteady transition to the upper burning branch occurs. If one starts on the burning branch and increases the dissipation rate moving to the left, one reaches the point Q where quenching occurs. This diagram is called the S-shaped curve. The middle branch between the point I and Q is unstable and therefore has no physical significance.

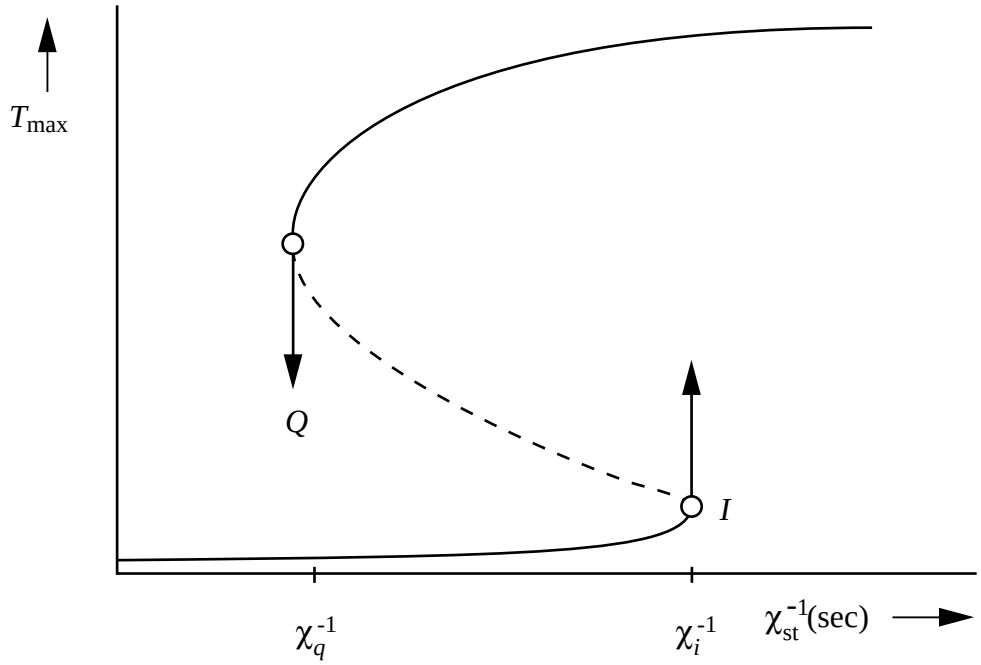

Figure 3.5: The S-shaped curve showing the maximum temperature in a diffusion flame as a function of the inverse of the scalar dissipation rate at stoichiometric mixture.

3.3 Diffusion Flamelets in Turbulent Combustion

The flamelet concept views a turbulent diffusion flame as an ensemble of laminar diffusion flamelets. The main advantage of the flamelet concept is the fact that chemical time and length scales need not be resolved ina multi-dimensional CFD code. In addition to the continuity, momentum and energy equations, equations describing turbulence quantities like $\widetilde{k}$ and $\widetilde{\varepsilon}$ and thereby the turbulent length and time scales, the balance equations for the mean mixture fraction (3.19) and the mixture fraction variance (3.20) need to be solved numerically. The flamelet structure can be calculated as a function of prescribed parameters by solving the one-dimensional equations (3.25) and (3.27). These solutions may be available either in form of steady state flamelet libraries or from an instationary calculation. The latter is used in the interactive approach [3.10] shown in Fig.3.6, where the time-dependent parameters $\widetilde{\chi}_{st}(t)$, $\tilde{p}(t)$, $T_1(t) = \widetilde{T}_{fuel}(t)$ and $T_2(t) = \widetilde{T}_{ox}(t)$ are fed into the flamelet code from the CFD code. Then the flamelet solution provides all scalars as functions of the mixture fraction at each time step. Mean values of these scalars may then be obtained by using the presumed pdf approach, where $\widetilde{P}(Z)$ is calculated from (1.26) for the given values of $\widetilde{Z}(\mathbf{x}, t)$ and $\widetilde{Z''^2}(\mathbf{x}, t)$ and equations like (1.28) are used to calculate the mean temperature and species mass fractions.

In previous presentations [3.1] the enthalpy h has been related to the mixture

fraction by the coupling relation

$$h = h_2 + Z(h_1 - h_2) \; . \tag{3.33}$$

For a general formulation, however, it is preferable to include the enthalpy as an additional variable modelled by the equation

$$\overline{\rho}\,\frac{\partial \widetilde{h}}{\partial t} + \overline{\rho}\,\widetilde{v}_\alpha\,\frac{\partial \widetilde{h}}{\partial x_\alpha} = \frac{\partial}{\partial x_\alpha}\left(\overline{\rho}\,\frac{\tilde{\nu}_t}{\mathrm{Pr}}\frac{\partial \tilde{h}}{\partial x_\alpha}\right) + \frac{\partial \overline{p}}{\partial t} - \overline{q_R}\,. \tag{3.34}$$

Here Pr is a turbulent Prandtl number. The terms containing the mean spatial pressure gradient have been neglected in the limit of zero Mach number, when fast acoustic waves are rapidly homogenizing the pressure field. The term describing temporal mean pressure changes $\partial\overline{p}/\partial t$ is important in internal combustion engines operating under non-premixed conditions, such as the Diesel engine. Also the mean volumetric heat loss term must be retained if radiative heat exchange has an influence on the local enthalpy balance. This may well be the case in large furnaces where it influences the prediction of NO_x formation which is very sensitive to temperature. Changes of the mean enthalpy may also occur due to heat loss at the boundaries and due to evaporation of a liquid fuel in a Diesel engine. Under these conditions the mean enthalpy can no longer be coupled to the mean mixture fraction by a linear relation analogue to (3.33).

No equation for enthalpy fluctuations is written here. In non-premixed turbulent combustion fluctuations of the enthalpy are mainly due to mixture fraction fluctuations and are described by those.

In (3.19), (3.20) and (3.34) diffusive terms containing molecular diffusivities have been neglected as small compared to the turbulent transport terms in the large Reynolds number limit. Diffusive effects have only been retained in the mean scalar dissipation $\widetilde{\chi}$ which is modelled by (3.22). Effects due to non-unity Lewis numbers on the mean mixture fraction and its variance are difficult to quantify and will also be neglected here.

An important additional quantity that needs modelling is the conditional scalar dissipation rate $\widetilde{\chi}_{\mathrm{st}}$. Equations (3.31) and (3.32) show that there is a dependence of the scalar dissipation rate on the mixture fraction. Since a CFD code will only provide the unconditioned average $\widetilde{\chi}$, for instance from (3.22), there is a need to relate $\widetilde{\chi}_{\mathrm{st}}$ to $\tilde{\chi}$ by using the information provided by (3.31) and (3.32). We may express (3.31) in the form

$$\chi(Z) = \chi(Z_{\mathrm{st}})\frac{f(Z)}{f(Z_{\mathrm{st}})} \tag{3.35}$$

where $f(Z)$ is the exponential term in (3.31). Then, as suggested by Hellström [3.9] one obtains the average

$$\widetilde{\chi} = \int_0^1 \chi(Z)\widetilde{P}(Z)dZ = \chi(Z_{\mathrm{st}})\int_0^1 \frac{f(Z)}{f(Z_{\mathrm{st}})}\widetilde{P}(Z)dZ \tag{3.36}$$

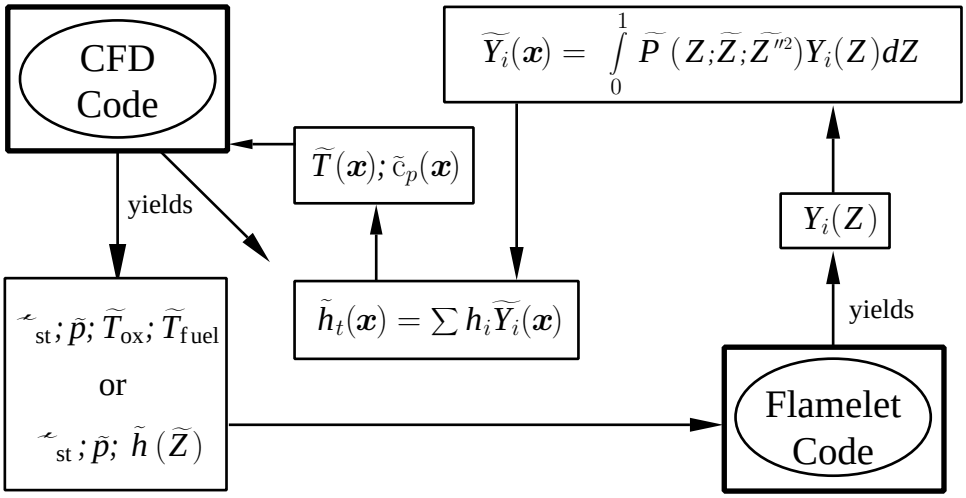

Figure 3.6: Code structure of Representative Interactive Flamelet concept.

which is given by (3.22). Therefore, the scalar dissipation at stoichiometric conditions $\widetilde{\chi}_{st} = \chi(Z_{st})$ can be expressed as

$$\widetilde{\chi}_{st} = \frac{c_\chi \frac{\tilde{\varepsilon}}{\tilde{k}} \widetilde{Z''^2}}{\int_0^1 \frac{f(Z)}{f(Z_{st})} \widetilde{P}(Z) dZ} \,. \tag{3.37}$$

Since the r.h.s describes averaged quantities, this may be interpreted as the conditional average value $\widetilde{\chi}_{st}$ required in the flamelet equations.

3.4 Turbulent Jet Diffusion Flames

Turbulent diffusion flames owe their name to the rate-determining mechanism that controls the combustion in many applications: laminar and turbulent diffusion. In technical furnaces, but also in gas turbine combustion chambers fuel and oxidizer are injected separately. Mixing then occurs essentially by turbulent diffusion. But only when fuel and oxidizer are mixed at the molecular scales, combustion can take place.

In many applications fuel enters into the combustion chamber as a turbulent jet, with or without swirl. To provide an understanding of the basic properties of jet diffusion flames, we will consider here at first the easiest case, the round jet flame into still air without buoyancy, for which we can obtain approximate analytical solutions to determine the flame length of a jet diffusion flame. The flame length is defined as the distance from the nozzle on the centerline of the flame to where the mean mixture fraction is equal to the stoichiometric value Z_{st}.

The flow configuration and the flame contour of a vertical jet diffusion flame are shown in Fig. 3.7. We consider a fuel jet issuing from a round nozzle with diameter d and exit velocity u_0 into quiescent air. The indices 0 and ∞ denote conditions at the nozzle and in the ambient air, respectively. Later on buoyancy will be included but then we restrict the analysis to a vertical jet.

With these assumptions we obtain a two-dimensional axisymmetric problem governed by equations for

Continuity

$$\frac{\partial}{\partial x}\left(\bar{\rho}\tilde{u}r\right) + \frac{\partial}{\partial r}\left(\bar{\rho}\tilde{v}r\right) = 0\,, \tag{3.38}$$

Momentum in x-direction

$$\bar{\rho}\tilde{u}r\frac{\partial\tilde{u}}{\partial x} + \bar{\rho}\tilde{v}r\frac{\partial\tilde{u}}{\partial r} = \frac{\partial}{\partial r}\left(\bar{\rho}\tilde{\nu}_t r\frac{\partial\tilde{u}}{\partial r}\right)\,, \tag{3.39}$$

Mean mixture fraction

$$\bar{\rho}\tilde{u}r\frac{\partial\tilde{Z}}{\partial x} + \bar{\rho}\tilde{v}r\frac{\partial\tilde{Z}}{\partial r} = \frac{\partial}{\partial r}\left(\frac{\bar{\rho}\tilde{\nu}_t r}{\mathrm{Sc}}\frac{\partial\tilde{Z}}{\partial r}\right)\,. \tag{3.40}$$

Here Sc is the turbulent Schmidt number. We have introduced the boundary layer assumption and neglected the viscous stress as compared to the Reynolds stress component which was modelled as

$$-\bar{\rho}\widetilde{u''v''} = \bar{\rho}\tilde{\nu}_t\frac{\partial\tilde{u}}{\partial r}\,. \tag{3.41}$$

We will not consider equations for $\tilde{k}$ and $\tilde{\varepsilon}$ or the mixture fraction variance but seek an approximate solution by introducing a model for the turbulent viscosity $\tilde{\nu}_t$. The system of equations may be reduced by introducing a similarity transformation [3.11]

$$\eta = \frac{\bar{r}}{\zeta}\,,\ \bar{r}^2 = 2\int_0^r \frac{\bar{\rho}}{\rho_\infty}r'\,dr'\,,\quad \zeta = x + x_0\,, \tag{3.42}$$

which contains a density transformation defining the density weighted radial coordinate $\bar{r}$. The new axial coordinate ζ starts from the virtual origin of the jet located at $x = -x_0$. With the stream function defined by

$$\bar{\rho}\tilde{u}r = \partial\psi/\partial r\,,\quad \bar{\rho}\tilde{v}r = -\partial\psi/\partial x \tag{3.43}$$

the continuity equation (3.38) is satisfied. Introducing the non-dimensional stream function

$$F(\xi,\eta) = \psi/\rho_\infty\nu_{tr}\zeta \tag{3.44}$$

one obtains with

$$\tilde{u} = \nu_{tr}F_\eta/\eta\zeta \quad \text{and} \quad \bar{\rho}\widetilde{v}r = -\rho_\infty\nu_{tr}(\zeta F_\zeta + F - F_\eta\eta) \tag{3.45}$$

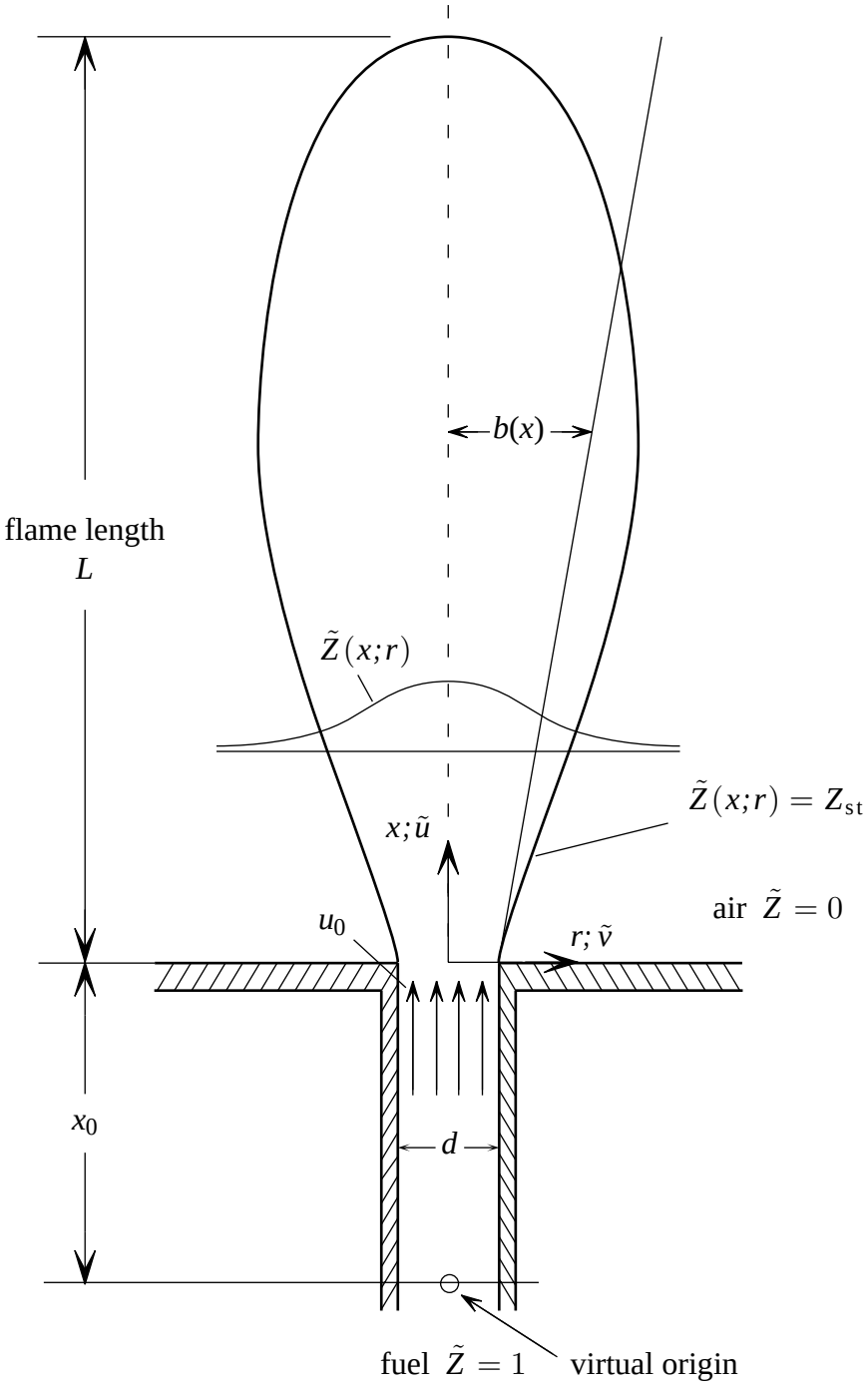

Figure 3.7: Schematic representation of a vertical jet flame into quiescent air.

in the similarity region of the jet

$$-\frac{\partial}{\partial\eta}\left(\frac{FF_\eta}{\eta}\right) = \frac{\partial}{\partial\eta}\left[C\eta\frac{\partial}{\partial\eta}\left(\frac{F_\eta}{\eta}\right)\right] \tag{3.46}$$

$$-\frac{\partial}{\partial\eta}(F\omega) = \frac{\partial}{\partial\eta}\left(\frac{C}{\mathrm{Sc}}\eta\frac{\partial\omega}{\partial\eta}\right) . \tag{3.47}$$

Here $\omega = \widetilde{Z}/\widetilde{Z}_{CL}$ stands for the mixture fraction normalized by that on the centerline.

The basic assumption introduced here is that the Chapman-Rubesin parameter

$$C = \frac{\bar{\rho}^2\tilde{\nu}_t r^2}{\rho_\infty^2\nu_{tr}\bar{r}^2} \tag{3.48}$$

is a constant in the entire jet. The reference eddy viscosity ν_{tr} is that of a jet with constant density. It is fitted to experimental data as

$$\nu_{tr} = \frac{u_0 d}{70} . \tag{3.49}$$

A similarity solution exists only for a zero free-stream velocity. Then one obtains

$$\begin{aligned} F &= C\gamma^2\eta^2/(1+(\gamma\eta)^2/4) \\ \omega &= (1+(\gamma\eta)^2/4)^{-2\mathrm{Sc}} . \end{aligned} \tag{3.50}$$

The axial velocity profile is then given by

$$\frac{\tilde{u}}{u_0} = \frac{2C\gamma^2\nu_{tr}}{\zeta}\left(1+\frac{(\gamma\eta)^2}{4}\right)^{-2} \tag{3.51}$$

where the jet spreading parameter

$$\gamma^2 = \frac{3\cdot 70^2}{64}\frac{\rho_0}{\rho_\infty C^2} \tag{3.52}$$

is obtained from the requirement of momentum conservation. The conservation of the mixture fraction on the centerline gives

$$\widetilde{Z}_{CL} = \frac{70(1+2\mathrm{Sc})}{32}\frac{\rho_0}{\rho_\infty C}\frac{d}{\zeta} \tag{3.53}$$

such that the mixture fraction profile is

$$\tilde{Z} = \frac{2.19\,(1+2\mathrm{Sc})\,d}{x+x_0}\frac{\rho_0}{\rho_\infty C}\left(1+\frac{(\gamma\eta)^2}{4}\right)^{-2\mathrm{Sc}} . \tag{3.54}$$

The flame length is obtained by setting $L = x$, $r = 0$ and $\tilde{Z} = Z_{\rm st}$

$$\frac{L + x_0}{d} = \frac{2.19(1 + 2{\rm Sc})}{Z_{\rm st}} \frac{\rho_0}{\rho_\infty C} \, . \tag{3.55}$$

Experimental data by [3.12] suggest that the flame length should scale as

$$\frac{L + x_0}{d} = \frac{5.3}{Z_{\rm st}} \left(\frac{\rho_0}{\rho_{\rm st}} \right)^{1/2} \, . \tag{3.56}$$

This fixes the turbulent Schmidt number as ${\rm Sc} = 0.71$ and the Chapman-Rubesin parameter as

$$C = \frac{(\rho_0 \rho_{\rm st})^{1/2}}{\rho_\infty} \, . \tag{3.57}$$

This may be introduced into (3.51) and (3.52) to obtain for the centerline velocity

$$\frac{\tilde{u}_{CL}}{u_0} = \frac{6.56\, d}{x + x_0} \left(\frac{\rho_0}{\rho_{\rm st}} \right)^{1/2} \, . \tag{3.58}$$

The distance of the virtual origin from $x = 0$ may be estimated by setting $\tilde{u}_{CL} = u_0$ at $x = 0$ in (3.58) so that

$$x_0 = 6.56\, d \left(\frac{\rho_0}{\rho_{\rm st}} \right)^{1/2} \, . \tag{3.59}$$

Since at the stoichiometric mixture the molecular weight is approximately that of nitrogen, the density ratio $\rho_0 / \rho_{\rm st}$ may be estimated as

$$\frac{\rho_0}{\rho_{\rm st}} = \frac{W_0}{W_{\rm N_2}} \frac{T_{\rm st}}{T_0} \, . \tag{3.60}$$

With the estimate $T_{\rm st} \approx 2000\,{\rm K}$ for methane this takes the value $\rho_0 / \rho_{\rm st} \sim 3.8$. The flame length may then be calculated with $Z_{\rm st} = 0.055$ as $L \sim 200\, d$.

3.5 Vertical Turbulent Jet Diffusion Flames with Buoyancy Effects

For flames with buoyancy effects a closed form solution of the governing equations cannot be derived. Here we seek an approximate solution by replacing the velocity and mixture fraction profiles by top hat profiles (cf. [3.13])

$$\tilde{u}, \tilde{Z} = \begin{cases} \hat{u}, \hat{Z} & \text{for } r \le b(x) \ ; \\ 0 & \text{for } r > b(x) \ , \end{cases} \tag{3.61}$$

where $b(x)$ is the half-width of the jet (cf. Fig. 3.7). The cross-sectional averages $\hat{u}(x)$, and $\hat{Z}(x)$ are defined by the area averages

$$\begin{aligned} \rho_\infty \hat{u}^2 b^2 &= 2\int_0^\infty \bar{\rho}\tilde{u}^2 r\, dr \\ \rho_\infty \hat{u} b^2 &= 2\int_0^\infty \bar{\rho}\tilde{u} r\, dr \\ \rho_\infty \hat{u}\hat{Z} b^2 &= 2\int_0^\infty \bar{\rho}\tilde{u}\tilde{Z} r\, dr\,. \end{aligned} \tag{3.62}$$

If the profiles are known, $\hat{u}$, $\hat{Z}$ and b can be calculated from (3.62). Introducing (3.51) and (3.54) into (3.62) leads for the non-buoyant jet flame to the solution

$$\begin{aligned} \frac{\hat{u}}{u_0} &= \hat{Z} = 2.19\frac{d}{x+x_0}\left(\frac{\rho_0}{\rho_{\rm st}}\right)^{1/2} \\ b(x) &= 0.23\, x\left(\frac{\rho_{\rm st}}{\rho_\infty}\right)^{1/2}. \end{aligned} \tag{3.63}$$

In order to derive an equation for the cross-sectional momentum we combine (3.38) and (3.39) and add for the case of a vertical jet flame the buoyancy term

$$\frac{\partial}{\partial x}(\bar{\rho}\tilde{u}^2 r) + \frac{\partial}{\partial r}(\bar{\rho}\tilde{u}\tilde{v} r) = \frac{\partial}{\partial r}\left(\bar{\rho}\tilde{\nu}_t r\frac{\partial \tilde{u}}{\partial r}\right) + r(\rho_\infty - \bar{\rho})g\,. \tag{3.64}$$

When this is integrated over r from $r = 0$ to $r = \infty$ the two terms containing radial derivatives disappear due to the boundary conditions $\tilde{v} = 0$ at $r = 0$, $\tilde{u} = 0$ at $r = \infty$ and $\partial\tilde{u}/\partial r = 0$ at $r = 0$ and $r = \infty$. We then obtain an integrated form of the momentum equation

$$\frac{d}{dx}[\hat{u}^2 b^2] = 2g\int_0^r \left(1 - \frac{\bar{\rho}}{\rho_\infty}\right) r\, dr\,. \tag{3.65}$$

Similarly, the integrated mixture fraction equation may be written as

$$\frac{d}{dx}\left[\hat{u}\hat{Z}b^2\right] = 0\,. \tag{3.66}$$

Applying the initial condition $\hat{Z} = 1$ at the nozzle, where $\widetilde{Z} = 1$, $\bar{\rho} = \rho_0$ and $\tilde{u} = u_0$ for r smaller than $d/2$ the right-hand side of $(3.62)_3$ is $\rho_0 u_0 d^2/4$, the integrated form of (3.66) is

$$\hat{u}\hat{Z}b^2 = \frac{d^2}{4}\frac{\rho_0}{\rho_\infty}u_0\,. \tag{3.67}$$

This allows to define an effective exit diameter as

$$d_{\text{eff}} = d \left(\frac{\rho_0}{\rho_\infty} \right)^{1/2} . \tag{3.68}$$

For a non-buoyant jet flame (3.65) can be integrated analytically

$$\hat{u}^2 b^2 = \frac{d^2}{4} \frac{\rho_0}{\rho_\infty} u_0^2 . \tag{3.69}$$

In the following we relate all velocities to the jet exit velocity and all lengths to the effective diameter. Then, with $u^* = \hat{u}/u_0$, $b^* = b/d_{\text{eff}}$, the solution for the velocity u^* from (3.69) may be written in terms of b^* as

$$u^* = \frac{1}{2\, b^*} . \tag{3.70}$$

The next step is to evaluate the half-width $b(x)$. We note that the spreading of turbulent jets is due to the entrainment of fluid from outside by large vortices generating an entrainment velocity v_e. Following a particle within the jet that moves with velocity $\hat{u}$ downstream one may, by dimensional analysis, relate the growth of the half-width to the entrainment velocity v_e as

$$\hat{u} \frac{db}{dx} \sim v_e . \tag{3.71}$$

The entrainment velocity is proportional to the velocity difference between the jet and its surrounding. Setting $v_e \sim \hat{u} - u_\infty$,where $u_\infty = 0$ for the jet into still air, we obtain the relation

$$\hat{u} \frac{db}{dx} = \beta \left(\hat{u} - u_\infty \right) , \tag{3.72}$$

where β is a proportionality constant. For a non-buoyant flame it follows from $(3.63)_2$ that $\beta = 0.23\, (\rho_{\text{st}}/\rho_\infty)^{1/2}$.

The flame length is defined by the location where $\tilde{Z}$ on the centerline is equal to Z_{st}. The area-averaged value $\hat{Z}$ is smaller than the centerline value, as $\hat{u}$ is smaller than the centerline velocity. Therefore, rather than using Z_{st} we use $\hat{Z} = Z_{\text{st}}/\alpha_1$, where α_1 is a correction factor for the mixing over the jet area. In order to determine the value of α_1 we consider again a jet into still air. From (3.63) we obtain

$$\frac{L + x_0}{d} = 2.19\, \alpha_1 \frac{1}{Z_{\text{st}}} \left(\frac{\rho_0}{\rho_{\text{st}}} \right)^{1/2} , \tag{3.73}$$

which is identical to (3.55), if α_1 is set equal to $(1 + 2\,\text{Sc}) = 2.42$. We adopt this value in the following.

Buoyancy becomes important in flames due to the density differences that combustion generates. The density decreases from ρ_0 at the nozzle to ρ_{st} at the

flame length. The integral on the r.h.s. of (3.65) may therefore be approximated by

$$2\int_0^\infty \left(1-\frac{\bar{\rho}}{\rho_\infty}\right) r\,dr = b^2\alpha_2\left(1-\frac{\rho_{\rm st}}{\rho_\infty}\right), \tag{3.74}$$

where α_2 is an empirical coefficient that takes the variable density into account. Introducing a modified Froude number

$$\mathrm{Fr}^* = \frac{u_0^2}{g d_{\rm eff}}\frac{\rho_\infty}{\alpha_2\,(\rho_\infty-\rho_{\rm st})} = \mathrm{Fr}\sqrt{\frac{\rho_0}{\rho_\infty}}\frac{\rho_\infty}{\alpha_2\,(\rho_\infty-\rho_{\rm st})}, \tag{3.75}$$

where $\mathrm{Fr}=u_0^2/gd$, we may replace (3.65) with $x^*=x/d_{\rm eff}$ by

$$\frac{d}{dx^*}\left[u^{*2}b^{*2}\right] = \frac{b^{*2}}{\mathrm{Fr}^*}. \tag{3.76}$$

With $b^*=\beta x^*$ from (3.72) for $u_\infty=0$ this leads to

$$\frac{du^{*2}}{db^*}+\frac{2u^{*2}}{b^*} = \frac{1}{\beta\mathrm{Fr}^*}, \tag{3.77}$$

which is a linear first-order differential equation for u^{*2} and may therefore be solved analytically. One obtains the solution

$$u^{*2} = \frac{c_0}{b^{*2}}+\frac{b^*}{3\beta\mathrm{Fr}^*}, \quad \text{where } c_0=\frac{1}{4}-\frac{1}{24\beta\mathrm{Fr}^*}, \tag{3.78}$$

with the initial condition $u^*=1$ for $b^*=1/2$. The first term describes the momentum-dominated part of the vertical flame and reduces to $u^*=1/(2b^*)$, identical to (3.70), for large Froude numbers. The second term, which increases with b^*, describes the influence of buoyancy. Using only this term the flame length L is obtained with $4u^*\hat{Z}b^{*2}=1$ from (3.67) and $\hat{Z}=Z_{\rm st}/\alpha_1$ as

$$\frac{L}{d_{\rm eff}} = \frac{1}{\beta}\left(\frac{3\beta\alpha_1^2}{16Z_{\rm st}^2}\mathrm{Fr}^*\right)^{1/5}. \tag{3.79}$$

This shows the 1/5-exponential dependence of the flame length on the Froude number. A comparison with experimental data reported in Sønju and Hustad [3.14] allows to determine the yet unknown empirical constant α_2 as $\alpha_2=1$. A general equation for the flame length is obtained by combining (3.78) and (3.79) as

$$\left(\frac{3}{4}\beta\mathrm{Fr}^*-\frac{1}{8}\right)\left(\frac{\beta L}{d_{\rm eff}}\right)^2+\left(\frac{\beta L}{d_{\rm eff}}\right)^5 = \frac{3\beta\alpha_1^2}{16Z_{\rm st}^2}\mathrm{Fr}^*, \tag{3.80}$$

which reduces for sufficiently large values of L to (3.79) and for large Froude numbers to the momentum-dominated flame described by (3.73). Equation (3.80)

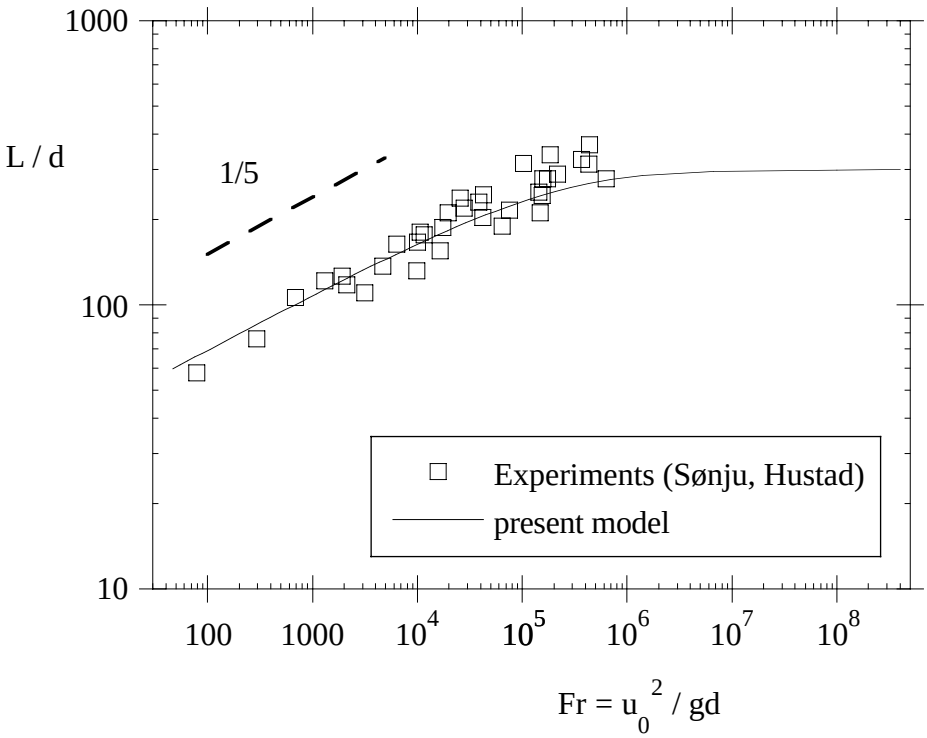

Figure 3.8: Dimensionless flame length, L/d, versus Froude number, Fr, for propane and comparison with experimental data of Sønju and Hustad [3.14].

has been evaluated for propane with $\rho_{st}/\rho_\infty \approx T_\infty/T_{st}$ and compared with experimental data from [3.14] shown in Fig. 3.8. The buoyancy-dominated regime is valid for Froude numbers Fr $< 10^5$ showing a slope of 1/5 in this range, whereas the Froude number independent solution is approached for Fr $> 10^6$. For lower Froude numbers there is an excellent agreement between the predictions of (3.80) and the experimental data.

3.6 Experimental Data Showing Non-Equilibrium Effects in Jet Diffusion Flames

While the flame length may be calculated on the basis of the mixture fraction field only, more details on scalars are needed if one wants to determine chemical effects and pollutant formation in jet flames. Flamelet extinction leading to lift-off will be considered in lecture 4. Here we want to discuss as an example data taken locally in a jet flame. They were obtained by Raman-scattering and laser-induced fluorescence in diluted hydrogen-air diffusion flames by Barlow et al. [3.15]. The fuel stream consisted of a mixture of 78 mole % H_2, 22 mole % argon, the nozzle inner diameter d was 5.2 mm and the co-flow air velocity was 9.2 m/s. The resulting

flame length was approximately $L = 60\,d$. Two cases of nozzle exit velocities were analyzed but only the case B with $u_0 = 150$m/s will be considered here.

The stable species H_2, O_2, N_2, and H_2O were measured using Raman-scattering at a single point with light from a flash-lamp pumped dye laser. In addition, quantitative OH radical concentrations from LIF measurements were obtained by using the instantaneous one-point Raman data to calculate quenching corrections for each laser shot. The correction factor was close to unity for stoichiometric and moderately lean conditions but increased rapidly for very lean and moderately rich mixtures. The temperature was calculated for each laser shot by adding number densities of the major species and using the perfect gas law for this atmospheric pressure flame. The mixture fraction was calculated similarly from the stable species concentrations. An ensemble of one-point, one-time Raman-scattering measurements of major species and temperature are plotted over mixture fraction in Fig. 3.9. They were taken at $x/d = 30$, $r/d = 2$ in the case B flame. Also shown are calculations based on the assumption of chemical equilibrium.

The overall agreement between the experimental data and the equilibrium solution is quite good. This is often observed for hydrogen flames where the chemistry is very fast. On the contrary, hydrocarbon flames at high strain rates are likely to exhibit local quenching effects and non-equilibrium effects due to slow conversion of CO to CO_2.

Fig. 3.10 shows temperature profiles versus mixture fraction calculated for counter-flow diffusion flames at different strain rates. These flamelet profiles display a characteristic decrease of the maximum temperature with increasing strain rates as shown schematically by the upper branch of the S-shaped curve in Fig. 3.5. The strain rates vary here between $a = 100$/s which is close to chemical equilibrium and $a = 10000$/s. For comparison, the mean strain rate in the jet flame, defined here as $\bar{a} = u(x)/b(x)$ may be estimated as $\bar{a} = 12.15$/s at $x/d = 30$ based on (3.63).

Data of OH-concentrations are shown in Fig. 3.11. They are to be compared to flamelet calculations in Fig. 3.12 for the different strain rates mentioned before. It is evident from Fig. 3.11 that the local OH-concentrations exceed those of the equilibrium profile by a factor 2 to 3. The flamelet calculations show an increase of the maximum values by a factor of 3 already at the low strain rates $a = 100$/s and $a = 1000$/s, while the OH-profile over mixture fraction decreases and broadens for the maximum value $a = 10000$/s. This value is close to extinction for the diluted flamelet considered here.

It should be mentioned that also Monte-Carlo simulations to solve a pdf-transport equation were performed for this experimental configuration. Since the prediction of chemically reacting flows by pdf-transport equations suffers from limitations of the turbulent mixing model, we will not discuss these results here.

In summary, it may be concluded that one-point, one-time experimental data for hydrogen flames when plotted as a function of mixture fraction, show qualitatively similar tendencies as flamelet profiles. Non-equilibrium effects are evident in

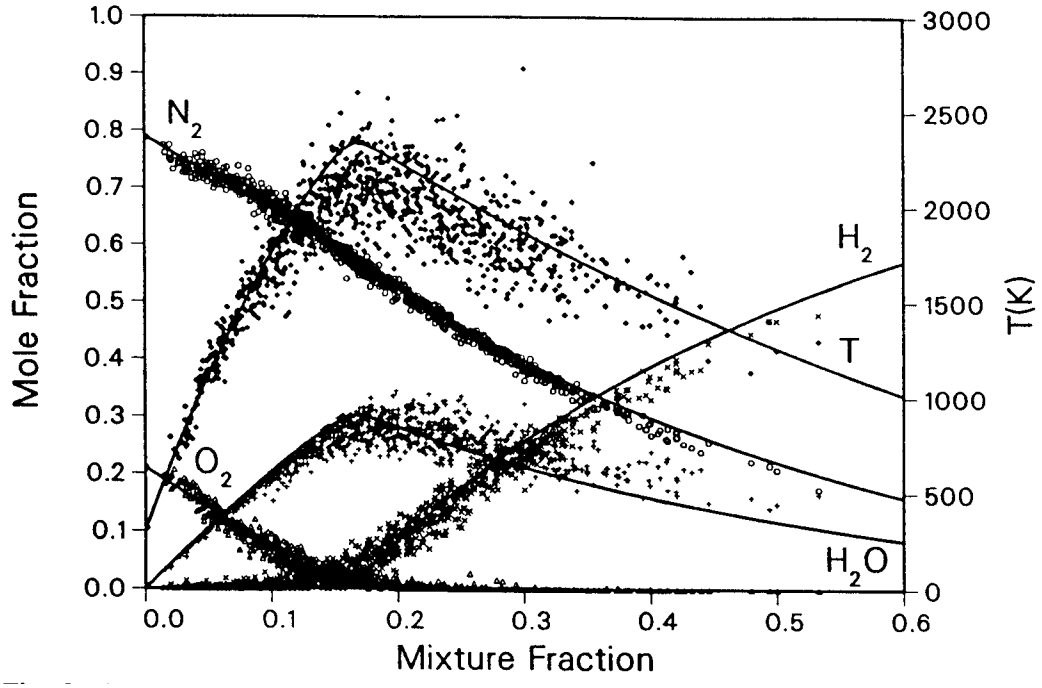

Figure 3.9: Ensemble of Raman scattering measurements of major species concentrations and temperatures at $x/d = 30, r/D = 2$. The solid curves show equilibrium conditions.

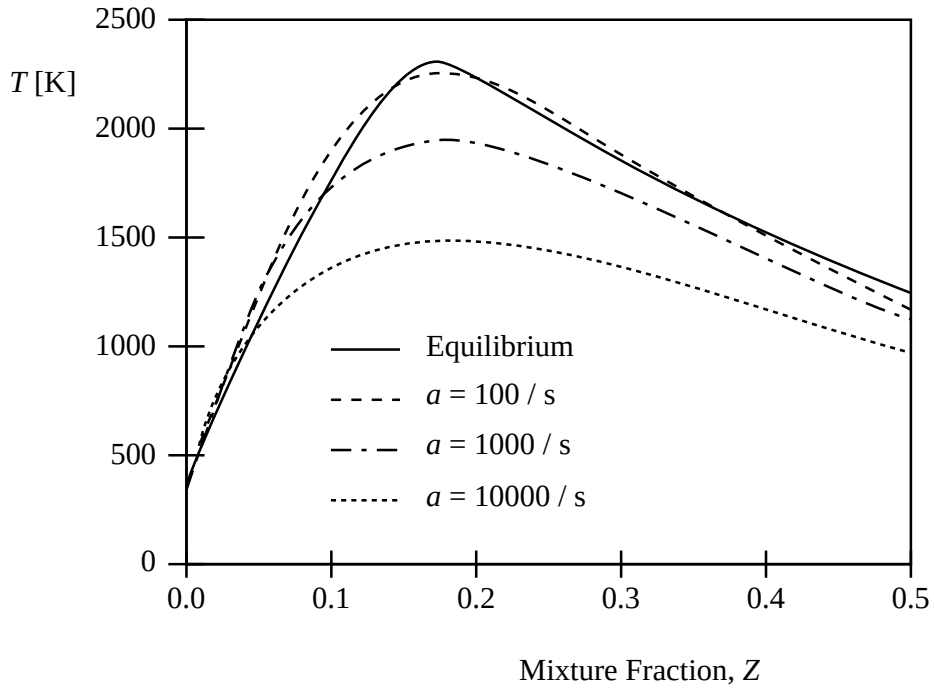

Figure 3.10: Temperature profiles from flamelet calculations at different strain rates.

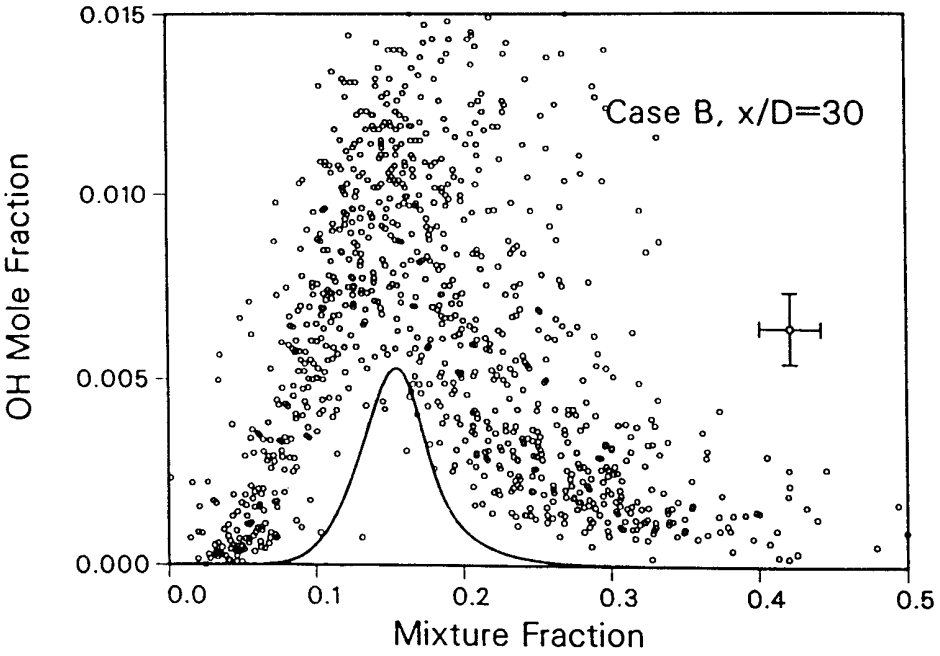

Figure 3.11: Ensemble of LIF measurements of OH concentrations at $x/d = 30, r/D = 2$. The solid curve shows equilibrium solution.

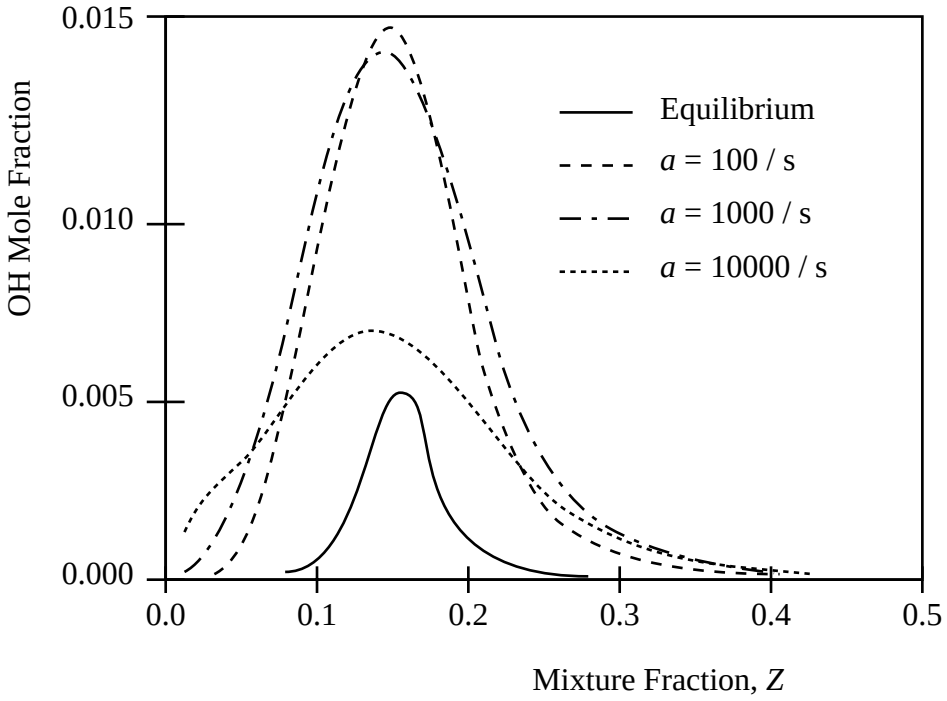

Figure 3.12: OH mole fractions from flamelet calculations at different strain rates.

both cases and lead to an increase of radical concentrations and a decrease of temperatures. This has an important influence on NO_x formation in turbulent diffusion flames.

Bibliography

[3.1] Peters, N., Progress in Energy and Combustion Science, **10** (1984) 319.

[3.2] Peters, N., Twenty-First Symp. (International) on Combustion, pp. 1231–1256, The Combustion Institute, 1986.

[3.3] Pitsch, H., Peters, N., A consistent Flamelet Formulation for Non-Premixed Combustion Considering Differential Diffusion Effects, submitted to Combust. Flame 1997

[3.4] Peters, N. in "Reduced Kinetic Mechanisms for Application in Combustion Systems" (N. Peters and B. Rogg, Eds.), Lecture Notes in Physics m15, Springer-Verlag 1993, pp. 3-14.

[3.5] Peters, N., Kee, R.J., Combust. Flame **68**, pp. 17-29 (1987).

[3.6] Tsuji, H., and Yamaoka, I., Thirteenth Symposium (International) on Combustion, p. 723, The Combustion Institute, 1971.

[3.7] Bilger, R.W., Twenty-Second Symposium (International) on Combustion, The Combustion Institute, Pittsburgh, pp. 475-488, 1988.

[3.8] Kim, J.S., Williams, F.A., SIAM J. Appl. Math. **53**, 1551-1556 (1993).

[3.9] Hellström, Th., private communication [3.10]

[3.10] Pitsch, H., Barths, H., Peters, N., SAE-paper 962057, 1996.

[3.11] Peters, N., Donnerhack, S., Eighteenth Symp. (International) on Combustion, The Combustion Institute, pp. 33–42, 1981.

[3.12] Hawthorne, W.R., Weddel, D.S. and Hottel, H.C., Third Symposium (International) on Combustion, The Combustion Institute, p. 266, 1949.

[3.13] Peters, N., Göttgens, J., Combust. Flame **85**, pp. 206-214 (1991).

[3.14] Sønju, O.K., Hustad, J., Prog. Astronaut. Aeronaut. **95**, p. 320 (1984).

[3.15] Barlow, R.S., Dibble, R.W., Chen, J.Y., Lucht, R.P., Combust. Flame **82**, p. 235 (1990).

Lecture 4

Partially Premixed Turbulent Combustion

In this lecture we present a unified approach for partially premixed combustion that combines the formulations for premixed combustion in lecture 2 and for non-premixed combustion in lecture 3. The approach will be based on the two scalar fields $G(\mathbf{x}, t)$ and $Z(\mathbf{x}, t)$ and the modeling assumptions that were introduced for each of these fields. While the mixture fraction Z determines the local equivalence ratio and thereby the value of the laminar burning velocity, the distance function G determines the location of the premixed flame front. When the laminar burning velocity is plotted as a function of mixture fraction the maximum lies close to stoichiometric mixture. Therefore, flames will propagate the fastest along surfaces $Z(\mathbf{x}, t) = Z_{\mathrm{st}}$ in a mixture field. If such a surface exists in a partially premixed field, flame propagation generates a flame structure that is called triple flame. Such a structure is shown schematically in Fig. 4.1 in a layered mixture. The leading edge of the flame, called the triple point, propagates along the surface of stoichiometric mixture. On the lean side of that surface there is a lean premixed flame branch and on the rich side there is a rich premixed flame branch, both propagating with a lower burning velocity. Behind the triple point, on the surface of stoichiometric mixture, a diffusion flame develops where the unburnt intermediates like H_2 and CO from the rich premixed flame branch burn with the remaining oxygen from the lean premixed flame branch.

Triple flames are the key element for flame propagation in partially premixed systems. An early paper demonstrating the structure of a triple flame is due to Phillips [4.1]. More recently, a number of theoretical and experimental papers have been devoted to this subject [4.2]–[4.8]. In this lecture we will first analyze the structure of triple flames and discuss numerical simulations. Then we will derive an expression for the turbulent burning velocity for partially premixed combustion and finally we apply this combustion model to determine the lift-off heights of turbulent jet diffusion flames.

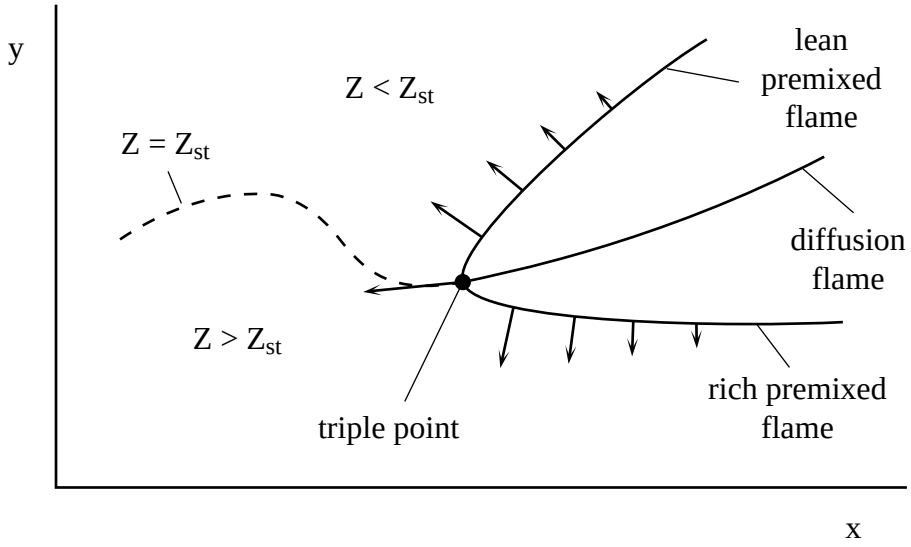

Figure 4.1: A schematic presentation of the triple flame structure showing the triple point, the two premixed flame branches and the trailing diffusion flame.

4.1 The Structure of Triple Flames

Fig. 4.2 shows the photograph of a methane-air triple flame stabilized in a laminar round jet 44 mm above the triple flame burner. This flame was analyzed in [4.9]. The burner generates a staged mixture by issuing a central flow of diluted fuel, surrounded by a lean co-flow, which is again surrounded by an air co-flow. These three mixtures have interdiffused at the stabilization height to form a partially premixed mixture ranging between $Z = 0.15$ on the centerline and $Z = 0$ in the air co-flow. Due to dilution of the central flow the stoichiometric mixture fraction is 0.0789. One can clearly distinguish in Fig. 4.2 (a) the bright rich premixed flame in the center, the broad diffusion flame surrounding it and extending further downstream and the thin lean premixed branches outside. The temperature field, obtained from Rayleigh measurements is compared with numerical simulations in Fig. 4.3. Here only the high temperature region generated by the diffusion flame is identified as a flame. The numerically calculated heat release rate shown in Fig. 4.4, however, indicates clearly the triple flame structure. The original data on the l.h.s of Fig. 4.4 show that the heat release by the lean premixed flame is the strongest, while the data multiplied by a factor 10 on the r.h.s show the heat release in all three branches. It is interesting to note that neither the rich premixed flame branch (as the chemiluminescence in Fig. 4.2 would suggest), nor the high temperature diffusion flame shown in Fig. 4.3 generates the strongest heat release.

Triple flames are always curved at the triple point. This is due to the fact that the burning velocity decreases as one moves from the stoichiometric contour to the lean and the rich. The triple point therefore propagates faster against the oncoming flow and the rich and lean premixed flame branches stay behind.

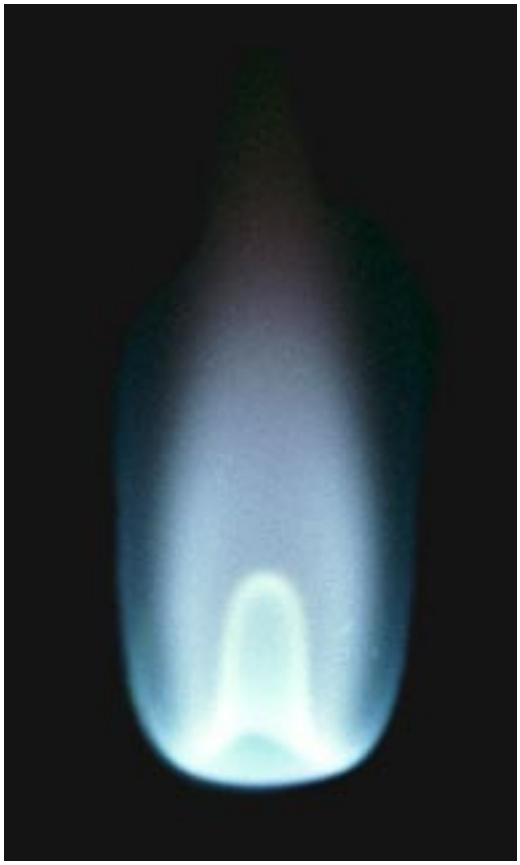

(a)

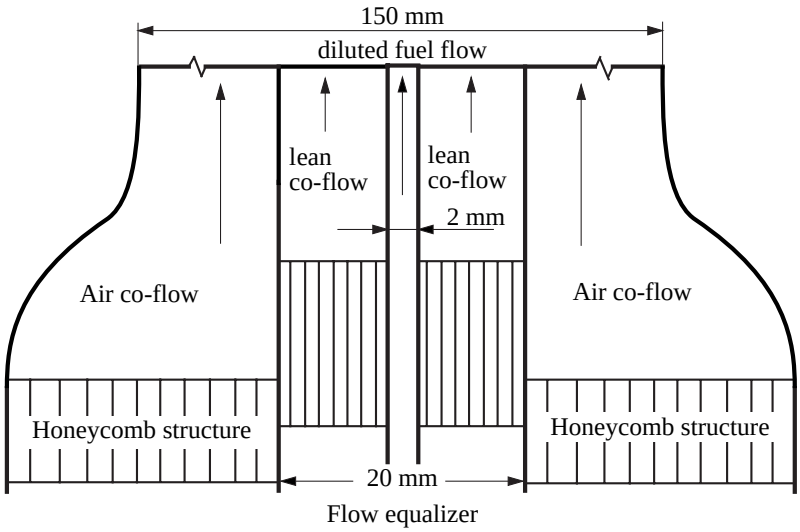

(b)

Figure 4.2: (a) Photograph of a laminar triple flame and (b) a schematic diagram of the triple flame burner.

Heat release in the premixed branches has a strong influence on the flow field ahead of the flame structure. Expansion in the premixed flame front generates a normal velocity away from the front into the unburnt mixture. Since the front is curved, this leads to a diverging flow field and a lower oncoming velocity directly ahead of the flame. The latter is shown in Fig. 4.5 where the axial velocity through the triple point is shown, both by PIV measurements and by numerical simulations. The oncoming velocity decreases from an upstream value of 0.9 m/s to 0.4 m/s, which roughly corresponds to the burning velocity of the mixture. The radial profiles of the axial velocity and the mixture fraction are shown in Fig. 4.6. The measured values of the mixture fraction were obtained from the Raman measurements of CH_4 and O_2. The triple point lies at stoichiometric mixture. The strong velocity minimum at that point clearly shows the expansion effect.

Due to the decrease of the oncoming velocity ahead of the flame we have to distinguish between the propagation velocity of the entire triple flame structure and the burning velocity of the premixed flames relative to the flow, which has a maximum close to the triple point. The ratio of the propagation velocity to the burning velocity at the triple point depends on the density ratio between the unburnt gas ahead of the triple point and the stoichiometric burnt gas behind. This velocity ratio should scale with the square root of the density ratio [4.6].

The burning velocity at the two premixed branches should depend to first approximation on the local mixture fraction. Numerical calculations of the mass burning rate $\rho_u s_L$ were performed in [4.9]. They showed, however, that the maximum of the mass burning rate normal to the flame front evaluated from the two dimensional simulations was significantly lower than the mass burning rate through a one-dimensional flame in a homogeneous mixture. The lowering of the burning velocity may in part be attributed to the local mixture fraction gradient. An ad-hoc expression that models this effect by a factor $(1-\alpha\chi(Z)/\chi_q)$ in terms of the scalar dissipation rate was proposed in [4.10] and was justified using asymptotic analysis in [4.11]. The mass flow rate is then given by the expression

$$(\rho s)(Z,\chi) = \rho_u(Z) s_L(Z) \left\{ 1 - \alpha \frac{\chi(Z)}{\chi_q} \right\} \tag{4.1}$$

which is compared in Fig. 4.7 with the values obtained from the simulations.

Here, the scalar dissipation rate at quenching of $\chi_q = 30\,\mathrm{s}^{-1}$ calculated for this diluted methane diffusion flame is used [4.12]. The parameter α was fixed to $\alpha = 0.96$. The scalar dissipation rate on the premixed flame contour rises from low values to about 6 s^{-1} for stoichiometric mixtures, and increases then up to 9.5 s^{-1} for rich mixtures. For very rich conditions the actual flow rate is higher than predicted by (4.1). This is due to the preheating from the diffusion flame. For close to stoichiometric mixtures, the flow rate is considerably lower which probably is due to increased heat loss resulting from flame front curvature in this region. It can be concluded that for a precise prediction of the local burning velocity in a triple flame, effects of preheating and heat loss need to be considered and a simple

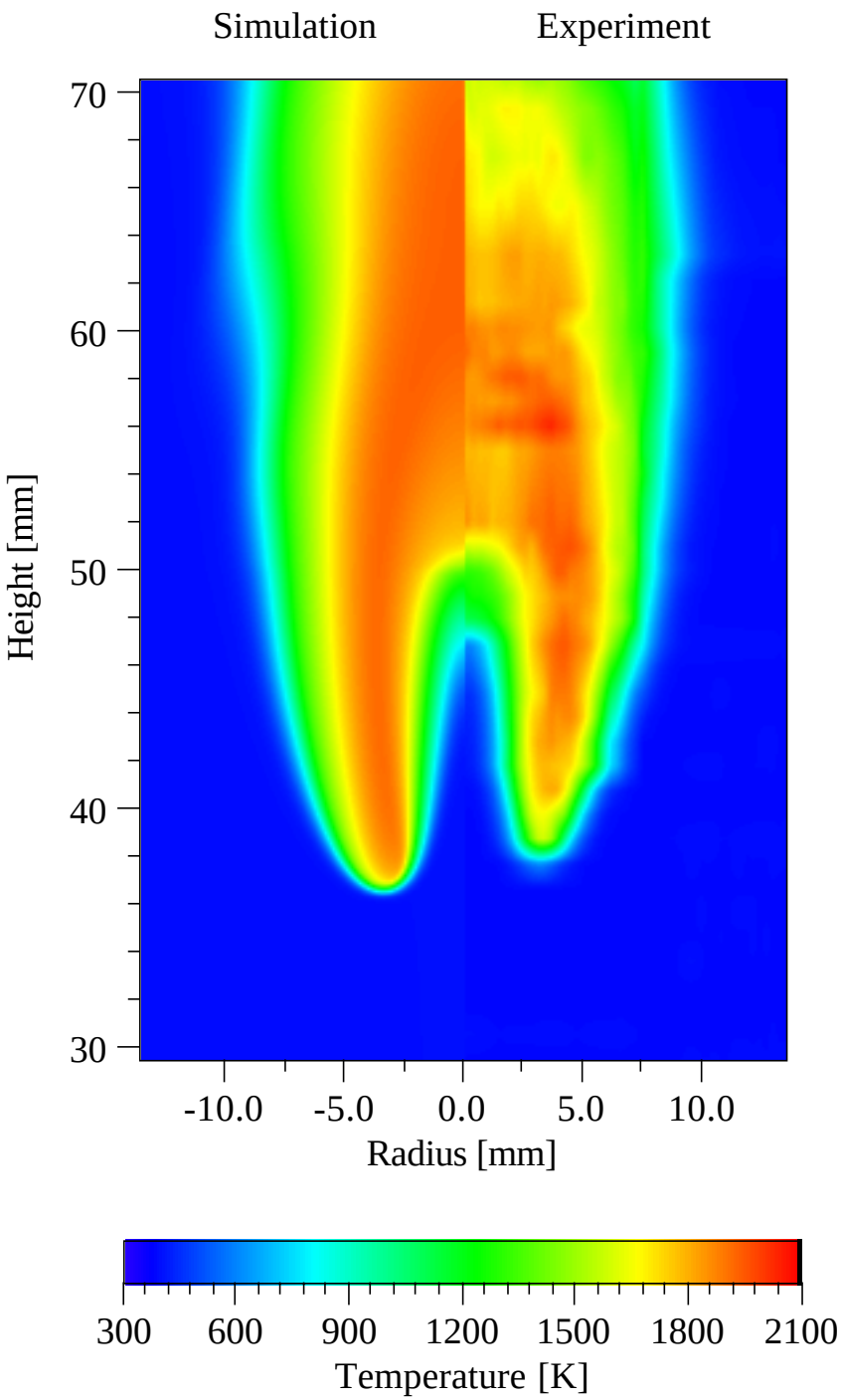

Figure 4.3: Calculated and measured temperature distribution.

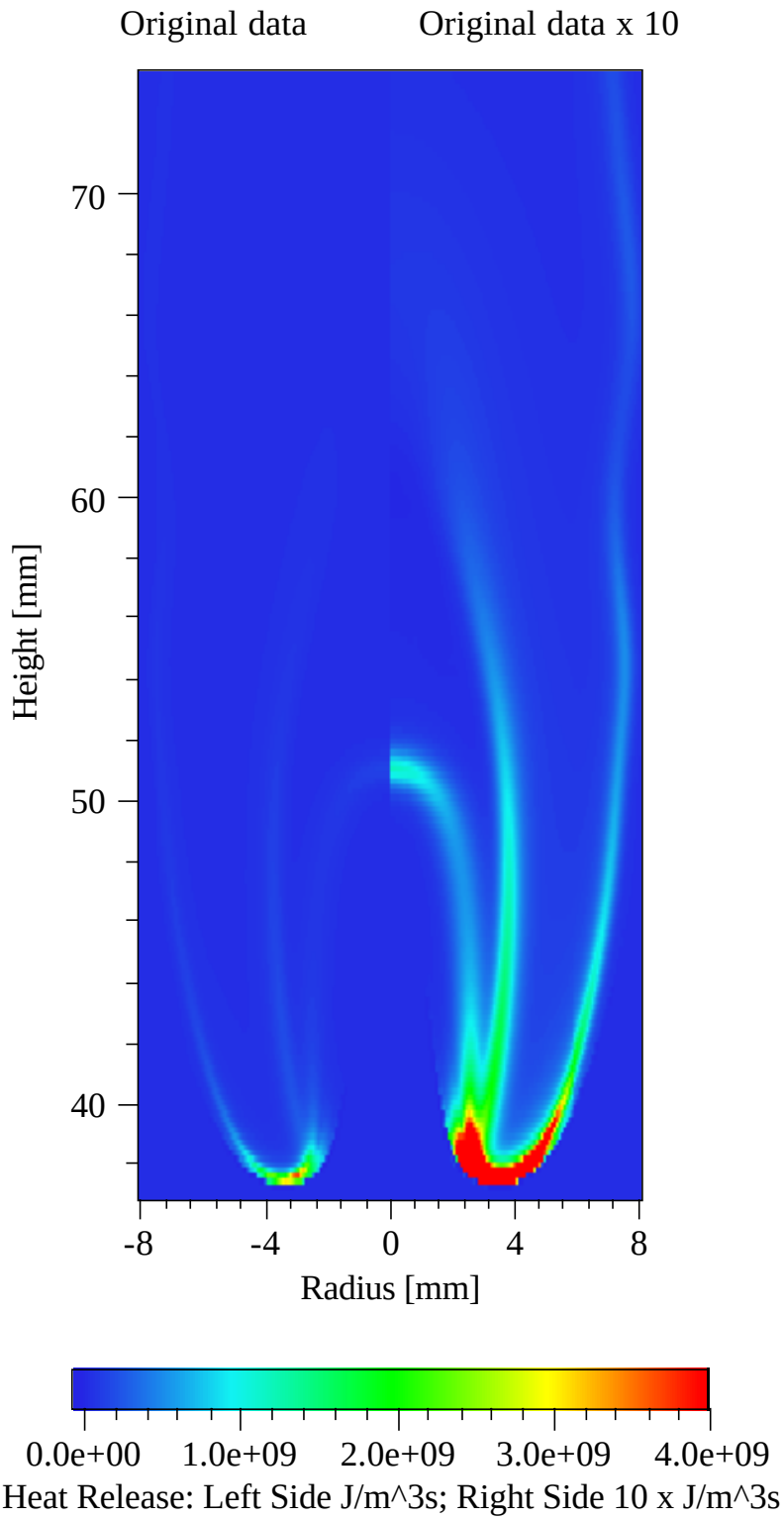

Figure 4.4: Calculated heat release. The left side illustrates the original data while the right side illustrates the data multiplied by 10 in order to show the structure of small values.

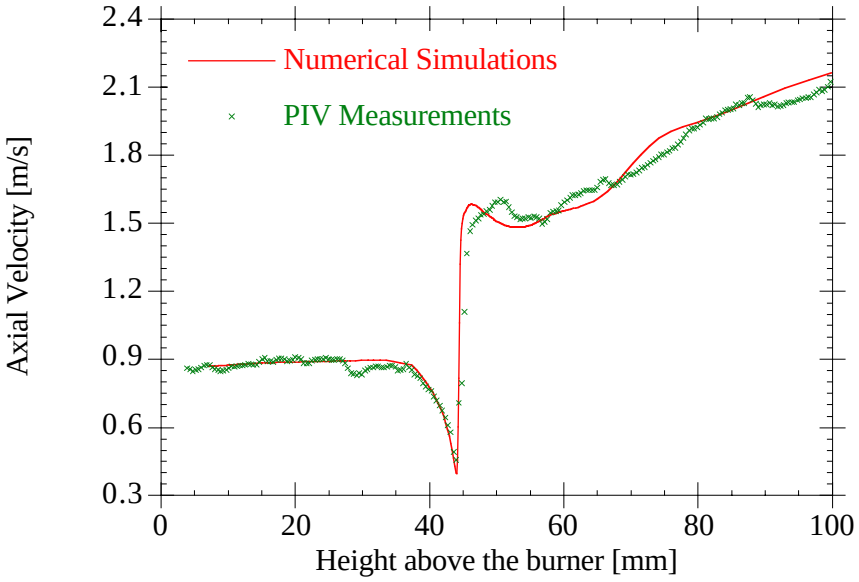

Figure 4.5: Axial velocity profiles at $r = 3.2$ mm through the triple points

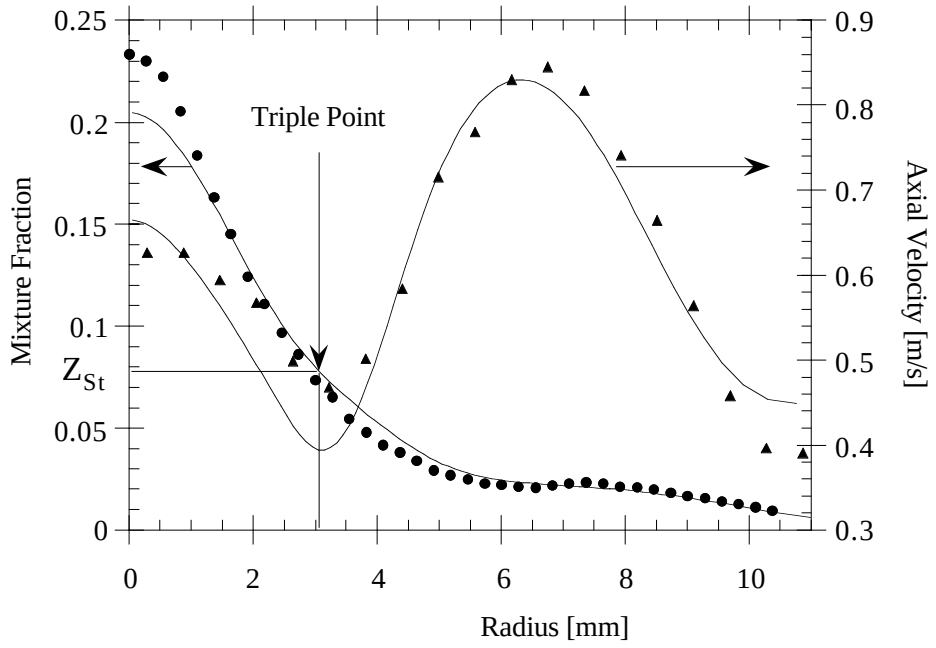

Figure 4.6: Measured (symbols) and calculated (solid lines) radial profiles of the axial velocity, u, and mixture fraction, Z, at the stabilization height of the triple flame.

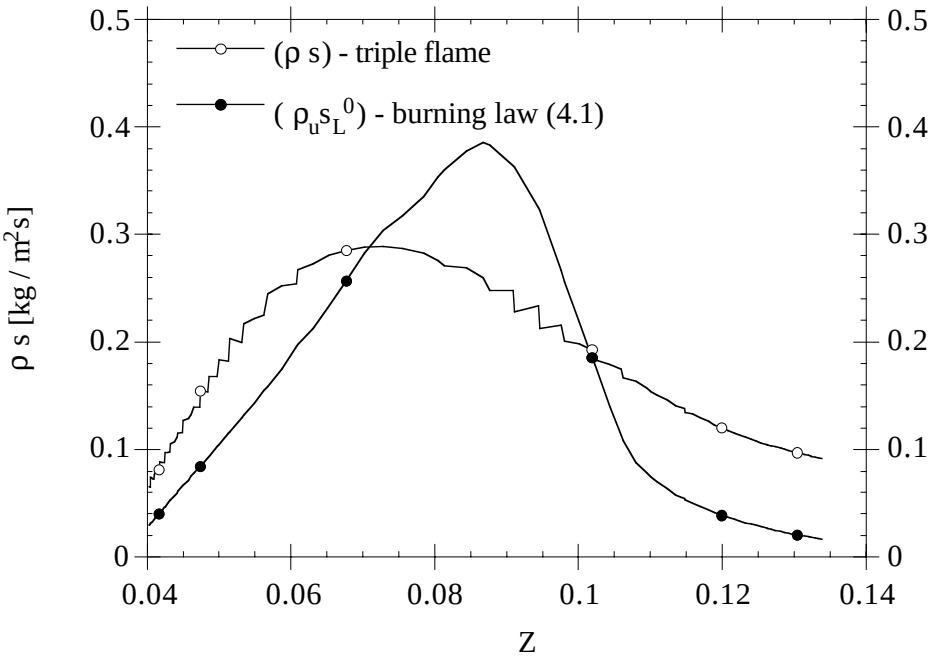

Figure 4.7: Mass flow rate through the triple flame contour compared to the flow rate of the burning law (4.1) together with local scalar dissipation rate along the flame contour.

expression like (4.1) may not be sufficient. However, in the following we will only use the qualitative behaviour of the burning velocity of a triple flame as a function of the mixture fraction, in order to derive an expression for the turbulent burning velocity in partially premixed systems.

4.2 Numerical Simulations of Auto-Ignition and Triple Flame Propagation

Numerical simulations of auto-ignition in non-uniform mixtures illustrate the role of triple flame structures in partially premixed turbulent combustion very convincingly. In [4.6] and [4.7] two dimensional simulations on a 256^2 grid have been performed using a sixth-order finite difference scheme and a one-step reaction with a Zeldovich number Ze $= 8$ and a heat release parameter $\alpha = (T_b - T_u)/T_b = 0.8$. The reaction rate was first order with respect to fuel and oxygen. In order to simulate the effect of compression, source terms were added to the temperature and the species equations. Thereby the temperature was increased up to conditions close to auto-ignition. The different stages of ignition and flame propagation may be described as follows

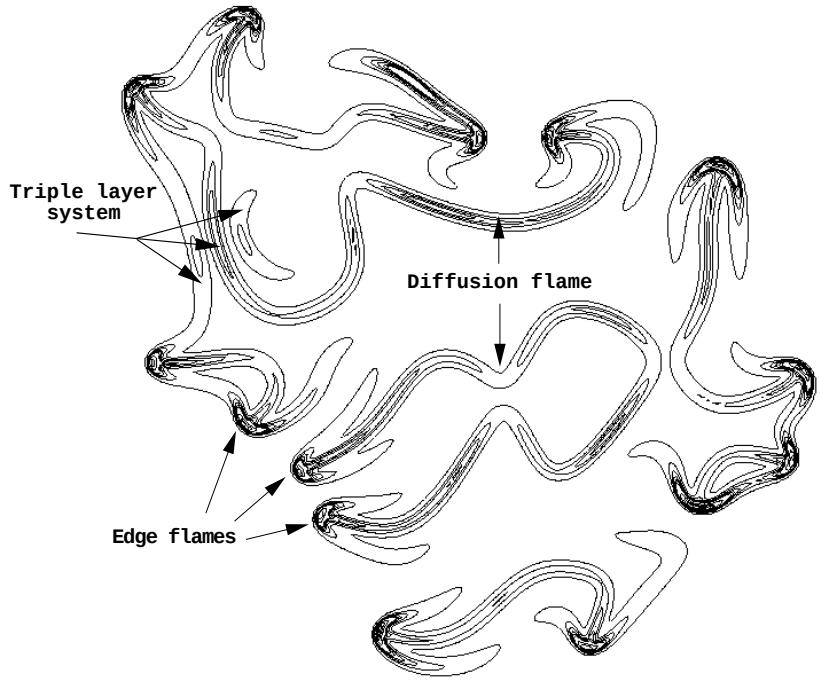

Figure 4.8: Triple flame propagation through a non-homogeneous mixture field [4.6].

1. Ignition occured in the vicinity of the stoichiometric line in regions where the scalar dissipation rate was low.

2. Two premixed flame fronts containing lean and rich branches propagate in opposite directions along the stoichiometric lines. They have the shapes of arrow-heads as shown in Fig. 4.8.

3. A diffusion flame develops on the stoichiometric line between the premixed flames. The tails of the premixed flames are lying nearly parallel to the diffusion flame and are propagating into the lean and rich mixture. As they depart from the diffusion flame they become weaker and finally disappear.

4. When premixed flame fronts try to propagate into regions of very high scalar dissipation rates, local extinction is likely to occur.

5. The dissipation rate and the heat release rate are inversely correlated. Maximum values of the dissipation rate correspond to minimum levels of heat release and vice versa.

It is concluded that the conditional mean value of the scalar dissipation rate at stoichiometric mixture $\tilde{\chi}_{st}$ rather than its unconditioned mean $\tilde{\chi}$ controls ignition and subsequent flame propagation in partially premixed systems.

4.3 Turbulent Flame Propagation in Partially Premixed Systems

We want to derive an expression for the mean turbulent burning velocity in a partially premixed system. We expect turbulent flame propagation to be the fastest in regions when the probability of finding stoichiometric mixture is the highest. This correspond to regions where the mean mixture fraction is in the vicinity of stoichiometric mixture. For a partially premixed system we also may formulate a kinematic or a diffusive G-equation that describes this propagation process, but now the laminar burning velocity will be a function of the mixture fraction

$$\frac{\partial G}{\partial t} + \mathbf{v} \cdot \nabla G = s_L(Z, \chi)\sigma - D_{\mathcal{L}} k \sigma + \mathcal{L}\mathbf{n} \cdot \nabla \cdot \mathbf{n}\sigma \ . \tag{4.2}$$

The turbulence modeling will be essentially the same as in lecture 2. Therefore the turbulent counterpart of (4.2) corresponding to (2.57) will then be

$$\frac{\partial \overline{G}}{\partial t} + \overline{\mathbf{v}} \cdot \nabla \overline{G} = s_{T,p} |\nabla \overline{G}| - (\mathcal{D}_{\mathcal{L}} + D_t) \bar{k}(\overline{G}) |\nabla \overline{G}| \ . \tag{4.3}$$

Here we have also combined the means of the first and the last term in 4.2 to define the turbulent burning velocity $s_{T,p}$ for partially premixed systems by

$$s_{T,p} = s_L(Z_{\mathrm{st}}) + \overline{s_L(Z, \chi)\sigma} \left(1 - b_3 \frac{\mathcal{L} v'}{\ell s_L^0(Z_{\mathrm{st}})} \right) \ . \tag{4.4}$$

Here, following (2.103) we have added the first term to cover the laminar limit. The turbulent burning velocity for partially premixed systems $s_{T,p}$ depends in a non-trivial manner on the laminar burning velocity $s_L(Z, \chi)$, on the statistics of σ and on the mixture fraction field.

In [4.10] a model for the turbulent burning velocity has been derived by considering the mean value of $s_L(Z, \chi)\sigma$ as a statistical mean depending on Z, χ and σ

$$\overline{s_L(Z, \chi)\sigma} = \int_0^\infty \int_0^\infty \int_0^\infty s_L(Z, \chi)\sigma \, P(Z, \chi, \sigma) dZ d\chi d\sigma \ . \tag{4.5}$$

Here $P(Z, \chi, \sigma)$ is a joint probability density function of Z, χ and σ. In general, one may not assume these quantities to be statistically independent. In fact, since $G = G_0$ represents the premixed flame fronts, iso-lines of G will tend to align with iso-lines of Z in very lean and rich parts of the mixture, while G is nearly normal to Z around $Z = Z_{\mathrm{st}}$.

We will for simplicity, however, assume statistical independence and furthermore neglect fluctuations of χ such that the pdf of χ is given by a delta function. The joint pdf is then written

$$P(Z, \chi, \sigma) = P(Z)P(\sigma)\delta(\chi - \overline{\chi}) \, . \tag{4.6}$$

Then, using (4.1) the integral in (4.5) takes the form

$$\overline{s_L(Z,\chi)\sigma} = \overline{\sigma}\left(1-\alpha\frac{\overline{\chi}_{\rm st}}{\chi_q}\right)\int_0^1 s_L(Z)P(Z)\,dZ\,. \tag{4.7}$$

Here we have introduced the conditioned mean scalar dissipation rate at stoichiometric mixture since this value determines the flame propagation process. Furthermore, a convenient representation of the integral in (4.7) is

$$\int_0^1 s_L(Z)P(Z)\,dZ = s_L(Z_{\rm st})P(Z_{\rm st})(\Delta Z)_{s_L} \tag{4.8}$$

which defines the width $(\Delta Z)_{s_L}$. This is essentially the range in mixture fraction space where the burning velocity is a significant fraction of the maximum burning velocity. It will depend on the shape of $s_L(Z)$ and via $P(Z)$ on $\tilde{Z}$ and $\widetilde{Z''^2}$. Numerical calculations using (4.7) show that using a beta-function pdf and assuming the mixture fraction variance to be proportional to the square of the mean mixture fraction, one obtains for methane flames a nearly constant value for $(\Delta Z)_{s_L} = 0.06$, which is in the vicinity of the stoichiometric mixture fraction $Z_{\rm st} = 0.055$.

Inserting (4.8) into (4.7) leads to

$$\overline{s_L\,(Z,\,\chi)\,\sigma} \;=\; \underbrace{s_L(Z_{\rm st})\bar{\sigma}}_{\substack{\text{premixed flame}\\ \text{propagation}}} \times \underbrace{P(Z_{\rm st})(\Delta Z)_{s_L}}_{\substack{\text{partial}\\ \text{premixing}}} \underbrace{\left(1-\alpha\frac{\overline{\chi}_{\rm st}}{\chi_q}\right)}_{\substack{\text{diffusion}\\ \text{flamelet}\\ \text{quenching}}}. \tag{4.9}$$

This formulation contains three contributions:

1. A term accounting for premixed turbulent flame propagation proportional to the maximum laminar burning velocity $s_L(Z_{\rm st})$ times the flame surface area ratio $\overline{\sigma}$, which may be calculated from (2.95).

2. A term due to partial premixing which restricts flame propagation to regions where the probability for stoichiometric conditions is high.

3. A term accounting for triple flame extinction at large scalar dissipation rates. This term takes into account that triple flamelets are less able to propagate as the dissipation rate increases and will extinguish when χ approaches χ_q.

4.4 Stabilization Heights of Lifted Jet Diffusion Flames

In order to protect the burner material from being affected by the high temperatures of the flame, industrial burners in general operate with lifted flames. If the nozzle

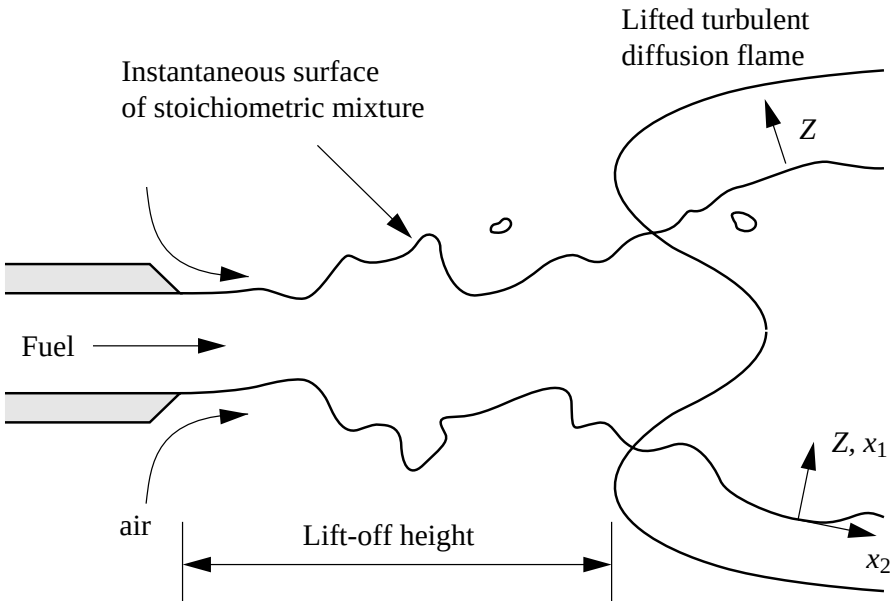

Figure 4.9: Schematic presentation of a lifted jet diffusion flame.

exit velocity of the fuel in a jet diffusion flame exceeds a characteristic value, the flame abruptly detaches from the nozzle. It now acquires a new position and stabilizes further downstream. The lift-off height is the centerline distance from the nozzle to the plane of flame stabilization (cf. Fig. 4.9). A further increase in the exit velocity increases the lift-off height without significantly modifying the turbulent flame length. The flame length was already considered in lecture 3.

There has been a long-term controversy about the stabilization mechanism in lifted turbulent diffusion flames. The mechanism proposed by Vanquickenborne and van Tiggelen [4.13] suggests that flame stabilization occurs on the contour of mean stoichiometric mixture at the position where the axial mean velocity equals the turbulent burning velocity for entirely premixed conditions. This model has been followed by Eickhoff et al. [4.14] and Kalghatgi [4.15]. On the contrary, Peters and Williams [4.16] have argued that in a non-premixed flow field flame propagation will proceed along instantaneous surfaces of stoichiometric mixtures up to the position where too many flamelets are quenched, so that flame propagation of the turbulent flame towards the nozzle cannot proceed further. Here the flame was viewed as a diffusion flamelet and flamelet quenching was thought to be the essential mechanism. A thorough review on the lift-off problem has been given by Pitts [4.17].

In Fig. 4.10 non-dimensional lift-off heights of methane flames are plotted as a function of the nozzle exit velocity u_0 for different nozzle diameters. Similar data were obtained for methane in diluted air. The scalar dissipation rate at quenching χ_q for diluted and undiluted methane-air flames taken from laminar flamelet calculations was multiplied with d/u_0 to obtain the non-dimensional quantity χ_q^* [4.18].

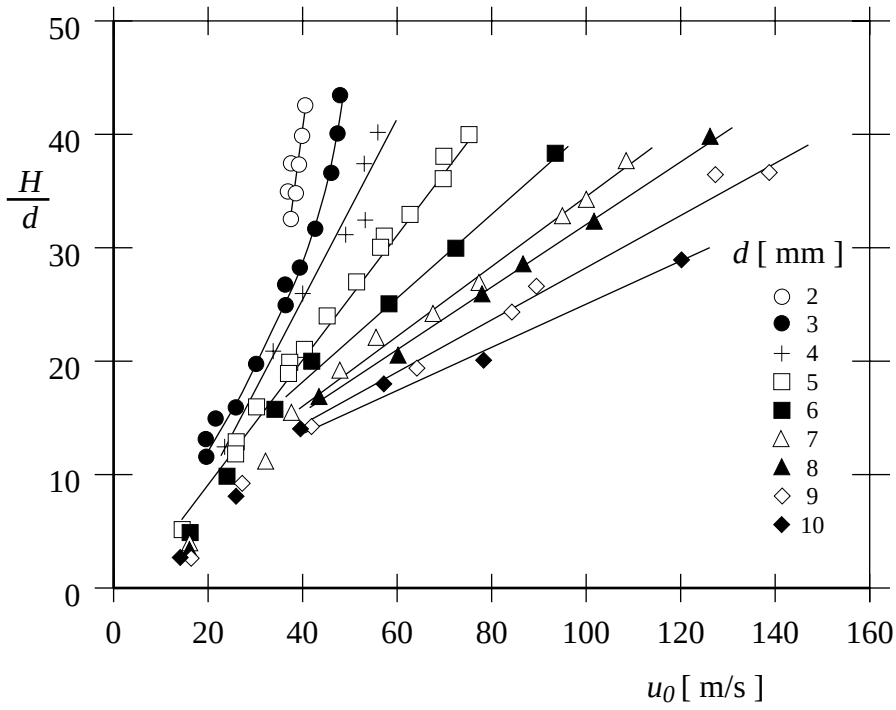

Figure 4.10: Non-dimensional lift-off heights for methane-air flames.

These data are plotted as a function of H/d in Fig. 4.11 for different dilutions of the oxidizer stream, characterized by the mole fraction of the oxygen in that stream. The straight line through these data has a slope of -1 and corresponds to

$$\frac{\chi_q d}{u_0} = 0.036 \left(\frac{H}{d} \right)^{-1} . \tag{4.10}$$

This leads immediately to the scaling

$$H = 0.036\, u_o / \chi_q \tag{4.11}$$

independent of the nozzle diameter. Different values of χ_q account for different fuels. Typical values to be used here are $\chi_q = 15$/s for methane and $\chi_q = 30$/s for propane in air at atmospheric pressure.

4.5 Numerical Simulation of Downward Flame Propagation and Lift-Off Heights

The turbulent burning velocity model described by (4.9) has been used to calculate the unsteady flame propagation and the stabilization in turbulent jet flames. For this purpose the KIVA II code was modified to include an equation for $\overline{G}$ similar to

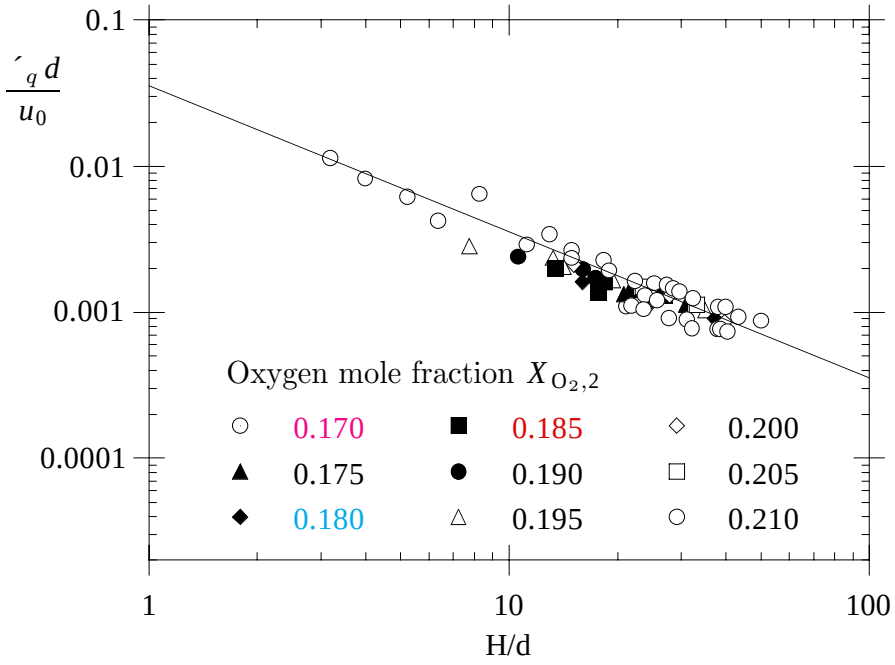

Figure 4.11: Lifted flames: Non-dimensional scalar dissipation as a function of the non dimensional lift-off height. Experimental data for different dilutions, where $X_{O_2,2}$ is the mole fraction of O_2 in the oxidizer stream.

(4.3). The $\overline{G}$ field was initialized with $\overline{G} = 0$ for unburnt conditions. Combustion was initiated by setting $\overline{G} = 0.1$ in one cell. The evolution of the $\overline{G}$ field then led to values $\overline{G} > G_0$, where G_0 was chosen to $G_0 = 1.0$. If $\overline{G}$ increases beyond $\overline{G} = 2.0$ it is set equal to that value.

The combustion model of KIVA II was removed, but equations for the mean mixture fraction $\tilde{Z}$ and its variance $\widetilde{Z''^2}$ were included. In addition, an equation for the mean total enthalpy $\tilde{h}$ was solved,

$$\frac{\partial \overline{\rho}\tilde{h}}{\partial t} + \nabla \cdot (\overline{\rho}\mathbf{v}\tilde{h}) = \frac{\partial \overline{p}}{\partial t} + \mathbf{v} \cdot \cdot \nabla \overline{p} + \nabla \cdot \left(\frac{\bar{\rho}\tilde{\nu}_t}{P_r} \nabla \tilde{h} \right) . \qquad (4.12)$$

This was necessary, because KIVA II is a compressible code which uses an Arbitrary Lagrangian Eulerian (ALE) algorithm, where in a first Lagrangian step the diffusion and acoustic terms are solved implicitly. In the second Eulerian step the convection terms are treated explicitly by subcycling the implicit time step. Therefore, the enthalpy equation cannot be coupled to the mixture fraction equation but must contain the first two acoustic terms on the r.h.s. of (4.12).

The mass fractions of the chemical species were determined by using a flamelet library for laminar counterflow diffusion flames for different values of the velocity counterflow gradient. There are two possible states for a diffusion flamelet which

are conditioned by the value of $\overline{G}$. If in a computational cell $\overline{G} \gg G_0$, it is considered to be completely burnt and the mass fractions are determined by

$$\tilde{Y}_{i,b}(\tilde{Z}, \widetilde{Z''^2}, \overline{a}) = \int_0^1 Y_i(Z, a)\tilde{P}(Z)\, dZ \tag{4.13}$$

where $Y_i(Z, a)$ is taken from the library of burning flamelets setting the velocity gradient a of the flamelet equal to the local strain rate

$$\overline{a} = \frac{\tilde{\varepsilon}}{\tilde{k}} \tag{4.14}$$

of the turbulent flow. In (4.13) a beta function pdf was used. The integration was performed in advance and values for $\tilde{Y}_{i,b}$ were tabulated as functions of $\tilde{Z}$, $\widetilde{Z''^2}$ and $\overline{a}$.

If $\overline{G} \ll G_0$ in a computational cell, the mass fractions are those of fuel and air in an unburnt mixture at the local value of $\tilde{Z}$

$$\tilde{Y}_{i,u} = Y_{i,u}(\tilde{Z})\ . \tag{4.15}$$

If the computation cell is located within the flame brush thickness, the weighted sum

$$\tilde{Y}_i = f\tilde{Y}_{i,b} + (1 - f)\tilde{Y}_{i,u} \tag{4.16}$$

is used. The fraction of burnt flamelets in each cell is calculated by assuming that G fluctuations are Gaussian distributed. Then

$$f = \int_{G=G_O}^{\infty} \frac{1}{\sqrt{2\pi\overline{G'^2}}} \exp\left\{-\frac{(G - \overline{G})^2}{2\overline{G'^2}}\right\} dG \tag{4.17}$$

where the variance $\overline{G'^2}$ is assumed to be proportional to the square of the integral length scale.

The temperature $\tilde{T}$ in the cell was calculated from the mean enthalpy by

$$\sum_{i=1}^{n} \tilde{Y}_i h_i(\tilde{T}) = \tilde{h}(\mathbf{x}, t) \tag{4.18}$$

where the specific enthalpies are taken from NASA polynomials. The temperature profile and the velocity change due to thermal expansions, at the flame front $\overline{G} = G_0$ are continuous over a few grid points due to the weighting used in (4.16).

To determine instationary propagation velocities in turbulent methane jets a simple experimental set-up consisting of a burner, an ignition device, a high speed camera and an Argon-Ion laser was used. The nozzles had a length of 115 mm and inner diameters D of 4, 6, and 8 mm. Methane was used as fuel, the fuel mass flow was measured by flowmeters.

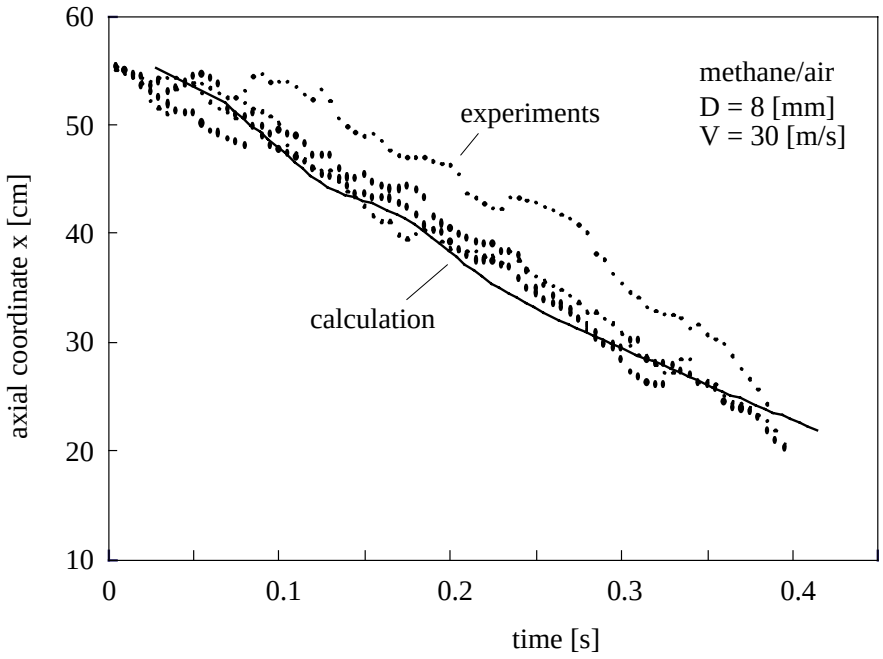

Figure 4.12: Axial coordinate of the flame base over time during unsteady propagation of a flame burning in an ignited turbulent cold jet of methane into still air.

To visualize the flame front, the fuel flow was seeded with club moss spores and illuminated with a laser light sheet. The club moss spores scatter the laser light in the unburnt mixture and burn in the flame front, thus there is no light scatter in the burned gas. Flame propagation is recorded with a high speed camera at 200 frames per second perpendicular to the laser light sheet. An electric spark is used to ignite the flame at a downstream position, where a fuel lean mixture is expected.

In order to determine the burning velocities, the lowest visible flame front position on each image of the film is marked visually and the positions are scanned. From the images it can be seen, that local propagation velocities are influenced by three-dimensional structures moving sometimes in spirals around the axis of symmetry.

In order to simulate the downward propagating flame front one computational cell of the steady cold flow field was initiated with $\bar{G} = G_0$ on the centerline downstream of the position of mean stoichiometric mixture. The flame ignition and propagation is then driven by the $\overline{G}$ gradient towards the neighboring cells. An example calculation is shown in Fig. 4.12 where the axial distance between the flame base and the nozzle is plotted versus time. The solid line denotes the calculation and the symbols represent the measured values from different experimental runs.

It is seen that the slope of the calculated curve and therefore the propagation velocity agrees well with that of the experimental runs. A closer inspection of the

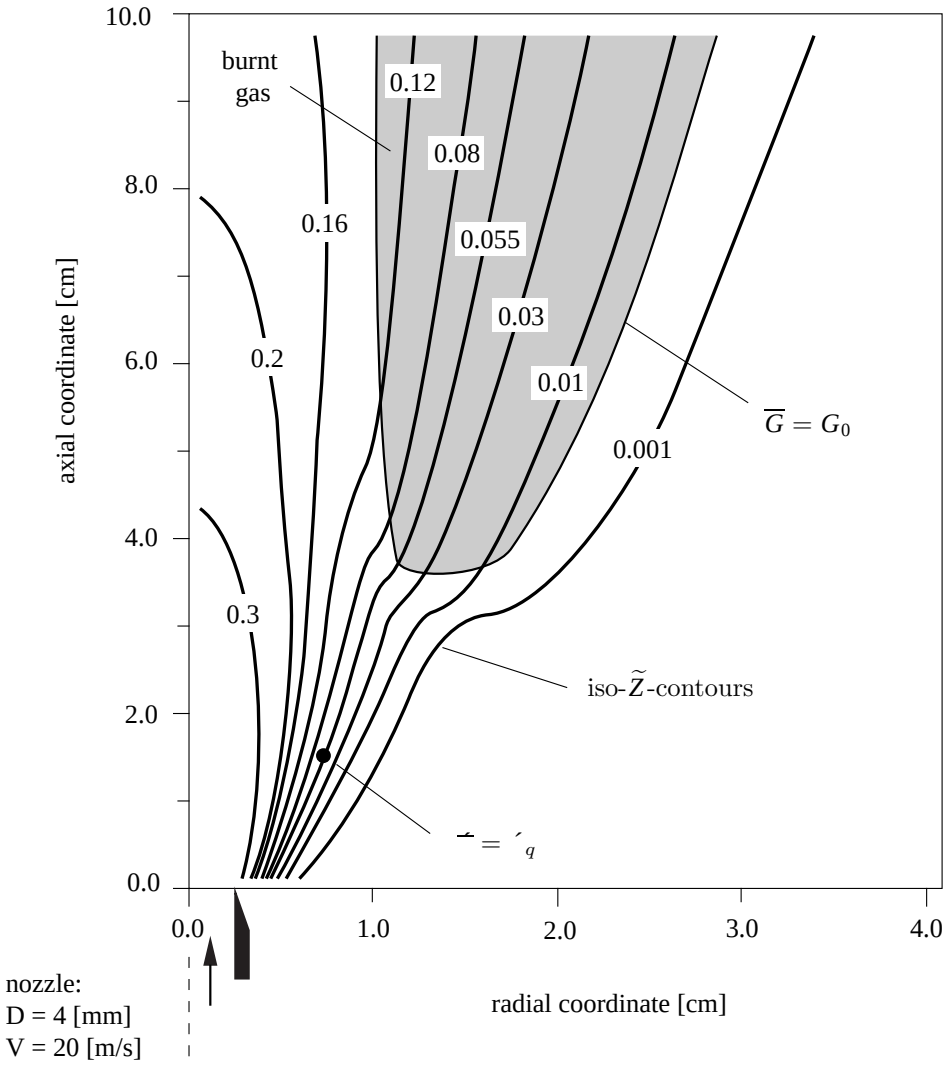

Figure 4.13: Stabilization region of a lifted turbulent jet diffusion flame.

calculations shows that flame propagation follows the surface of mean stoichiometric mixture and depends on the velocity fluctuations there. The experiments, on the one side, seem to show a transport of the flame by the large structures at the edge of the jet. Therefore, there remains a substantial difference between the very crude turbulence modeling based on the k-ε-model and the large scale dynamics in a jet.

When the unsteady flame front propagation reaches a steady state, the lift-off height can be determined. Fig. 4.13 shows a blow-up of the stabilization region in a turbulent methane jet flame with a diameter $D = 4$ mm and a fuel exit velocity of 20 m/s. The shadowed area indicates the burnt gas region $\overline{G} > G_0$ and the solid lines are iso-contours of the mixture fraction. The expansion by the flame deflects the stream lines and thereby the mixture fraction iso-contours at the flame base.

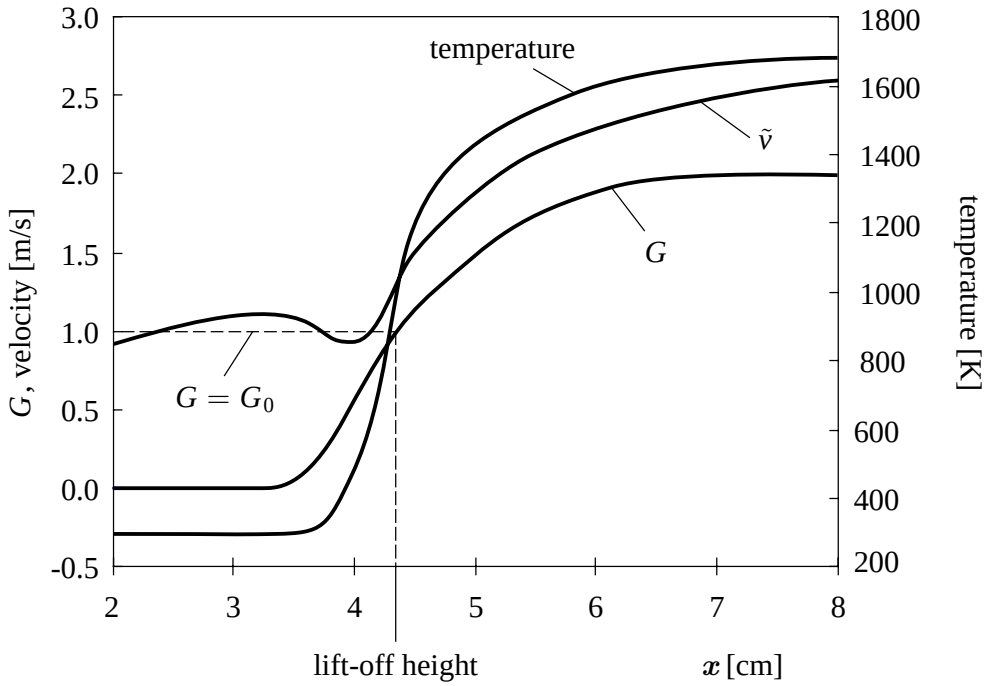

Figure 4.14: A cut following the line of mean stoichiometric mixture at the stabilization height.

In Fig. 4.14 a cut following the line of mean stoichiometric mixture at the stabilization height is shown. The absolute values of the velocity $\tilde{\mathbf{v}}$ along this line and the $\tilde{G}$-profile are plotted. The expansion effect by the rising temperature leads first to a decrease of the velocity $\tilde{\mathbf{v}}$ with a local minimum in front of the flame and then to a velocity acceleration further downstream.

In Fig. 4.15 calculated non-dimensional lift-off heights H/D of turbulent methane jet diffusion flames are plotted over the jet exit velocity. They are compared with experiments of different authors. The calculations have been performed for two nozzle diameters, $D = 4$ mm and $D = 8$ mm, and a wide range of jet exit velocities. The computed lift-off heights depend on the value of the parameters α and χ_q in (4.9). This also indicates that the last term in (4.9) becomes important at the stabilization height. The calculations also show that this term is nearly unity during most of the downward propagation process and becomes approximately 0.3 at the lift-off height. Since the flow velocity and therefore s_{Tp} are non-zero, $\overline{\chi}$ must be smaller there than χ_q at the stabilization height. If the stabilization height was determined by $\overline{\chi} = \chi_q$, as by the flamelet quenching criterion, the lift-off height is underpredicted. This is evident from Fig. 4.13 where the position of $\overline{\chi}/\chi_q = 5.0$ lies upstream of the stabilization region. Therefore, both effects, premixed flame propagation and flamelet quenching add to the stabilization mechanism.

It may be concluded that flame propagation and lift-off in jet diffusion flames may be predicted using an expression for the turbulent burning velocity (4.9) that

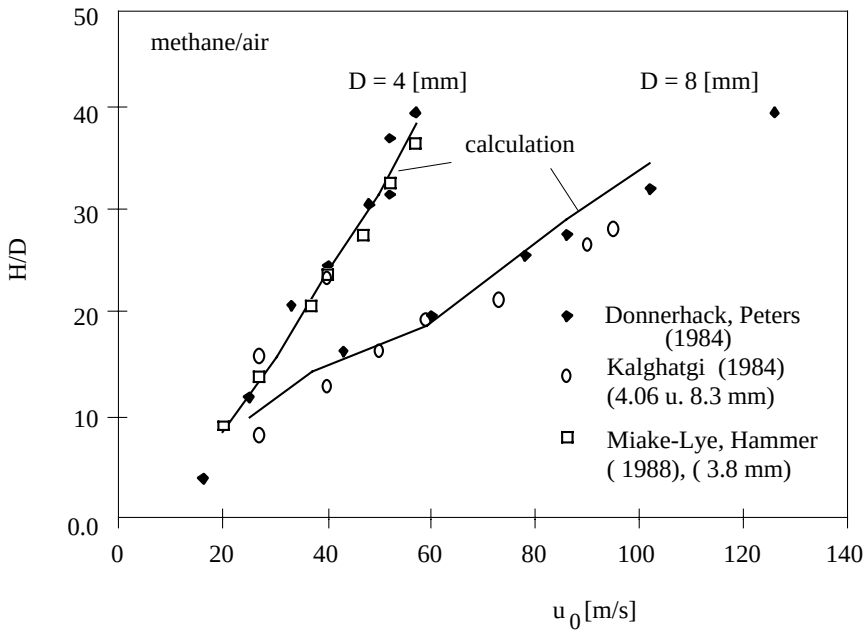

Figure 4.15: Measured and calculated lift-off heights of methane/air jet diffusion flames.

includes the two different physical mechanisms proposed in [4.13]–[4.16] to explain the stabilization mechanisms, namely premixed flame propagation along the surface of mean stoichiometric mixture and flamelet quenching. While unsteady flame propagation is essentially dominated by the first mechanism, the flame is stabilized close to, but downstream of the position $\overline{\chi} = \chi_q$, indicating that flamelet quenching is important for flame stabilization of lifted flames.

Bibliography

[4.1] Phillips, H., Tenth Symposium (International) on Combustion, The Combustion Institute, Pittsburgh, 1965, pp. 1277–1283.

[4.2] Buckmaster, J. and Matalon, M., Twenty-Second Symposium (International) on Combustion, The Combustion Institute, Pittsburgh, 1989, pp. 1527–1535.

[4.3] Dold, J. W., Combust. Flame **76**:71–88 (1988).

[4.4] Hartley, L. J. and Dold, J. W., Combust. Sci. Tech. **80**:23–46 (1991).

[4.5] Kioni, P., Rogg, B., Bray, K. N. C., and Linãn, A., Combust. Flame **95**:276–290 (1993).

[4.6] Veyante, D., Vervisch, L., Linãn, and Ruetsch, G.R., Triple Flame Structure and Diffusion Flame Stabilization, In Proc. of Summer Prog. 1994, Center for Turbulence Research, Stanford University, CA, 1994.

[4.7] Domingo, P. and Vervisch, L., Twenty-Sixth Symposium (International) on Combustion, The Combustion Institute, Pittsburgh, 1996, pp. 233–240.

[4.8] Echekki, T. and Chen, H., Structure and Propagation of Methanol-Air Triple Flames, submitted to Combustion and Flame, 1997.

[4.9] Plessing, T., Terhoeven, P., Mansour, M. S., and Peters, N., An Experimental and Numerical Study on a Laminar Triple Flame, submitted to Combustion and Flame, 1997.

[4.10] Müller, C. M., Breitbach, H., and Peters, N., Twenty-Fifth Symposium (International) on Combustion, The Combustion Institute, Pittsburgh, 1994, pp. 1099–1106.

[4.11] Buckmaster, J., Edge Flames, J. Eng. Math. **31**:269–284 (1977).

[4.12] Pitsch, H., private communication.

[4.13] Vanquickenborne, L. and Van Tiggelen, A., Combust. Flame **10**:59 (1966).

[4.14] Eickhoff, H., Lenze, B. and Leukel, W., Twentieth Symposium (International) on Combustion, The Combustion Institute, Pittsburgh, 1985, p. 311.

[4.15] Kalghatgi, G. T., Combust. Sci. Tech. **41**:17 (1984).

[4.16] Peters, N. and Williams, F. A., AIAA J. **21**:423 (1983).

[4.17] Pitts, W. M., Twenty-Second Symposium (International) on Combustion, The Combustion Institute, Pittsburgh, 1989, pp. 809–816.

[4.18] Donnerhack, S., Peters, N., Combust. Sci. Tech. **41**:101–108 (1984).